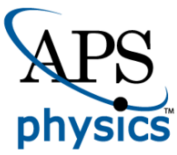

Postquench dynamics and prethermalization in a resonant Bose gas

Xiao Yin and Leo Radzihovsky

Phys. Rev. A **93**, 033653 — Published 31 March 2016

DOI: 10.1103/PhysRevA.93.033653

Post-quench dynamics and pre-thermalization in a resonant Bose gas

Xiao Yin* and Leo Radzihovsky†
Department of Physics, University of Colorado, Boulder, CO 80309

We explore the dynamics of a resonant Bose gas following its quench to a strongly interacting regime near a Feshbach resonance. For such deep quenches, we utilize a self-consistent dynamic field approximation and find that after an initial regime of many-body Rabi-like oscillations between the condensate and finite-momentum quasiparticle pairs, at long times, the gas reaches a pre-thermalized nonequilibrium steady state. We explore the resulting state through its broad stationary momentum distribution function, that exhibits a power-law high momentum tail. We study the dynamics and steady-state form of the associated enhanced depletion, quench-rate dependent excitation energy, Tan's contact, structure function and radio frequency spectroscopy. We find these predictions to be in a qualitative agreement with recent experiments.

PACS numbers: 67.85.De, 67.85.Jk

I. INTRODUCTION

A. Background and motivation

Degenerate atomic gases have radically expanded the scope of quantum many-body physics beyond the traditional solid-state counter part, offering opportunity to study highly coherent, strongly interacting, and well-characterized, defects-free systems. Atomic field-tuned Feshbach resonances (FRs) [1–4] have become a powerful experimental tool that has been extensively utilized to explore strong resonant interactions in these systems. Feshbach resonances have thus led to a seminal realization of paired s-wave fermionic superfluidity, with the associated BCS-to-Bose-Einstein condensate (BEC) crossover [3–6] through a universal unitary regime [7–9], and phase transitions driven by species imbalance [10, 11] and by Mott-insulating physics in an optical lattice [12–16]. Numerous other promising many-body states and phase transitions, such a p-wave fermionic superfluidity [17–19] and Stoner ferromagnetism [20] have been proposed and continue to be explored.

Unmatched by their extreme coherence and high tunability of system parameters, such as FR interactions and single-particle (trap and lattice) potentials, atomic gases have also enabled numerous experimental realizations of highly *nonequilibrium*, strongly-interacting many-body states and associated phase transitions [2, 6, 12].

This has motivated extensive theoretical studies [21–23], with a particular focus on nonequilibrium dynamics following a quench of Hamiltonian parameters, $\hat{H}_i \to \hat{H}_f$. In addition to studies of specific physical systems, experiments on these closed and highly coherent systems have driven theory to address fundamental questions in quantum statistical mechanics. These include the conditions for and nature of thermalization under unitary time evolution $|\hat{\psi}(t)\rangle = e^{i\hat{H}_f t}|\hat{\psi}_i(0)\rangle$ of a closed quantum system vis-á-vis eigenstate thermalization hypothesis [24, 25], role of conservation laws and obstruction to full equilibration of integrable models argued to instead be characterized by a generalized Gibb's ensemble (GGE), emergence of statistical mechanics under unitary time evolution for equilibrated and nonequilibrium stationary states [26, 27]. These questions of post-quench dynamics have been extensively explored in a large number of systems [28–43].

Early studies of a Feshbach-resonant Fermi gas predicted persistent coherent post-quench oscillations [30, 44] and, more recently found topological nonequilibrium steady states and phase transitions [45, 46].

Resonant Bose gas quenched dynamics studies date back to seminal experiments on ^{85}Rb [47, 48], that demonstrated coherent Rabi-like oscillations between atomic and molecular condensates [49], enabling a measurement of the molecular binding energy. More recently, oscillations in the dynamic structure function have also been observed in quasi-2D bosonic ^{133}Cs [38] and studied theoretically [37, 50] for shallow quenches between weakly-repulsive interactions (small gas parameter $na_s^3 \ll 1$ where a_s is the s-wave scattering length).

Such resonant bosonic gases were also predicted to exhibit distinct atomic and molecular superfluid phases, separated by a quantum Ising phase transition (rather than just a fermionic smooth BCS-BEC crossover) and other rich phenomenology [51–55], thereby providing additional motivation for their studies.

Important recent developments are experiments by Makotyn, et al, [56], that explored dynamics of ^{85}Rb following a *deep* quench to the vicinity of the unitary point on the molecular (positive scattering length, $a_s > 0$) side of the Feshbach resonance. It was discovered that even near the unitary point, where a Bose gas is expected to be unstable [57], the three-body decay rate γ_3 (on the order of an inverse milli-second) appears to be more than an order of magnitude slower than the two-body equilibration rate γ_2 (both measured to be proportional to Fermi energy, as expected [58, 59]. This thereby opened a window of time scales from a microsecond (a scale of the

*xiao.yin@colorado.edu
†radzihov@colorado.edu

quench) to a milli-second for observation of a metastable strongly-interacting nonequilibrium dynamics.

Stimulated by these fascinating experimental developments and motivated by the aforementioned earlier work, in a recent brief publication [39] we reported on results for the upper-branch repulsive dynamics of a resonant Bose gas following a deep-detuning quench close to the unitary point on the molecular side ($a_s > 0$) of the FR [56]. Taking the aforementioned slowness of $\gamma_3 \ll \gamma_2$ as an empirical fact, consistent with experimental observations we predicted a fast evolution to a pre-thermalized strongly-interacting stationary state, characterized by a broad, power-law steady-state momentum distribution function, n_k^{ss}, with a time scale $\tau_k = \hbar/E_k$ for the pre-thermalization of momenta k set by the inverse of the excitation spectrum, E_k. The associated condensate depletion was found to exhibit a monotonic growth to a nonequilibrium value exceeding that of the corresponding ground state. In the current manuscript we present the details of the analyses that led to these results as well as a large number of other predictions.

B. Outline

The rest of the paper is organized as follows. We conclude the Introduction with a summary of our key results. In Section II, starting with a one-channel model of a Feshbach-resonant Bose gas, we develop its approximate Bogoliubov and self-consistent dynamic field forms. In Section III, as a warmup we analyze the equilibrium self-consistent model for the strongly interacting case and compare its predictions to that of the Bogoliubov approximation. In Section IV we utilize the Bogoliubov model to study the *nonequilibrium* dynamics following a shallow-quench, computing the momentum distribution function $n_k(t)$ probed in the time-of-flight, the radio-frequency (RF) spectroscopy signal, $I(\omega, t)$, and the structure function $S_k(t)$ probed via Bragg spectroscopy. Then in Section V we generalize the quench to a more experimentally realistic case of a finite-rate ramp and study the effect of ramp rate. In Section VI we employ the self-consistent dynamic field theory to study these and a number of other observables for deep quenches in a strongly interacting regime relevant to JILA experiments [56]. In Section VII we study excitation energy, an important measure of long time nonequilibrium stationary state, for both sudden quench and finite ramp-rate cases, and discuss its dependence on quench depth and ramp rate. We generalize Tan's contact to nonequilibrium process and study its long time behavior in Section VIII. Finally in Section IX we conclude with a discussion of our predictions for experiments and of the future directions for this work. We relegate the details of most calculations to Appendices.

C. Summary of results

Before turning to the derivation and analysis, we briefly summarize the key predictions of our work. Working within the upper-branch of a single-channel model of a resonantly interacting Bose gas we studied an array of nonequilibrium observables following its Feshbach resonance quench toward the unitary point. One central quantity extensively studied in recent time of flight measurements [38, 56] is the momentum distribution function, $n_k(t) = \langle gs_i|\hat{a}_k^\dagger(t)\hat{a}_k(t)|gs_i\rangle$ at time t after a quench from a ground state $|gs_i\rangle$ of an initial Hamiltonian $\hat{H}_i$ to a final Hamiltonian $\hat{H}_f$. Motivated by experiments we take $|gs_i\rangle$ to be a superfluid BEC ground state in the upper branch of the repulsive Bose gas [61]. For a shallow quench in the scattering length $a_i \to a_f$, away from the immediate vicinity of the unitary point, the calculation is controlled by an expansion in a small interaction parameter, $na_{i,f}^3 \ll 1$. Within the lowest, Bogoliubov approximation the momentum distribution function is given by (choosing units where $\hbar = 1$ and $k_B = 1$ throughout) [37]

$$n_{\hat{k}}(\hat{t}) = \frac{\hat{k}^2 + \sigma + \frac{2(1-\sigma)}{\hat{k}^2+2}\sin^2(\hat{t}\sqrt{\hat{k}^2(\hat{k}^2+2)})}{2\sqrt{\hat{k}^2(\hat{k}^2+2\sigma)}} - \frac{1}{2}, \quad (1.1)$$

where $\sigma \equiv a_i/a_f$ characterizes the "depth" of the quench, and we have rescaled the momentum k and time t with the coherence length $\xi \equiv 1/\sqrt{2mng_f}$ and pre-thermalization timescale $t_0 = 1/ng_f$, as $\hat{k} = k\xi$ and $\hat{t} = t/t_0$. Above, n and m are the atom density and mass, respectively, and $g_f = 4\pi a_f/m$ is the post-quench (final) interaction strength. We start the system in a weakly interacting state, characterized by a short positive scattering length a_i and quench it to $a_f > a_i$ ($\sigma \leq 1$). Following coherent oscillations, the gas then exhibits pre-thermalization dynamics, where after a dephasing time τ_k, set by the inverse of the excitation spectrum $1/E_k = 1/\sqrt{\hat{k}^2(\hat{k}^2+2)}$ consistent with experiments [56], the initial narrow Bogoliubov momentum distribution evolves to a stationary state, characterized by a broadened distribution function

$$n_{\hat{k}}^{ss} = \frac{1}{2}\left[\frac{(\hat{k}^2+\sigma)(\hat{k}^2+2)+1-\sigma}{(\hat{k}^2+2)\sqrt{\hat{k}^2(\hat{k}^2+2\sigma)}} - 1\right], \quad (1.2a)$$

$$\sim \begin{cases} C^{ss}/k^4, & \text{for } k\xi \gg 1, \\ 1/k^2, & \text{for } \sigma \ll k\xi \ll 1, \\ 1/k, & \text{for } k\xi \ll \sigma, \end{cases} \quad (1.2b)$$

where we defined C^{ss} as the nonequilibrium analog of Tan's contact[76],

$$C^{ss} = (4\pi a_f n)^2[1 + (1-\sigma)^2], \quad (1.3)$$

derived for the nonequilibrium stationary state in Section VIII. Within above approximation the quasi-particles

do not scatter, precluding full thermalization, and the above final state remains nonequilibrium, completely determined by the depth-quench parameter σ, with the associated diagonal density matrix ensemble.

The associated condensate depletion $n_d(t) = \frac{1}{N}\sum_{\mathbf{k}\neq 0} n_k(t)$ is then straightforwardly computed and monotonically pre-thermalizes to

$$n_d^{ss}(\sigma) = \frac{8}{3\sqrt{\pi}}\left(na_f^3\right)^{1/2}\left[\sigma^{3/2} + \frac{3}{2}\sqrt{1-\sigma}\arccos(\sqrt{\sigma})\right], \tag{1.4}$$

a value exceeding that for the ground state of the final scattering length a_f and greater than the initial ground state depletion $n_d^i = n_d^{ss}(\sigma = 1) = \frac{8}{3\sqrt{\pi}}\left(na_i^3\right)^{1/2}$ at scattering length a_i.

With the goal of understanding deep quenches of a strongly interacting Bose gas [39, 56, 62] near a Feshbach resonance, we developed a self-consistent dynamic field theory of coupled Gross-Petaevskii equation for the condensate $n_c(t)$ and a Heisenberg equation for atoms $\hat{a}_{\mathbf{k}\neq 0}(t)$ excited out of the condensate. It accounts for strong time-dependent depletion of the condensate, with feedback on dynamics of excitations. Within this nonpertubative (but uncontrolled) approximation this amounts to solving for a Heisenberg evolution of $\hat{a}_{\mathbf{k}}(t)$ with a time-dependent Bogoliubov-like Hamiltonian, parameterized by a condensate density $n_c(t)$. The latter is self-consistently determined by the atom-number constraint equation, $n_c(t) = n - \sum_{\mathbf{k}} n_k(t, [n_c(t)])$ [30, 39]. Our treatment here is closely related to the analysis of post-quench quantum coarsening dynamics of the $O(N)$ [36] and Ising [35] models. The resulting momentum distribution function, $\tilde{n}_{\mathbf{k}_\perp}(t)$ (projected column density measured in experiments [56]) and the corresponding depletion $n_d(t)$ are illustrated in Figs. 1,3.

We also studied the excitation energy (defined by Eq. (7.1)) after a constant ramp rate γ (infinite in the case of a sudden quench) between the initial and final scattering lengths a_i and a_f. As illustrated in Fig. 4, we found that it displays a $\sqrt{\gamma}$ form

$$\frac{E_{exc}(\gamma)}{V} = \frac{4(\sigma-1)^2 n^2 a_f}{m} a_f \Lambda f(\gamma/E_\Lambda), \tag{1.5a}$$

$$\propto (1-\sigma)^{3/2}\sqrt{\gamma}, \quad \text{for } \gamma \ll E_\Lambda,$$
$$\propto (1-\sigma)^2 a_f \Lambda\,, \quad \text{for } \gamma \gg E_\Lambda, \tag{1.5b}$$

for a ramp-rate below the microscopic energy cutoff $E_\Lambda = \Lambda^2/2m$.

To further characterize the post-quench evolution and the resulting pre-thermalized steady-state we have also computed a time dependent structure function $S(q,t) = \langle gs_i|n(-\mathbf{q},t)n(\mathbf{q},t)|gs_i\rangle$, a Fourier transform of the density-density connected correlation function. For the weakly interacting, shallow-quench regime, at temperature $1/\beta$ it is given by

$$S(q,t) = \frac{n_0\epsilon_q}{E_{qf}^2}\coth(\beta E_{qi}/2)\left[1 + \frac{E_{qi}^2 - E_{qf}^2}{E_{qf}^2}\sin^2(E_{qf}t)\right], \tag{1.6}$$

first computed and measured in Ref. [38], and after pre-

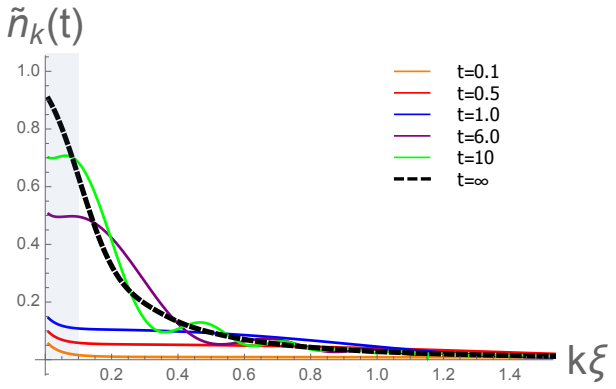

FIG. 1: (Color online) Time evolution of the (column-density) momentum distribution function, $\tilde{n}_{\hat{k}}(\hat{t}) \equiv \int d\hat{k}_z n_{\hat{k}}(\hat{t})$ following a deep scattering length quench $k_n a_i = 0.01 \to k_n a_f = 1$ in a resonant Bose gas (where $k_n \equiv n^{1/3}$), computed within a self-consistent dynamic field approximation. Here momentum is rescaled by the coherence length ξ as $\hat{k} = k\xi \equiv k/\sqrt{2mng_f}$. Lowest curve corresponds to earlier time at $\hat{t} \equiv t/t_0 = 0.1$ in units of pre-thermalization timescale $t_0 = 1/ng_f = m/(4\pi a_f n)$ while the dashed-thick black one represents the asymptotic steady-state distribution. The figure illustrates the initial narrow momentum distribution (lowest curve) evolving to a much broader momentum distribution (highest curve), corresponding to a pre-thermalized steady state. The grey region indicates a range of momenta not resolved in JILA experiments, due to initial inhomogeneous real space density profile and finite trap size.

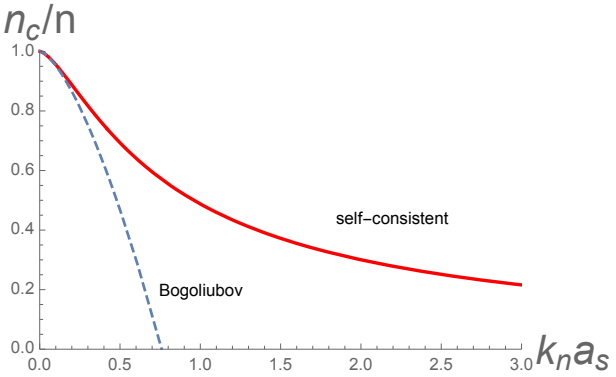

FIG. 2: (Color online) Ground state condensate fraction as a function of a dimensionless measure of atom density and interaction, $k_n a_s$(with $k_n \equiv n^{1/3}$), computed within a self-consistent dynamic field approximation (solid red curve), as compared to Bogoliubov approximation result (dashed blue curve).

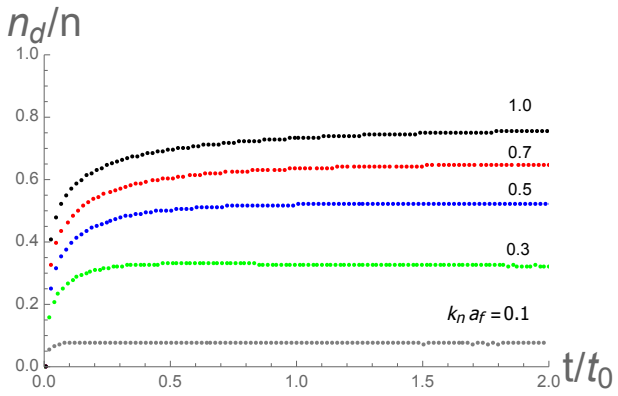

FIG. 3: (Color online) Time evolution of the condensate depletion fraction $n_d(t)/n$ (treated within a self-consistent dynamic field analysis), following a scattering length quench from $k_n a_i = 0.01$ to various $k_n a_f$ in a resonant Bose gas. Here we normalize the time with the pre-thermalization timescale $t_0 = 1/ng_f = m/(4\pi a_f n)$ associated with $k_n a_f = 1$ (where $k_n \equiv n^{1/3}$).

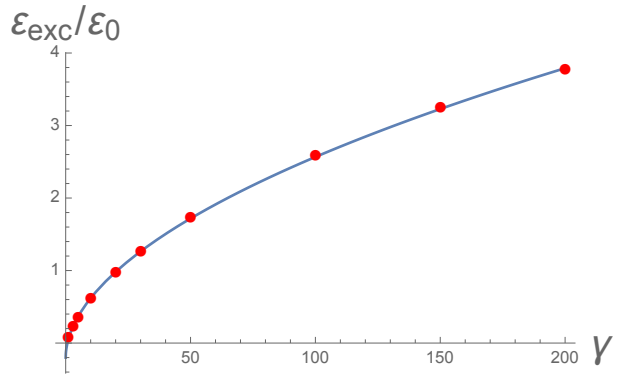

FIG. 4: (Color online) Excitation energy (scaled by LHY correction to the ground state energy) following a scattering length ramp as a function of ramp rate γ (as a "zoom-in" for Fig. 22, see Sec. VII). The red data points are obtained for by varying the ramp rate γ at $a_i/a_f = 1/2$, with scaled dimensionless momentum cutoff $\hat{\Lambda} = \Lambda\xi = 100$ ($\xi \equiv 1/\sqrt{2mng_f}$ is the coherence length); the blue curve is a power-law fit to the numerical data given by $y = 0.24x^{0.53} - 0.2$, with the exponent close to 1/2 predicted by our scaling theory.

thermalization reduces to a time-independent form [39],

$$S_q^{ss} = \frac{n_0\epsilon_q}{2E_{qf}^2}\coth(\beta E_{qi}/2)\left(1+\frac{E_{qi}^2}{E_{qf}^2}\right). \qquad (1.7)$$

Above, $\epsilon_q = q^2/(2m)$ and $E_{qi} = \sqrt{{\epsilon_q}^2 + 2ng_i\epsilon_q}$, $E_{kf} = \sqrt{{\epsilon_q}^2 + 2ng_f\epsilon_q}$ are the pre- and post-quench Bogoliubov dispersions, respectively.

Utilizing our self-consistent dynamic field theory we extended above calculation of $S(q,t)$ to deep quenches of strongly interacting resonant condensates. The resulting time-dependent structure function and its steady-state form are illustrated in Fig. 5.

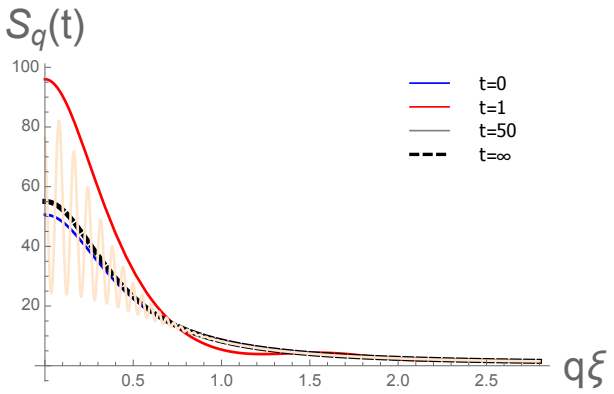

FIG. 5: (Color online) Time evolution of the structure function $S_{\mathbf{q}}(t)$ defined in the text following a scattering length quench from $0.1a_f \to a_f$ with $k_n a_f = 0.7$ (where $k_n \equiv n^{1/3}$), referring to Eq. (6.17) using quasi-adiabatic self-consistent approximation (see Sec. VI A). It illustrates the initial ground state structure function (blue curve), that following the quench develops oscillations and after a pre-thermalization time approaches a steady-state distribution (dashed black curve), which within-quasi-adiabatic approximation almost collapses with the initial ground state curve. Here momentum and time are rescaled with $\xi \equiv 1/\sqrt{2mng_f}$ and $t_0 \equiv 1/(ng_f)$, respectively.

We also computed the RF spectroscopy signal $I(\omega_{RF})$ [63, 64], that measures the transition rate of atoms from two resonantly interacting hyperfine states into a third weakly interacting hyperfine state, for the quench process. Within the Bogoliubov approximation the response is given by

$$I(\omega_{RF}) = \frac{\sqrt{2}\tau V I_0^2}{4\sqrt{\pi m}}\frac{(4\pi n a_f)^2}{\omega_{RF}^{3/2}}, \qquad (1.8)$$

as measured experimentally, with the amplitude proportional to Tan's contact, that in the simplest Bogoliubov approximation is given by $C = (4\pi n a_f)^2$. Here I_0 is the Gaussian RF pulse amplitude and ω_{RF} is the RF pulse carrier frequency, as defined in Eq. (4.32) of Section IV C.

We next turn to a single-channel Feshbach resonant model, followed by its detailed analysis that led to above and other results.

II. MODEL OF A RESONANT SUPERFLUID

A resonant gas of bosonic atoms can be modeled by a single-channel grand-canonical Hamiltonian, (defining $\int_{\mathbf{r}} \equiv \int d^3r$)

$$\hat{H} = \int_{\mathbf{r}}[\hat{\psi}^\dagger(\hat{\epsilon}-\mu)\hat{\psi} + \frac{g}{2}\hat{\psi}^\dagger\hat{\psi}^\dagger\hat{\psi}\hat{\psi}], \qquad (2.1)$$

where $\hat{\psi}(\mathbf{r})$ is a bosonic atom field operator, $\hat{\epsilon} = -\frac{\nabla^2}{2m}$ is a single-particle Hamiltonian, μ is the chemical potential,

and the pseudo-potential g characterizes the atomic two-body interaction on the scale longer than its microscopic range $r_0 = 1/\Lambda$, typically on the order of ten angstroms. For simplicity, we have set $\hbar = 1$.

As discussed in detail in Ref. [4] and references therein, near a Feshbach resonance the magnetic field-dependent coupling $g(B)$ controls the s-wave scattering length a_s through the renormalized coupling (T-matrix) $\tilde{g}^{-1} = g^{-1} + \int_{\mathbf{k}} \frac{1}{2\epsilon_k} = g^{-1} + m\Lambda/(2\pi^2)$,

$$\tilde{g} = \frac{g}{1 + g/g_c}, \tag{2.2}$$

related to the scattering length via $\tilde{g} = 4\pi a_s/m$. As illustrated in Fig. 6, for a sufficiently strong attractive interaction, in a vacuum, the two-atom scattering length diverges at $g_c = 2\pi^2/(m\Lambda) = 2\pi^2 r_0/m$, as the two-body bound state forms for $g < -g_c$ and a_s turns positive on the so-called "BEC" side of the Feshbach resonance. r_0 is the range of the potential and Λ is the corresponding momentum cutoff. It is this scattering-length tunability that enables studies of phase transitions in resonant Bose [51–55] (and BCS-BEC crossover in Fermi [1–3, 3–6]) gases and quenched dynamics [38, 39, 56, 62] that is our focus here.

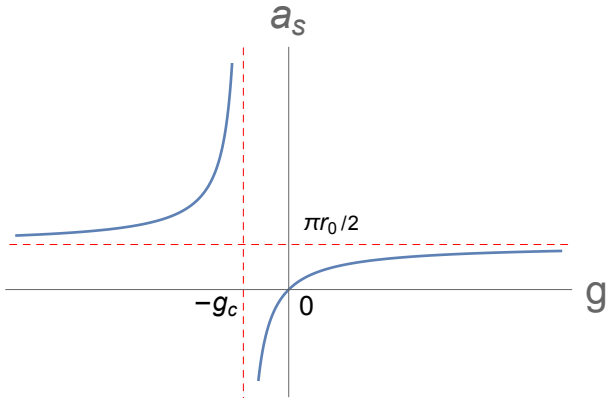

FIG. 6: (Color online) A plot of the s-wave scattering length a_s (renormalized coupling $\tilde{g}$) as a function of bare coupling g in a Feshbach resonance. Here $g_c = 2\pi^2 r_0/m$ is the critical coupling strength at which a_s diverges.

To allow for dynamics within a Bose-condensed state explored experimentally [38, 56], we decompose the atomic field operator $\hat{\psi}(\mathbf{r}) = \frac{1}{\sqrt{V}} \sum_{\mathbf{k}} \hat{a}_{\mathbf{k}} e^{i\mathbf{k}\cdot\mathbf{r}}$, into a c-field condensate Ψ_0 and a fluctuation field $\hat{a}(\mathbf{r})$,

$$\hat{\psi} = \Psi_0 + \hat{a}. \tag{2.3}$$

Expressing the Hamiltonian, (2.1) in terms of the operator $\hat{a}$, it decomposes into

$$\hat{H} = \hat{H}_0 + \hat{H}_1 + \hat{H}_2 + \hat{H}_3 + \hat{H}_4, \tag{2.4}$$

where

$$\hat{H}_0 = \int_{\mathbf{r}} [\Psi_0^*(\hat{\epsilon} - \mu)\Psi_0 + \frac{g}{2}|\Psi_0|^4], \tag{2.5}$$

is the lowest order mean-field ground-state energy, and

$$\hat{H}_1 = \int_{\mathbf{r}} [\hat{a}^\dagger(\hat{\epsilon} + g|\Psi_0|^2 - \mu)\Psi_0] + h.c., \tag{2.6a}$$

$$\hat{H}_2 = \int_{\mathbf{r}} \left[\hat{a}^\dagger \left(\hat{\epsilon} + 2g|\Psi_0|^2 - \mu\right) \hat{a} + \frac{g}{2}\left(\Psi_0^{*2}\hat{a}\hat{a} + \Psi_0^2 \hat{a}^\dagger \hat{a}^\dagger\right)\right], \tag{2.6b}$$

$$\hat{H}_3 = g \int_{\mathbf{r}} [\Psi_0 \hat{a}^\dagger \hat{a}^\dagger \hat{a} + \Psi_0^* \hat{a}^\dagger \hat{a}\hat{a}], \tag{2.6c}$$

$$\hat{H}_4 = \frac{g}{2} \int_{\mathbf{r}} \hat{a}^\dagger \hat{a}^\dagger \hat{a}\hat{a}. \tag{2.6d}$$

are the operator components organized by respective orders in the excitation $\hat{a}$.

A. Bogoliubov approximation for weakly interacting bosons

We set the stage for the study of dynamics following a shallow quench [38] and of a self-consistent dynamic field treatment [39] of a deep quench [56] by first briefly summarizing the results for the ground state and excitations in the Bogoliubov approximation [65, 66].

In the weakly interacting limit the atomic gas is characterized by a small gas parameter $na_s^3 \ll 1$, well-approximated by the Bogoliubov quadratic Hamiltonian, neglecting the nonlinear $\hat{H}_{3,4}$ components of $\hat{H}$. Focusing on the uniform (bulk) condensate and eliminating the chemical potential in favor of the condensate density by requiring the vanishing of the $\hat{H}_1$ component (equivalent to a minimization of $\hat{H}_0$ over Ψ_0), $\mu = g|\Psi_0|^2 \approx gn$, neglecting the difference between the condensate density, $|\Psi_0|^2 \equiv n_c$ and total atom density, n, the grand-canonical Hamiltonian reduces to $\hat{H} \approx -\frac{1}{2}Vgn^2 + \hat{H}_B$,

$$\begin{aligned}
\hat{H}_B &= -\frac{1}{2}\sum_{\mathbf{k}\neq 0} \varepsilon_k + \frac{1}{2}\sum_{\mathbf{k}\neq 0} \begin{pmatrix} \hat{a}_{\mathbf{k}}^\dagger & \hat{a}_{-\mathbf{k}} \end{pmatrix} \begin{pmatrix} \varepsilon_k & gn_c \\ gn_c & \varepsilon_k \end{pmatrix} \begin{pmatrix} \hat{a}_{\mathbf{k}} \\ \hat{a}_{-\mathbf{k}}^\dagger \end{pmatrix}, \\
&= -\frac{1}{2}\sum_{\mathbf{k}\neq 0} \varepsilon_k + \frac{1}{2}\sum_{\mathbf{k}\neq 0} \hat{\Phi}_{\mathbf{k},i}^\dagger h_{\mathbf{k},ij} \hat{\Phi}_{\mathbf{k},j}, \\
&= -\frac{1}{2}\sum_{\mathbf{k}\neq 0} \varepsilon_k + \frac{1}{2}\sum_{\mathbf{k}\neq 0} E_k \hat{\Psi}_{\mathbf{k},s}^\dagger \hat{\Psi}_{\mathbf{k},s}, \\
&= -\frac{1}{2}\sum_{\mathbf{k}\neq 0} (\varepsilon_k - E_k) + \sum_{\mathbf{k}\neq 0} E_k \hat{\alpha}_{\mathbf{k}}^\dagger \hat{\alpha}_{\mathbf{k}},
\end{aligned} \tag{2.7}$$

where the quadratic Hamiltonian was straightforwardly diagonalized in terms of the Bogoliubov quasi-particles $\hat{\Psi}_{\mathbf{k}} = (\hat{\alpha}_{\mathbf{k}}, \hat{\alpha}_{-\mathbf{k}}^\dagger)$, related to the atomic Nambu spinor $\hat{\Phi}_{\mathbf{k}} = (\hat{a}_{\mathbf{k}}, \hat{a}_{-\mathbf{k}}^\dagger)$ by a pseudo-unitary transformation, $U_{\mathbf{k}}$

$$\begin{pmatrix} \hat{a}_{\mathbf{k}} \\ \hat{a}_{-\mathbf{k}}^\dagger \end{pmatrix} = \begin{pmatrix} u_{\mathbf{k}} & v_{\mathbf{k}} \\ v_{\mathbf{k}}^* & u_{\mathbf{k}}^* \end{pmatrix} \begin{pmatrix} \hat{\alpha}_{\mathbf{k}}, \\ \hat{\alpha}_{-\mathbf{k}}^\dagger, \end{pmatrix} \tag{2.8a}$$

$$\hat{\Phi}_{\mathbf{k}} = U_{\mathbf{k}} \hat{\Psi}_{\mathbf{k}}. \tag{2.8b}$$

$U_{\mathbf{k}}$ satisfies a pseudo eigenvalue equation $h_{\mathbf{k}}U_{\mathbf{k}} = E_{\mathbf{k}}\sigma^z U_{\mathbf{k}}$ and preserves the canonical commutation relation, $[a_{\mathbf{k}}, a^\dagger_{\mathbf{k}'}] = \delta_{\mathbf{k},\mathbf{k}'}$, corresponding to $[\hat\Phi_{i\mathbf{k}}, \hat\Phi^\dagger_{j\mathbf{k}'}] = \sigma^z_{ij}\delta_{\mathbf{k},\mathbf{k}'}$, defined by

$$U\sigma_z U^\dagger = \sigma_z, \tag{2.9}$$

with $|u_{\mathbf{k}}|^2 - |v_{\mathbf{k}}|^2 = 1$ and σ^z the third Pauli matrix.

With $\varepsilon_k = k^2/2m + gn$ in (2.7), the Bogoliubov spectrum is given by a well-known gapless form,

$$E_k = \sqrt{\varepsilon_k^2 - g^2n^2} = \sqrt{\epsilon_k^2 + 2gn\epsilon_k} = ck\sqrt{1+\xi^2k^2/2}, \tag{2.10}$$

that interpolates between the low-momentum zeroth-sound with velocity $c = \sqrt{gn/m}$ (a Goldstone mode of the $U(1)$ symmetry breaking) and the high-momentum quadratic dispersion, with crossover scale set by the correlation length $\xi = 1/\sqrt{2mgn}$. The corresponding coherence factors defining $U_{\mathbf{k}}$ are given by

$$u_k^2 = \frac{1}{2}\left(\frac{\varepsilon_k}{E_k} + 1\right), \quad v_k^2 = \frac{1}{2}\left(\frac{\varepsilon_k}{E_k} - 1\right). \tag{2.11}$$

The ground state is a vacuum of Bogoliubov quasiparticles, $\hat\alpha_{\mathbf{k}}|gs\rangle = 0$, with the energy density $\mathcal{E}_{gs} = V^{-1}\langle gs|\hat H|gs\rangle$ given by

$$\mathcal{E}_{gs} = \frac{1}{2}gn^2 - \frac{1}{V}\sum_{\mathbf{k}\neq 0} E_k n_k, \tag{2.12a}$$

$$= \frac{2\pi a_s}{m}n^2\left[1 + \frac{128}{15\sqrt{\pi}}(na_s^3)^{1/2}\right]. \tag{2.12b}$$

Above, the second term in Eq. (2.12b) is the well-known Lee-Huang-Yang (LHY) correction to the mean field ground state energy (first term)[68].

At $T = 0$ the momentum distribution function is

$$n_k = \langle gs|\hat a_k^\dagger \hat a_k|gs\rangle = |v_k|^2 \approx_{k\to\infty} C/k^4, \tag{2.13}$$

with Tan's contact $C = \partial\mathcal{E}_{gs}/\partial a_s^{-1} = 16\pi^2n^2a_s^2[(1 + \frac{64}{3\sqrt{\pi}}(na_s^3)^{1/2}]$ and

$$\mu = \frac{4\pi an}{m}\left[1 + \frac{32}{3\sqrt{\pi}}(na_s^3)^{1/2}\right]. \tag{2.14}$$

The interaction-driven condensate depletion, $n_d \equiv n - n_c$ is given by

$$n_d = \frac{1}{V}\sum_{\boldsymbol{k}\neq 0} n_k \approx \frac{8}{3\sqrt{\pi}}\left(na_s^3\right)^{1/2} n, \tag{2.15}$$

and provides an important measure of the validity of the Bogoliubov approximation that neglects the difference between n and n_c.

Clearly, for a large gas parameter, $na_s^3 \gg 1$ the depletion is substantial and must be accounted for. Although there is no currently available systematic analysis in this non-perturbative limit, as we will show in subsequent sections, an uncontrolled self-consistent method, akin to a spherical, large-N model [35, 36, 59, 67, 69] captures important qualitative physics in this resonantly interacting regime.

B. Generalization for large scattering length

To extend the analysis to a large na_s^3 we need to account (even if approximately) for the nonlinear components of the Hamiltonian, $\hat H_{3,4}$ neglected in the Bogoliubov model. To this end, in the spirit of variational theory or a spherical model [69], we replace these nonlinear operators by their "best" approximation in terms of operators up to a quadratic order in fluctuation field $\hat a$. Using Wick's theorem, we have

$$\begin{aligned}\hat a^\dagger\hat a^\dagger\hat a\hat a &\to 4\langle\hat a^\dagger\hat a\rangle\hat a^\dagger\hat a + \langle\hat a^\dagger\hat a^\dagger\rangle\hat a\hat a + \langle\hat a\hat a\rangle\hat a^\dagger\hat a^\dagger \\ &\quad -2\langle\hat a^\dagger\hat a\rangle\langle\hat a^\dagger\hat a\rangle - \langle\hat a^\dagger\hat a^\dagger\rangle\langle\hat a\hat a\rangle, \\ &\approx 4n_d\hat a^\dagger\hat a - 2n_d^2, \end{aligned} \tag{2.16a}$$

$$\hat a^\dagger\hat a\hat a \to 2\langle\hat a^\dagger\hat a\rangle\hat a \approx 2n_d\hat a, \tag{2.16b}$$

$$\hat a^\dagger\hat a^\dagger\hat a \to 2\hat a^\dagger\langle\hat a^\dagger\hat a\rangle \approx 2n_d\hat a^\dagger, \tag{2.16c}$$

where we kept the depletion density $n_d = \langle\hat a^\dagger\hat a\rangle$ and neglected "anomalous" averages (e.g., $\langle\hat a\hat a\rangle = 0$) and high order correlators (e.g., $\langle\hat a^\dagger\hat a\hat a\rangle = 0$) that we expect to be subdominant.

With these we approximate $\hat H_3$ and $\hat H_4$ by a linear and quadratic forms

$$\hat H_3 = g\int_{\mathbf{r}}[\Psi_0\hat a^\dagger\hat a^\dagger\hat a + \Psi_0^*\hat a^\dagger\hat a\hat a] \to \delta\hat H_1, \tag{2.17}$$

where

$$\delta\hat H_1 = g\int_{\mathbf{r}}(2\Psi_0 n_d\hat a^\dagger + h.c.), \tag{2.18}$$

and

$$\hat H_4 = \frac{g}{2}\int_{\mathbf{r}}\hat a^\dagger\hat a^\dagger\hat a\hat a \to \delta\hat H_0 + \delta\hat H_2, \tag{2.19}$$

where

$$\delta\hat H_0 = -gVn_d^2, \tag{2.20a}$$

$$\delta\hat H_2 = 2g\int_{\mathbf{r}} n_d\hat a^\dagger\hat a. \tag{2.20b}$$

The grand-canonical Hamiltonians now take the following forms: $\hat H \approx \hat H_0' + \hat H_1' + \hat H_2'$, where

$$\begin{aligned}\hat H_0' &= \hat H_0 + \delta\hat H_0, \\ &= \int_{\mathbf{r}}\left[\Psi_0^*(\hat\epsilon - \mu)\Psi_0 + \frac{g}{2}n_c^2 - gn_d^2\right],\end{aligned} \tag{2.21a}$$

$$\begin{aligned}\hat H_1' &= \hat H_1 + \delta\hat H_1, \\ &= \int_{\mathbf{r}}\left[\hat a^\dagger(\hat\epsilon + gn_c + 2gn_d - \mu)\Psi_0\right] + h.c.,\end{aligned} \tag{2.21b}$$

$$\begin{aligned}\hat H_2' &= \hat H_2 + \delta\hat H_2, \\ &= \int_{\mathbf{r}}\left[\hat a^\dagger(\hat\epsilon + 2g(n_c + n_d) - \mu)\hat a + \frac{gn_c}{2}(\hat a\hat a + \hat a^\dagger\hat a^\dagger)\right].\end{aligned} \tag{2.21c}$$

Above, for simplicity, we have defined $n_c \equiv |\Psi_0|^2$ and $n_d \equiv \langle \hat{a}^\dagger \hat{a} \rangle$ and in Eqs. (2.21a),(2.21b),(2.21c) have discarded the "anomalous average" term $\tilde{m} \equiv \langle \hat{a}\hat{a} \rangle$ to satisfy the constraint of Goldstone theorem, which requires a gapless excitation spectrum. This amounts to the widely used Popov approximation [70].

Following what was done in the last subsection, we fix the chemical potential μ by requiring $\hat{H}_1' = 0$

$$(\hat{\epsilon} + g|\Psi_0|^2 + 2gn_d)\Psi_0 = \mu\Psi_0. \tag{2.22}$$

For a uniform system, this gives

$$\mu = gn_c + 2gn_d. \tag{2.23}$$

Thus we obtain the grand-canonical Hamiltonian

$$\begin{aligned}\hat{H} &= \int_{\mathbf{r}} \left[\hat{a}^\dagger(\hat{\epsilon} + gn_c)\hat{a} + \frac{g}{2}n_c(\hat{a}\hat{a} + \hat{a}^\dagger\hat{a}^\dagger)\right] - E_0 \\ &= \sum_{\boldsymbol{k}\neq 0}\left[(\epsilon_k + gn_c)\hat{a}^\dagger_{\mathbf{k}}\hat{a}_{\mathbf{k}} + \frac{1}{2}gn_c(\hat{a}^\dagger_{\mathbf{k}}\hat{a}^\dagger_{-\mathbf{k}} + \hat{a}_{\mathbf{k}}\hat{a}_{-\mathbf{k}})\right] - E_0,\end{aligned} \tag{2.24}$$

where $E_0/V = \frac{g}{2}n_c^2 + 2gn_cn_d + gn_d^2$. It exhibits the standard Bogoliubov form with gapless spectrum, but also approximately accounts for a potentially strong depletion through the condensate density n_c replacing the full density n as the self-consistently determined parameter of the Hamiltonian.

III. SELF-CONSISTENT ANALYSIS FOR STRONGLY INTERACTING GROUND STATE

Before turning to our main focus of nonequilibrium post-quench dynamics, we examine the ground state properties of a strongly interacting resonant Bose gas, characterized by a large scattering length and gas parameter $na_s^3 \gg 1$. This regime lies beyond the scope of the standard Bogoliubov theory. Nevertheless we expect to be able to treat it qualitatively correctly (even if quantitatively uncontrolled) by taking into account the large depletion $n - n_c > 0$ through the Hamiltonian (2.24) and the self-consistency condition through the atom number conservation

$$\begin{aligned} n &= n_c + \frac{1}{V}\sum_{\boldsymbol{k}\neq 0}\langle \hat{a}^\dagger_{\mathbf{k}}\hat{a}_{\mathbf{k}}\rangle, &(3.1a)\\ &= n_c + \frac{8}{3\sqrt{\pi}}\left(n_c a_s^3\right)^{1/2} n_c, &(3.1b)\end{aligned}$$

where in the second line we calculated the depletion by diagonalizing (2.24) as in Sec. II A of the conventional Bogoliubov theory, but with n_c replacing n. Such treatment is quite close in spirit to the self-consistent Hartree-Fock approximations, and the BCS and other mean-field gap equations.

In the dimensionless form for $\hat{n}_c = n_c/n$, the self-consistency equation reduces to

$$1 - \hat{n}_c - \lambda \hat{n}_c^{3/2} = 0, \tag{3.2}$$

where $\lambda = 8(na_s^3)^{1/2}/(3\sqrt{\pi}) \equiv 8(k_n a_s)^{3/2}/(3\sqrt{\pi})$, with $k_n \equiv n^{1/3}$ the mometum scale set by the boson density n.

The solution to Eq. (3.2) is illustrated in Fig. 2. We find that the self-consistency constraint suppresses condensate depletion, leading to a higher condensate fraction n_c than the Bogoliubov approximation for the same strength of the interaction parameter $k_n a_s$. We also observe that, as expected the correction to Bogoliubov theory from the self-consistency condition grows (from zero) with increasing gas parameter $k_n a_s$, thereby avoiding the spurious transition to a vanishing condensate state appearing in the Bogoliubov theory.

IV. DYNAMICS FOR SHALLOW QUENCH

We now turn to nonequilibrium dynamics following a change in the scattering length a_s from its initial value a_i to the final value a_f, as can be realized experimentally in a Feshbach resonant Bose gas by a change in the external magnetic field [56]. Here we assume the change is instantaneous (sudden quench), allowing analytical analysis. In this section, we focus on shallow quenches characterized by both $na_i^3 \ll 1$ and $na_f^3 \ll 1$, so that the Bogoliubov approximation remains rigorously valid.

For shallow quenches, the system is well approximated by Hamiltonian (2.7) with g_i and g_f for the initial and final Hamiltonians, respectively, with corresponding Bogoliubov quasi-particle bases $(\hat{\alpha}_{\mathbf{k}}, \hat{\alpha}^\dagger_{\mathbf{k}})$ prior to the quench and $(\hat{\beta}_{\mathbf{k}}, \hat{\beta}^\dagger_{\mathbf{k}})$ post the quench. Focussing on a sudden quench, the two sets of bases are related to the atomic basis $(\hat{a}_{\mathbf{k}}, \hat{a}^\dagger_{\mathbf{k}})$ via a pseudo-unitary transformations

$$\begin{aligned}\begin{pmatrix}\hat{a}_{\mathbf{k}}\\ \hat{a}^\dagger_{-\mathbf{k}}\end{pmatrix} &= \begin{pmatrix}u_k' & v_k'\\ v_k' & u_k'\end{pmatrix}\begin{pmatrix}\hat{\alpha}_{\mathbf{k}}\\ \hat{\alpha}^\dagger_{-\mathbf{k}}\end{pmatrix}, &(4.1a)\\ \hat{\Phi}_{\mathbf{k}}(0) &= U_k(0^-)\hat{\Psi}_{\mathbf{k}}(0^-), &(4.1b)\end{aligned}$$

and

$$\begin{aligned}\begin{pmatrix}\hat{a}_{\mathbf{k}}\\ \hat{a}^\dagger_{-\mathbf{k}}\end{pmatrix} &= \begin{pmatrix}u_k & v_k\\ v_k & u_k\end{pmatrix}\begin{pmatrix}\hat{\beta}_{\mathbf{k}}\\ \hat{\beta}^\dagger_{-\mathbf{k}}\end{pmatrix}, &(4.2a)\\ \hat{\Phi}_{\mathbf{k}}(0) &= U_k(0^+)\hat{\Psi}_{\mathbf{k}}(0^+), &(4.2b)\end{aligned}$$

where

$$u_k' = \sqrt{\frac{1}{2}\left(\frac{\epsilon_k + ng_i}{E_{ki}} + 1\right)}, \quad v_k' = -\sqrt{\frac{1}{2}\left(\frac{\epsilon_k + ng_i}{E_{ki}} - 1\right)}, \tag{4.3a}$$

$$u_k = \sqrt{\frac{1}{2}\left(\frac{\epsilon_k + ng_f}{E_{kf}} + 1\right)}, \quad v_k = -\sqrt{\frac{1}{2}\left(\frac{\epsilon_k + ng_f}{E_{kf}} - 1\right)}, \tag{4.3b}$$

define Bogoliubov transformations for Hamiltonians $\hat{H}_i$ (with interaction $g_i \equiv g(0^-)$) before and $\hat{H}_f$ (with interaction $g_f \equiv g(0^+)$) after the quench, respectively. The corresponding excitation spectra are

$$E_{ki} = \sqrt{{\epsilon_k}^2 + 2ng_i\epsilon_k}, \quad E_{kf} = \sqrt{{\epsilon_k}^2 + 2ng_f\epsilon_k}, \tag{4.4}$$

and the two quasi-particle bases are related by

$$\begin{aligned} \begin{pmatrix} \hat{\beta}_{\mathbf{k}} \\ \hat{\beta}^\dagger_{-\mathbf{k}} \end{pmatrix} &= U_k^{-1}(0^+)U_k(0^-) \begin{pmatrix} \hat{\alpha}_{\mathbf{k}} \\ \hat{\alpha}^\dagger_{-\mathbf{k}} \end{pmatrix}, \\ &= \begin{pmatrix} \cosh\Delta\theta_k & \sinh\Delta\theta_k \\ \sinh\Delta\theta_k & \cosh\Delta\theta_k \end{pmatrix} \begin{pmatrix} \hat{\alpha}_{\mathbf{k}} \\ \hat{\alpha}^\dagger_{-\mathbf{k}} \end{pmatrix}, \end{aligned} \tag{4.5}$$

with

$$\Delta\theta_k = \frac{1}{2}\cosh^{-1}\left[\frac{1}{2}\left(\frac{E_{kf}}{E_{ki}} + \frac{E_{ki}}{E_{kf}}\right)\right]. \tag{4.6}$$

We take the initial state $|0^-\rangle$ to be the ground state of the pre-quenched Hamiltonian $\hat{H}_i$ [61], and thus a vacuum of $\hat{\alpha}$ quasi-particles, $\hat{\alpha}_{\mathbf{k}}|0^-\rangle = 0$. At finite temperature this generalizes to Bose-Einstein distribution of $\hat{\alpha}$ quasi-particle occupation,

$$\langle\hat{\alpha}^\dagger_{\mathbf{k}}\hat{\alpha}_{\mathbf{k}}\rangle_{0^-} = \frac{1}{e^{E_{ki}/T} - 1}. \tag{4.7}$$

Because experiments probe physical observables expressed in terms of atomic operators, we need to compute time evolution of $\hat{\Phi}_{\mathbf{k}}(t) = (\hat{a}_{\mathbf{k}}(t), \hat{a}^\dagger_{\mathbf{k}}(t))$. Using free post-quench evolution of $\hat{\beta}$ quasi-particles

$$\begin{pmatrix} \hat{\beta}_{\mathbf{k}}(t) \\ \hat{\beta}^\dagger_{-\mathbf{k}}(t) \end{pmatrix} = \begin{pmatrix} e^{-iE_{kf}t} & 0 \\ 0 & e^{iE_{kf}t} \end{pmatrix} \begin{pmatrix} \hat{\beta}_{\mathbf{k}}(0) \\ \hat{\beta}^\dagger_{-\mathbf{k}}(0) \end{pmatrix} \equiv T_k(t)\hat{\Psi}_{\mathbf{k}}(0^+), \tag{4.8}$$

the relation (4.5), together with the simplicity of matrix elements of $\hat{\alpha}$ quasi-particles in the pre-quench ground state (vacuum of $\hat{\alpha}_{\mathbf{k}}$), we find

$$\begin{aligned} \begin{pmatrix} \hat{a}_{\mathbf{k}}(t) \\ \hat{a}^\dagger_{-\mathbf{k}}(t) \end{pmatrix} &= U_k(0^+) \begin{pmatrix} \hat{\beta}_{\mathbf{k}}(t) \\ \hat{\beta}^\dagger_{-\mathbf{k}}(t) \end{pmatrix}, && (4.9a) \\ &= U_k(0^+)T_k(t) \begin{pmatrix} \hat{\beta}_{\mathbf{k}}(0) \\ \hat{\beta}^\dagger_{-\mathbf{k}}(0) \end{pmatrix}, && (4.9b) \\ &= U_k(0^+)T_k(t)U_k^{-1}(0^+)U_k(0^-) \begin{pmatrix} \hat{\alpha}_{\mathbf{k}}(0) \\ \hat{\alpha}^\dagger_{-\mathbf{k}}(0) \end{pmatrix}, && (4.9c) \\ \hat{\Phi}_{\mathbf{k}}(t) &= U_k(t)\hat{\Psi}_{\mathbf{k}}(0^-) = R_k(t)U_k(0^-)\hat{\Psi}_{\mathbf{k}}(0^-), && (4.9d) \end{aligned}$$

where the matrix

$$\begin{aligned} R_{ij}(t) &= U_{il}T_{lm}(t)U^{-1}_{mn}, && (4.10a) \\ &= (\cos E_{kf}t)I_{ij} + i\frac{\sin E_{kf}t}{E_{kf}} \begin{pmatrix} \epsilon_k + g_f n & g_f n \\ -g_f n & -\epsilon_k - g_f n \end{pmatrix}, && (4.10b) \end{aligned}$$

evolves the initial Bogoliubov spinor $(u_k(0^-), v_k(0^-)) \to (u_k(t), v_k(t))$, and

$$\begin{aligned} U_k(t) &= U_k(0^+)T_k(t)U_k^{-1}(0^+)U_k(0^-), && (4.11a) \\ &= \begin{pmatrix} u_k e^{-iE_{kf}t} & v_k e^{iE_{kf}t} \\ v_k e^{-iE_{kf}t} & u_k e^{iE_{kf}t} \end{pmatrix} \begin{pmatrix} \cosh\Delta\theta_k & \sinh\Delta\theta_k \\ \sinh\Delta\theta_k & \cosh\Delta\theta_k \end{pmatrix}. && (4.11b) \end{aligned}$$

Having derived the evolution of the atomic fields $\hat{\Phi}_{\mathbf{k}}(t) = (\hat{a}_{\mathbf{k}}(t), \hat{a}^\dagger_{\mathbf{k}}(t))$, we can now compute the basic atomic bilinear correlator (suppressing the momentum $\mathbf{k}$ argument on the right hand-side):

$$\begin{aligned} C^{ij}_{\mathbf{k}}(t,t') &= \langle\hat{\Phi}^\dagger_i(t)\hat{\Phi}_j(t')\rangle, \\ &= \langle\hat{\Psi}^\dagger_m(0^-)U^\dagger_{mi}(t)U_{jn}(t')\hat{\Psi}_n(0^-)\rangle, \\ &= U^\dagger_{mi}(t)N_{mn}U_{jn}(t'), \end{aligned} \tag{4.12}$$

in terms of the pre-quench ($t = 0^-$) quasi-particle occupation matrix

$$\begin{aligned} N_{mn} &= \langle\hat{\Psi}^\dagger_m(0^-)\hat{\Psi}_n(0^-)\rangle, && (4.13a) \\ &= \begin{pmatrix} \langle\hat{\alpha}^\dagger_{\mathbf{k}}\hat{\alpha}_{\mathbf{k}}\rangle & \langle\hat{\alpha}^\dagger_{\mathbf{k}}\hat{\alpha}^\dagger_{-\mathbf{k}}\rangle \\ \langle\hat{\alpha}_{-\mathbf{k}}\hat{\alpha}_{\mathbf{k}}\rangle & \langle\hat{\alpha}_{-\mathbf{k}}\hat{\alpha}^\dagger_{-\mathbf{k}}\rangle \end{pmatrix}_{mn}, && (4.13b) \\ &= \begin{pmatrix} n_k(0^-) & 0 \\ 0 & n_{-k}(0^-) + 1 \end{pmatrix}_{mn}, && (4.13c) \\ &= \begin{pmatrix} 0 & 0 \\ 0 & 1 \end{pmatrix}_{mn}, \quad \text{for } T = 0, && (4.13d) \end{aligned}$$

from which physical observables, such as the momentum distribution function, structure function, RF spectroscopy signal, and many others can be obtained. We turn to their computation in the following subsections.

A. Time of flight: momentum distribution function

Time of flight measurements, where a gas is released from its trap and its density profile is measured at long times, is one of the central experimental probes dating back to the realization of BEC in dilute alkali gases [71, 72]. A straightforward analysis demonstrates [11], that at long times the density profile is proportional to the momentum distribution function. At $T = 0$, that is our main focus here, we obtain

$$\begin{aligned} n_k(t) &= \langle 0^-|\hat{a}^\dagger_{\mathbf{k}}(t)\hat{a}_{\mathbf{k}}(t)|0^-\rangle = C^{11}_k(t,t), \\ &= |(u_k e^{-iE_{kf}t}\sinh\Delta\theta_k + v_k e^{iE_{kf}t}\cosh\Delta\theta_k)|^2, \\ &= \frac{\epsilon_k + g_i n + \frac{2g_f(g_f - g_i)n^2}{\epsilon_k + 2g_f n}\sin^2(E_{kf}t)}{2\sqrt{\epsilon_k(\epsilon_k + 2g_i n)}} - \frac{1}{2}, \end{aligned} \tag{4.14}$$

at $t = 0$ reducing to the ground-state momentum distribution Eq. (2.13), as expected by continuity of evolution. Rescaling momentum as $\hat{k} = k\xi \equiv k/\sqrt{2mng_f}$ and time

as $\hat{t} = t/t_0 \equiv tng_f$, we obtain the momentum distribution in terms of dimensionless variables as

$$n_{\hat{k}}(\hat{t}) = \frac{[\hat{k}^2 + \sigma + \frac{2(1-\sigma)}{\hat{k}^2+2}\sin^2(\hat{t}\sqrt{\hat{k}^2(\hat{k}^2+2)})]}{2\sqrt{\hat{k}^2(\hat{k}^2+2\sigma)}} - \frac{1}{2}, \tag{4.15}$$

where the initial-to-final scattering length ratio, $\sigma \equiv a_i/a_f$ characterizes the "depth" of the quench.

The column momentum distribution $\tilde{n}_{\hat{k}}(\hat{t}) \equiv \int d\hat{k}_z n_{\hat{k}}(\hat{t})$ is a more experimentally relevant quantity that we plot at different times in Fig. 7. We observe

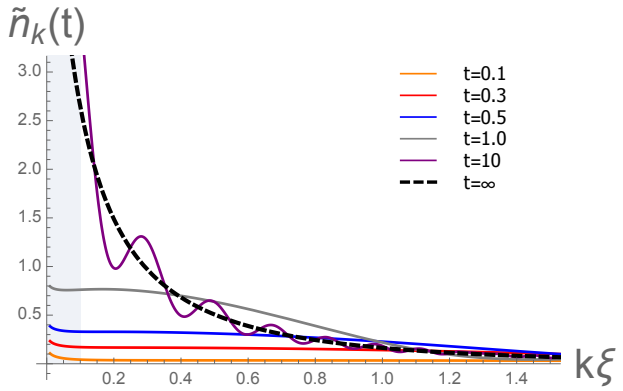

FIG. 7: (Color online) Time evolution of the column momentum distribution defined in the text following a scattering length quench from $0.1a_f \to a_f$, referring to Eq. (4.15) using Bogoliubov approximation. It illustrates the initial narrow momentum distribution (lowest curve) evolving to a much broader momentum distribution (highest curve), corresponding to a pre-thermalized steady state. Here momentum and time are rescaled with $\xi \equiv 1/\sqrt{2mng_f}$ and $t_0 \equiv 1/(ng_f)$, respectively. The grey region indicates a range of momenta not resolved in JILA experiments, due to initial inhomogeneous real space density profile and finite trap size.

that starting with a narrow BEC peak, the column momentum distribution function quickly broadens and develops a large momentum tail. The momentum distribution approaches a pre-thermalized steady-state $\tilde{n}_k^{ss}$ from high momenta, with momenta $k > k_{pth}(t)$ taking time $t_{pth}(k) \approx 1/E_{kf}$ to pre-thermalize [61]. Thus we obtain

$$t_{pth}(\hat{k}) = 1/\sqrt{\hat{k}^2(\hat{k}^2+2)}, \tag{4.16}$$

consistent with experiments [56] scaling as $1/k$ and $1/k^2$ at small and large momenta, respectively.

The steady-state momentum distribution, n_k^{ss} for a $a_i = 0.1a_f \to a_f$ is plotted in Fig. 8 and compared to the ground state n_k for the same a_f as well as thermal state n_k at finite temperature. We observe that this steady-state momentum distribution lies above the ground state one, indicating that even in the long time limit the post-quench system remains in the excited states, as required by energy conservation. However, it also differs significantly from the corresponding finite-temperature thermal-equilibrium distribution, $n_k^T = (u_k^2 + v_k^2)\langle\hat{\alpha}_{\mathbf{k}}^\dagger\hat{\alpha}_{\mathbf{k}}\rangle_{0^-} + v_k^2 = 1/(e^{E_{kf}/T} - 1) + v_k^2\coth(E_{kf}/2T)$, demonstrating that even in the long time, stationary state limit the system is only *pre-thermalized*. This is expected because of the quadratic, fully integrable form of the Bogoliubov Hamiltonian. The latter guarantees the absence of scattering of the Bogoliubov quasi-particles $\hat{\beta}_{\mathbf{k}}$, with a conserved momentum distribution function, that is directly related to the initial distribution by (4.5).

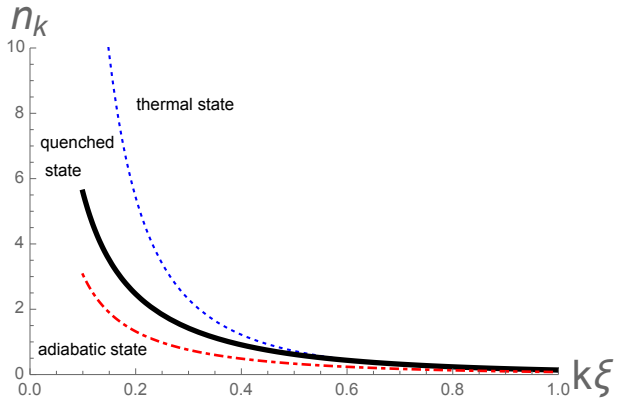

FIG. 8: (Color online) Quenched steady-state momentum distribution function n_k^{ss} following a scattering length quench $a_i = 0.1a_f \to a_f$ (thick black curve), as compared to the ground state momentum distribution at a_f (dash-dotted red) and the corresponding Bogoliubov thermalized distribution (dotted blue) at temperature $T = 0.45ng_f$.

A simpler measure of the post-quench dynamics is the evolution of the condensate depletion, obtained from the momentum distribution function, $n_k(t)$, (4.14),

$$\begin{aligned} n_d(t) &= \sum_{\mathbf{k}} n_k(t) = V\int \frac{d^3k}{(2\pi)^3} n_k(t), \\ &= n_d^0 F_d(\sigma, t), \end{aligned} \tag{4.17}$$

where $n_d^0 = 8/(3\sqrt{\pi})(na_f^3)^{1/2}$ is the ground-state depletion for $a_s = a_f$.

$$\begin{aligned} F_d(\sigma,t) &= (\sigma)^{3/2} + \frac{3}{2}\sqrt{1-\sigma}\mathrm{Arccos}(\sqrt{\sigma}) \\ &- \frac{3\sqrt{2}}{2}\int ydy\frac{(1-\sigma)\cos(2ty\sqrt{y^2+2})}{(y^2+2)(y^2+2\sigma)^{1/2}} \end{aligned} \tag{4.18}$$

is the nonequilibrium depletion enhancement factor above the corresponding ground state, that interpolates between $\sigma^{3/2}$ (giving the initial depletion at $t = 0^-$ for $a_s = a_i$) and the asymptotic depletion

$$F_d^{ss}(\sigma) \equiv F_d(\sigma, t\to\infty) = \sigma^{3/2} + \frac{3}{2}\sqrt{1-\sigma}\mathrm{Arccos}(\sqrt{\sigma}) \tag{4.19}$$

of the pre-thermalized state, plotted in Fig. 10.

As is clear from the asymptotics of $F_d(\sigma,t)$ defined by (4.19) and illustrated in Fig. 9, the depletion fraction monotonically increases as $\sqrt{t}$ over a characteristic time

$$t_{pth} \approx \frac{1}{ng_f}, \tag{4.20}$$

approaching its asymptotic pre-thermalized value, that is always higher than that of the ground state with the same scattering length $a_s = a_f$. The quenched steady-state depletion enhancement, $F_d^{ss}(\sigma)$ monotonically increasing with decreasing σ (deeper quench), reaching a minimum at $\sigma = 1$ (no quench), and exhibiting a maximum at $\sigma = 0$, corresponding to initially noninteracting gas or a quench deep into unitary regime, where $a_f \to \infty$. We note, however, that the latter strongly-interacting resonant regime, clearly lies outside of the perturbative Bogoliubov theory. We will treat this $k_n a_f \gg 1$ nonperturbative regime in a subsequent section, using an approximate self-consistent treatment.

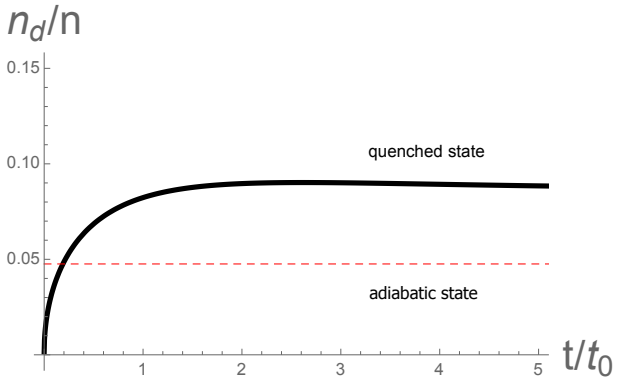

FIG. 9: (Color online) Post quench dynamics of the condensate depletion fraction as a function of rescaled time in units of pre-thermalization timescale $t_0 = \hbar/(ng_f) = m/(4\pi a_f n\hbar)$ (solid black curve), following a scattering length quench from $0.1a_f \to a_f$ with $k_n a_f = 0.1$ (where $k_n \equiv n^{1/3}$), as compared to the ground state depletion at $k_n a_f$ (dashed red line). For a typical ^{85}Rb experiment with $n = 5\times 10^{12} cm^{-3}$, $a_f = 1100 a_0$ (here $a_0 = 5.29\times 10^{-11} m$ is the Bohr radius), $t_0 \approx 360\mu s$.

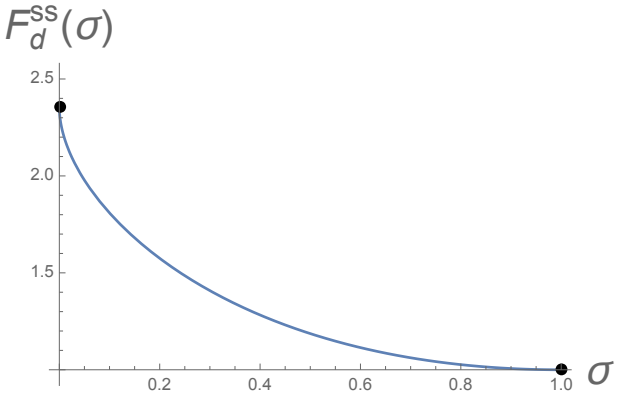

FIG. 10: (Color online) Quenched steady-state depletion enhancement factor $F_d^{ss}(\sigma)$ above the corresponding ground state value as a function of $\sigma = a_i/a_f$ following a quench from $a_i \to a_f$. The two dots correspond to the maximum enhancement $F_d^{ss}(0) = 3\pi/4$ (quenching a non-interacting gas or quenching to unitarity) and minimum enhancement $F_d^{ss}(1) = 1$ (no quench), respectively.

B. Bragg spectroscopy: structure function

A two-time structure function $S_{\mathbf{q}}(t,t') = \langle \delta\hat{n}(-\mathbf{q},t)\delta\hat{n}(\mathbf{q},t')\rangle$ is another central probe of the nonequilibrium dynamics of degenerate atomic gases. It can be measured via Bragg spectroscopy through a stimulated two-photon transitions [73], and via a correlation function of a measured density excitation, $\delta\hat{n}(\mathbf{q},t)$ at momentum $\mathbf{q}$ and time t [38]. The former thus allowed measurements of the excitation spectrum of a strongly interacting (^{85}Rb) BEC, near unitarity ($na_s^3 \gg 1$), demonstrating a large deviation from the Bogoliubov and Lee-Huang-Yang (LHY) prediction of Sec. (II A). The latter technique was used to characterize dynamics of a Feshbach-resonant Cesium gas, following a shallow quench in its scattering length [38].

With current experiments in mind, for simplicity we focus on the equal-time $t = t'$ structure function (nontrivial for nonequilibrium dynamics),

$$\begin{aligned} S_{\mathbf{q}}(t) &= \langle \delta\hat{n}(-\mathbf{q},t)\delta\hat{n}(\mathbf{q},t)\rangle, \\ &= \frac{1}{V}\int_{\mathbf{r},\mathbf{r}'} e^{i\mathbf{q}\cdot(\mathbf{r}-\mathbf{r}')}\langle\hat{\psi}^\dagger(\mathbf{r},t)\hat{\psi}(\mathbf{r},t)\hat{\psi}^\dagger(\mathbf{r}',t)\hat{\psi}(\mathbf{r}',t)\rangle_c, \\ &\approx S^0_{\mathbf{q}}(t) + \delta S^B_{\mathbf{q}}(t), \end{aligned} \tag{4.21}$$

where

$$\begin{aligned} S^0_{\mathbf{q}}(t) &= n_c\Big[\langle\hat{a}^\dagger_{\mathbf{q}}(t)\hat{a}_{\mathbf{q}}(t)\rangle + \langle\hat{a}_{-\mathbf{q}}(t)\hat{a}^\dagger_{-\mathbf{q}}(t)\rangle \\ &\quad + \langle\hat{a}_{-\mathbf{q}}(t)\hat{a}_{\mathbf{q}}(t)\rangle + \langle\hat{a}^\dagger_{\mathbf{q}}(t)\hat{a}^\dagger_{-\mathbf{q}}(t)\rangle\Big], \qquad (4.22a) \\ &= n_c\left[C^{11}_q(t) + C^{22}_q(t) + C^{21}_q(t) + C^{12}_q(t)\right], \qquad (4.22b) \end{aligned}$$

and

$$\begin{aligned} \delta S^B_{\mathbf{q}}(t) &= \frac{1}{V}\sum_{\mathbf{k}\neq 0}\Big[\langle\hat{a}^\dagger_{\mathbf{k}}(t)\hat{a}_{\mathbf{k}}(t)\rangle\langle\hat{a}_{\mathbf{k}-\mathbf{q}}(t)\hat{a}^\dagger_{\mathbf{k}-\mathbf{q}}(t)\rangle \\ &\quad + \langle\hat{a}^\dagger_{\mathbf{k}}(t)\hat{a}^\dagger_{-\mathbf{k}}(t)\rangle\langle\hat{a}_{\mathbf{k}-\mathbf{q}}(t)\hat{a}_{-\mathbf{k}+\mathbf{q}}(t)\rangle\Big], \\ &= \frac{1}{V}\sum_{\mathbf{k}\neq 0}\Big[C^{11}_k(t)C^{22}_{-k+q}(t) + C^{(12)}_k(t)C^{(21)}_{-k+q}(t)\Big], \end{aligned} \tag{4.23}$$

are, respectively the quadratic and quartic contribution to $S_{\mathbf{q}}(t)$, both computed within the Bogoliubov approximation.

Utilizing the Bogoliubov analysis of the nonequilibrium quenched dynamics from the previous subsection,

(Eqs.(4.9), (4.10b), (4.11), (4.12), (4.13)) the leading quadratic contribution to $S^B_{\mathbf{q}}(t)$ is given by [38]

$$S^0_{\mathbf{q}}(t) \;=\; S^0_q\left[1+\frac{E^2_{qi}-E^2_{qf}}{E^2_{qf}}\sin^2(E_{qf}t)\right], \quad (4.24)$$

where as a check, at initial time $S^0_{\mathbf{q}}(t=0)$ and/or for no-quench $g_i = g_f$ above expression reduces to the pre-quench $t = 0^-$ structure function,

$$S^0_q \;=\; n\frac{\epsilon_q}{E_{qi}}\coth\left(\frac{1}{2}\beta E_{qi}\right), \quad (4.25)$$

at temperature $T = 1/\beta$.

In dimensionless units $\hat{q} = q/\sqrt{2mng_f}$, $\hat{t} = ng_f t$ and $\hat{\beta} = ng_f\beta$, it is given by

$$S^0_{\hat{q}}(\hat{t}) = \frac{\hat{q}\coth(\hat{\beta}\hat{q}\sqrt{\hat{q}^2+2\sigma})}{\sqrt{\hat{q}^2+2\sigma}}\left[1-\frac{2(1-\sigma)}{\hat{q}^2+2}\sin^2\left(\hat{t}\hat{q}\sqrt{\hat{q}^2+2}\right)\right] \quad (4.26)$$

and plotted in Fig.(11).

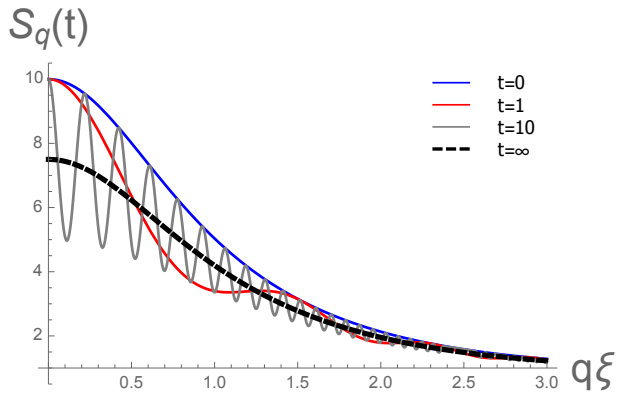

FIG. 11: (Color online) Time evolution of the structure function $S_{\mathbf{q}}(t)$ defined in the text following a scattering length quench from $0.5a_f \to a_f$, referring to Eq. (4.26) using Bogoliubov approximation. It illustrates, following the quench, that the initial ground state structure function (highest curve) develops oscillations and becomes lower, and after some pre-thermalization timescale approaches the steady-state distribution (lowest dashed black curve). Here momentum and time are rescaled by $\xi \equiv 1/\sqrt{2mng_f}$ and $t_0 \equiv 1/(ng_f)$, respectively. The temperature $T = 10ng_f$, for a typical ^{85}Rb experiment with $n = 5\times10^{12}cm^{-3}$, $a_f = 1100a_0$, corresponds to 16 nK.

Utilizing above Bogoliubov analysis, we have further shown that the higher-order correction, $\delta S^B_{\mathbf{q}}(t)$ in 3d at $T = 0$ is given by

$$\begin{aligned}\delta S^B_{\mathbf{q}}(0) \;&=\; \int_{\mathbf{k}}\left[u_{ki}v_{ki}u_{-\mathbf{k}+\mathbf{q},i}v_{-\mathbf{k}+\mathbf{q},i}+u^2_{ki}v^2_{-\mathbf{k}+\mathbf{q},i}\right],\\ &=\; \int_{\mathbf{k}}\left[\frac{g_i^2n^2+(\varepsilon_{ki}+E_{ki})(\varepsilon_{-\mathbf{k}+\mathbf{q},i}-E_{-\mathbf{k}+\mathbf{q},i})}{4E_{ki}E_{-\mathbf{k}+\mathbf{q},i}}\right],\\ &\approx\; \frac{g_i^2n^2}{2c_i^2}\int_{\mathbf{k}}\left[\frac{1}{k^2+\xi_i^2k^4}+O(q)\right],\\ &\propto\; n(na_i^3)^{1/2}\left[1+O(q)\right], \end{aligned} \quad (4.27)$$

and for weak interaction ($na_s^3 \ll 1$) it is subdominant to $S^0_{\mathbf{q}}(t)$. It can, however, become important at finite temperature, lower dimensions and strong interactions.

C. RF spectroscopy

Radio frequency (RF) spectroscopy is another important probe that has been fruitfully utilized to study spectroscopy and dynamics of resonant Fermi [6] and Bose [64] gases. Quite closely related to photoemission spectroscopy of solid state materials, the RF signal is the number of atoms $N_b(\omega_{RF})$, that undergoes a hyperfine transition from the many-body state of interest, E_a to a weakly interacting state $E_b = E_a + \omega_0$, in response to the stimulated RF pulse at frequency ω_{RF}.

For a weak RF pulse, the governing Hamiltonian

$$\begin{aligned}\hat{H} \;&=\; \hat{H}(\hat{a}_{\mathbf{k}},\hat{a}^\dagger_{\mathbf{k}})+\sum_{\mathbf{k}}(\epsilon_{\mathbf{k}}+\omega_0)\hat{b}^\dagger_{\mathbf{k}}\hat{b}_{\mathbf{k}}+\sum_{\mathbf{k}}I(t)\hat{b}^\dagger_{\mathbf{k}}\hat{a}_{\mathbf{k}}+h.c.,\\ &\equiv\; \hat{H}_0+\hat{H}_{RF}(t), \end{aligned} \quad (4.28)$$

is a sum of the interacting Hamiltonian for the system of $\hat{a}_{\mathbf{k}}$ bosons studied in previous subsections, the non-interacting vacuum Hamiltonian for the $\hat{b}_{\mathbf{k}}$ bosons, and the RF pulse coupling operator $\hat{H}_{RF}(t)$ that drives the transitions between the two hyperfine states, allowing a conversion of $\hat{a}_{\mathbf{k}}$ into $\hat{b}_{\mathbf{k}}$.

The RF spectroscopy signal $N_b(\omega)$ measures the number of $\hat{b}$ atoms transferred for an RF pulse at frequency ω. It can be evaluated via $N_b(\omega) = \int_0^\infty dt\langle\hat{J}(t)\rangle$, where $\hat{J}(t)$ is the $\hat{a}\to\hat{b}$ "current" operator

$$\begin{aligned}\hat{J}(t)\equiv\dot{\hat{N}}_b \;&=\; -i\sum_{\mathbf{k}}[\hat{b}^\dagger_{\mathbf{k}}\hat{b}_{\mathbf{k}},\hat{H}],\\ &=\; -i\sum_{\mathbf{k}}\left[I(t)\hat{b}^\dagger_{\mathbf{k}}\hat{a}_{\mathbf{k}}-I^*(t)\hat{a}^\dagger_{\mathbf{k}}\hat{b}_{\mathbf{k}}\right]. \end{aligned} \quad (4.29)$$

Appropriate for experiments, we focus on a weak RF pulse and calculate the response signal perturbatively

in $I(t)$, working in the interaction representation, with $\hat{J}_I(t) = e^{i\int_0^t dt'\hat{H}_0}\hat{J}e^{-i\int_0^t dt'\hat{H}_0}$,

$$\begin{aligned}\langle\hat{J}(t)\rangle &= -i\int_0^t dt'\langle\psi|\left[\hat{J}_I(t),\hat{H}^I_{RF}(t')\right]|\psi\rangle, \quad (4.30)\\ &= \int_0^t dt'\sum_{\mathbf{k}} I^*(t')I(t)\langle\alpha_0|\hat{a}^\dagger_{\mathbf{k}}(t')\hat{a}_{\mathbf{k}}(t)|\alpha_0\rangle \\ &\quad\times e^{i(\epsilon_k+\omega_0)(t-t')} + c.c.. \quad (4.31)\end{aligned}$$

Guided by the experimental protocol [56], above we have taken the initial $t = 0^-$ state $|\psi\rangle = |\alpha_0\rangle|0_b\rangle$ to be a product of a vacuum of $\hat{b}$ atoms, $|0_b\rangle$ and a SF condensate of $\hat{a}$ atoms, $|\alpha_0\rangle$, a vacuum of the Bogoliubov quasi-particles, $\hat{\alpha}_{\mathbf{k}}|\alpha_0\rangle = 0$ for the pre-quench interaction g_i. The analysis can be straightforwardly generalized to other initial conditions and finite temperature.

It is clear from (4.31) that the RF signal is not generically proportional to the momentum distribution function $n_k(t) = \langle\hat{a}^\dagger_{\mathbf{k}}(t)\hat{a}_{\mathbf{k}}(t)\rangle$. The latter requires a sufficiently narrow pulse so as to keep $t \approx t'$. Furthermore, a narrow excitation bandwidth is required. Under these conditions indeed we expect that at time t the number of atoms $\hat{b}_{\mathbf{k}}$ produced by the RF pulse is proportional to the number of atoms $\hat{a}_{\mathbf{k}}$ with momentum $\mathbf{k}$, such that the resonance condition $E_{kf} - \epsilon_k - \omega_0 = \omega_{RF}$ is satisfied.

Following the experiment [64], we take the RF pulse to be a real part of

$$I(t) = I_0 e^{-(t-t_0)^2/\tau^2}e^{-i\omega_{RF}t}, \quad (4.32)$$

with a carrier frequency ω_{RF} and a Gaussian envelope of width $\tau \gg 1/\omega_{RF}$, ensuring that the excitation is at a well-defined frequency. At the same time, in order to probe the evolving condensate dynamics at a specific time t, a short pulse that is narrow on the time scale of the ramp time (that can be made as short as a few microseconds) and on the characteristic many-body time scale (experimentally on the order of few hundred microseconds) that controls the condensate evolution, is required. In JILA experiment [64], the width τ ranges from $25\mu s$ to $200\mu s$ with $\omega_{RF} \approx 2\pi \times 50$kHz.

From the analysis of the previous section, the correlator inside Eq. (4.31) is given by

$$\begin{aligned}\langle\hat{a}^\dagger_k(t')\hat{a}_k(t)\rangle &= C^{11}_k(t',t), \quad (4.33)\\ &= u_k^2\sinh^2\Delta\theta_k e^{iE_{kf}(t'-t)} + v_k^2\cosh^2\Delta\theta_k e^{-iE_{kf}(t'-t)} \\ &\quad + u_k v_k\cosh\Delta\theta_k\sinh\Delta\theta_k(e^{iE_{kf}(t'+t)} + e^{-iE_{kf}(t'+t)}).\end{aligned}$$

Using it inside Eq. (4.31) and leaving the detailed analysis to Appendix D 3, in the limit of $t \gg t_0 \gg \tau \gg \omega^{-1}_{RF}$ we obtain

$$\begin{aligned}N_b(\omega_{RF}) &= 2\pi\tau^2 I_0^2\sum_{\mathbf{k}}\Big[e^{-\frac{1}{2}(\epsilon_k+\omega_0-\omega_{RF}-E_k)^2\tau^2}u_k^2\sinh^2\Delta\theta_k + e^{-\frac{1}{2}(\epsilon_k+\omega_0-\omega_{RF}+E_k)^2\tau^2}v_k^2\cosh^2\Delta\theta_k \\ &\quad + u_k v_k\sinh 2\Delta\theta_k e^{-\frac{1}{2}((\epsilon_k+\omega_0-\omega_{RF})^2+E_k^2)\tau^2}\cos 2Et_0\Big]. \quad (4.34)\end{aligned}$$

Although the general result is quite involved, it simplifies considerably in various important limits. For the case of broad pulse $\tau\omega_{RF} \gg 1$ with a well-defined frequency, the Gaussian factors reduce to energy-conserving δ-functions. In the simplest equilibrium case, where the ground state's n_k (= v_k^2 in the Bogoliubov approximation) is probed, $\Delta\theta_k = 0$, and we find

$$\begin{aligned}N_b^{gs}(\omega_{RF}) &= (2\pi)^{3/2}\tau I_0^2\sum_{\mathbf{k}}\delta(\omega_{RF}-\omega_0-\epsilon_k-E_k)n_k \\ \omega_{RF}\gg\omega_0 &= \frac{\tau I_0^2 V}{\sqrt{2\pi m}}\frac{C_{gs}}{|\omega_{RF}-\omega_0|^{3/2}}. \quad (4.35)\end{aligned}$$

In the last equality we focussed on the large frequency tail probed in the experiments [64] and C_{gs} is Tan's contact, that in the Bogoliubov approximation is given by $C^B_{gs} = 16\pi^2 n^2 a_s^2$.

For a measurement of the large frequency tail, $\omega_{RF} \gg \omega_0$ following a quench at $t = 0$, it is clear from Eq. (4.34) that only the second term contributes, giving

$$\begin{aligned}N_b(\omega_{RF}) &= (2\pi)^{3/2}\tau I_0^2\sum_{\mathbf{k}}\delta(\omega_{RF}-\omega_0-\epsilon_k-E_k) \\ &\quad\times n_k^f\cosh^2\Delta\theta_k \\ \omega_{RF}\gg\omega_0 &= \frac{\tau I_0^2 V}{\sqrt{2\pi m}}\frac{C_f}{|\omega_{RF}-\omega_0|^{3/2}}. \quad (4.36)\end{aligned}$$

where within Bogoliubov approximation

$$C_f = 16\pi^2 n^2 a_f^2. \quad (4.37)$$

This indicates that, while the overall momentum distribution function $n_k(t)$ exhibits nontrivial post-quench dynamics, the large tail of RF spectrum is *not* affected by the quench dynamics, and provides information about short-scale correlations in the ground state of the final state.

V. FINITE-RATE RAMP

Having studied the idealized case of a *sudden* $g_i \to g_f$ *quench*, we now analyze the dynamics following a more experimentally realistic *finite*-rate ramp. We model it by an idealized time-dependent coupling

$$g(t) = \begin{cases} g_i + (g_f - g_i)t/\tau, & \text{for } t < \tau, \\ g_f, & \text{for } t > \tau, \end{cases} \quad (5.1)$$

with ramp time τ, illustrated in Fig. 12.

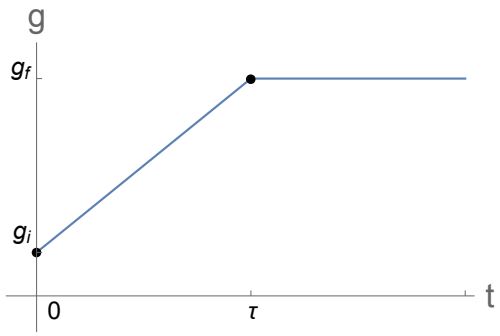

FIG. 12: (Color online) Protocol of a linear ramp of coupling strength g. Starting with $g = g_i$ at $t = 0$, the coupling strength is ramped to $g = g_f$ over ramp time τ.

To this end, we solve the corresponding Heisenberg equations of motion

$$i \begin{pmatrix} \dot{\hat{a}}_{\mathbf{k}} \\ -\dot{\hat{a}}^\dagger_{-\mathbf{k}} \end{pmatrix} = \begin{pmatrix} \epsilon_k + ng(t) & ng(t) \\ ng(t) & \epsilon_k(t) + ng(t) \end{pmatrix} \begin{pmatrix} \hat{a}_{\mathbf{k}}(t) \\ \hat{a}^\dagger_{-\mathbf{k}}(t) \end{pmatrix} \quad (5.2)$$

by expressing the atomic operators $\hat{a}_{\mathbf{k}}(t)$, $\hat{a}^\dagger_{\mathbf{k}}(t)$ in terms of the Bogoliubov quasi-particles $\hat{\alpha}_{\mathbf{k}}$, $\hat{\alpha}^\dagger_{\mathbf{k}}$ of $\hat{H}(t = 0)$ at the start of the ramp

$$\begin{pmatrix} \hat{a}_{\mathbf{k}} \\ \hat{a}^\dagger_{-\mathbf{k}} \end{pmatrix} = \begin{pmatrix} u_k(t) & v^*_k(t) \\ v_k(t) & u^*_k(t) \end{pmatrix} \begin{pmatrix} \hat{\alpha}_{\mathbf{k}} \\ \hat{\alpha}^\dagger_{-\mathbf{k}} \end{pmatrix} \equiv U_k(t) \begin{pmatrix} \hat{\alpha}_{\mathbf{k}} \\ \hat{\alpha}^\dagger_{-\mathbf{k}} \end{pmatrix}. \quad (5.3)$$

The dynamics is then encoded in the time evolution of a spinor $(u_k(t), v_k(t))$, with components satisfying

$$i\dot{u}_{\hat{k}} = (\hat{k}^2 + \hat{g}(t))u_{\hat{k}} + \hat{g}(t)v_{\hat{k}}, \quad (5.4a)$$
$$-i\dot{v}_{\hat{k}} = (\hat{k}^2 + \hat{g}(t))v_{\hat{k}} + \hat{g}(t)u_{\hat{k}}, \quad (5.4b)$$

where $\hat{g}(t) \equiv g(t)/g_f$, $\hat{t} \equiv ng_f t$ and $\hat{k}^2 \equiv k^2/(2mng_f)$. In term of above dimensionless variables, Eq. (5.1) becomes

$$\hat{g}(\hat{t}) = \begin{cases} \sigma + \gamma\hat{t}, & \text{for } t < \tau, \\ 1, & \text{for } t > \tau, \end{cases} \quad (5.5)$$

where we have defined a dimensionless ramp rate $\gamma \equiv (1-\sigma)/(ng_f\tau)$. We then solve these numerically, subject to the initial conditions

$$u_k(0) = \frac{1}{2^{1/2}} \left(\frac{\hat{k}^2 + \sigma}{\sqrt{\hat{k}^2(\hat{k}^2 + 2\sigma)}} + 1 \right)^{1/2}, \quad (5.6a)$$

$$v_k(0) = -\frac{1}{2^{1/2}} \left(\frac{\hat{k}^2 + \sigma}{\sqrt{\hat{k}^2(\hat{k}^2 + 2\sigma)}} - 1 \right)^{1/2}, \quad (5.6b)$$

that diagonalize the initial Hamiltonian at $t = 0$.

We focus on the momentum distribution at $T = 0$

$$n_k(t) = \langle 0^- | a^\dagger_k(t) a_k(t) | 0^- \rangle = |v_k(t)|^2, \quad (5.7)$$

and condensate fraction

$$n_c(t) = 1 - n_d(t) = 1 - V \int \frac{d^3k}{(2\pi)^3} n_k(t). \quad (5.8)$$

We apply this analysis to interpret experiments by Claussen, et al., [48], where dynamics of finite-rate ramp pulse was studied as a function of ramp time τ and heretofore remained unexplained.

In Fig. 13 we plot the time dependence of the resulting condensate fraction for two densities, following a constant-rate ramp, as illustrated in Fig. 12. Using the parameters reported in Ref. [48], we obtain results in qualitative agreement with these experimental measurement. More specifically, we find that even for a zero hold time, the condensate density drops by 10%-20%, consistent with the experimental observation in Ref. [48]. We attribute this condensate depletion to the finite ramp duration, τ.

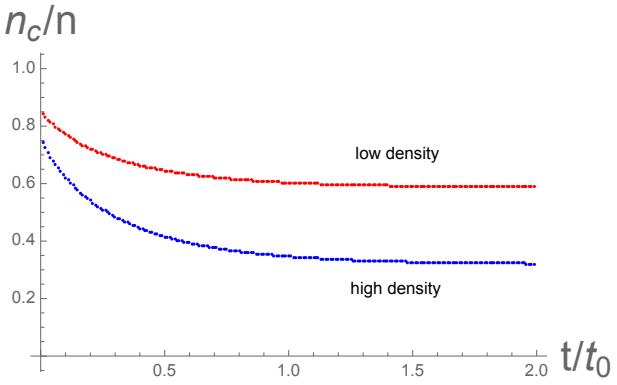

FIG. 13: (Color online) Dynamics of the condensate fraction $n_c(t)/n$ for high density $n = 1.9\times10^{13}cm^{-3}$ (lower blue curve) and low density $n = 0.7 \times 10^{13}cm^{-3}$ (upper red curve), after a linear interaction ramp $g(t)$ from $g_i = 0.001g_f$ to g_f with dimensionless ramp rate $\hat{\gamma} \equiv (1-\sigma)/(\tau ng_f) = 5$. Following the experiments of Ref.[48], above we used $a_f = 2700a_0$ for the final scattering length and find the pre-thermalization timescale $t_0 = 1/(ng_f) = 150\mu s$, that compares favorably to the experimental value of $t_{0exp} \approx 80\mu s$.

To explore the ramp rate dependence of the dynamics as studied by Claussen, et al., [48], in Fig. 14 we plot

the condensate fraction as a function of ramp time τ (inverse ramp rate, in units of $(1-\sigma)/(ng_f)$). As illustrated there, we find that the dependence on the ramp time τ is non-monotonic and is a function of the hold time t. This can be understood by noting that for a sudden quench (vanishing τ) at long hold times, the condensate is depleted more strongly than the ground state depletion for g_f. On the other hand, at short hold times the quenched depletion is given by the ground state for g_i. In contrast, for a slow adiabatic ramp (large τ) the condensate fraction asymptotes to the adiabatic limit corresponding to that of a ground state for g_f.

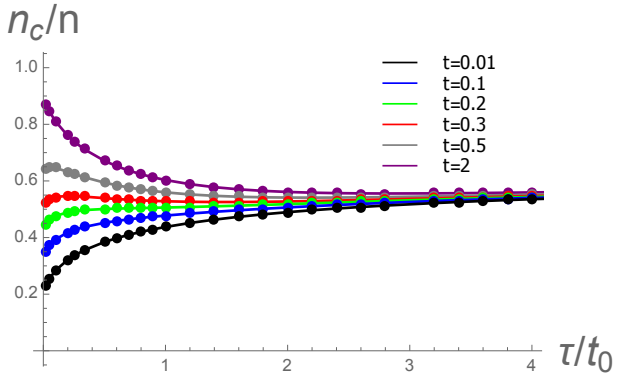

FIG. 14: (Color online) Dependence of condensate fraction n_c/n on the ramp duration τ for various hold time t in units of pre-thermalization timescale $t_0 = \hbar/(ng_f)$ (From lowest curve to highest one, the hold times are $\hat{t} = 0.01, 0.1, 0.2, 0.3, 0.5, 2$, respectively). Following the experiments in Ref. [48] we take the final scattering length to be $a_f = 2700a_0$ with $a_i = 0.001a_f$ and $n = 1.9 * 10^{12} cm^{-3}$.

Thus, for short hold time the condensate fraction *decreases* from $n_c^{g_i}$ to $n_c^{g_f}$ with increasing τ. For long hold times, the condensate fraction *increases* from pre-thermalized value n_c^{ss} to $n_c^{g_f}$ with increasing τ. This behavior is qualitatively quite similar to that found in experiments of Ref. [48].

VI. DYNAMICS FOR DEEP QUENCH

In the present and subsequent sections we study the non-perturbative dynamics following a deep quench, $na_f^3 \gg 1$, a regime of JILA recent experiment [56] that is our main focus [39]. In contrast to the well-controlled, perturbative dynamics of a shallow quench discussed in Sec. IV, for deep quenches the condensate depletion dynamics is significant and cannot be neglected.

From the outset, we acknowledge that no rigorous solution in such a non-perturbative regime is available even for a purely repulsive Bose gas ground state. Nevertheless, to make progress we treat this strongly interacting nonequilibrium dynamics utilizing a non-perturbative but uncontrolled self-consistent Bogoliubov treatment. This is analogous to a BCS dynamic mean-field theory [30, 44], with the condensate fraction $n_c(t)$ playing the role of the time-dependent order parameter. We thus reduce the problem to a solution of the Bogoliubov dynamics with a time-dependent condensate fraction that is self-consistently determined. This is a dynamical generalization of our analysis of the strongly interacting Bose gas ground state in Sec. III.

Another challenge of this system is the resonant nature of the Bose gas interaction. To handle this we employ a second beyond-Bogoliubov approximation by replacing the scattering length a_f by the density dependent scattering amplitude $|f(k_n, a_f)| = a_f/\sqrt{1+k_n^2 a_f^2} \equiv \tilde{a}_f$, and the Hartree interaction energy $g_f n$ by $\tilde{g}_f n \equiv \frac{8\pi\epsilon_F}{\sqrt{1/(k_n a_f)^2+1}}$. This qualitatively captures the crossover from the two-atom regime, $a_f \ll n^{-1/3}$ to a finite density limit, when a_f reaches inter-particle spacing and the scattering amplitude saturates at $\sim k_n^{-1}$. While the detailed nature of this crossover is ad hoc, our qualitative predictions are insensitive to these details and only depend on the limiting values of the two regimes.

Motivated by the experiments [56], we focus on an initial state that is a well-established condensate. This allows us to make progress in treating the resonant interactions by expanding in finite-momentum quasi-particle fluctuations about a macroscopically occupied $\mathbf{k} = 0$ state. Following a sudden quench, $g_i \to g_f$, we approximate the Hamiltonian by a quadratic time-dependent form,

$$\begin{aligned}\hat{H}_f(t) &= \frac{1}{2}\sum_{\mathbf{k}\neq 0}\left(\hat{a}_{\mathbf{k}}^\dagger \;\; \hat{a}_{-\mathbf{k}}\right)\begin{pmatrix}\epsilon_k + g_f n_c(t) & g_f n_c(t)\\ g_f n_c(t) & \epsilon_k + g_f n_c(t)\end{pmatrix}\begin{pmatrix}\hat{a}_{\mathbf{k}}\\ \hat{a}_{-\mathbf{k}}^\dagger\end{pmatrix}\\ &\equiv \frac{1}{2}\sum_{\mathbf{k}\neq 0}\hat{\Phi}_{\mathbf{k}}^\dagger(t)\cdot\hat{h}_{kf}(t)\cdot\hat{\Phi}_{\mathbf{k}}(t). \qquad (6.1)\end{aligned}$$

The key new ingredient (in contrast to Bogoliubov theory of Sec. II A) is the nontrivial time-dependent condensate density, that is self-consistently determined by the total atom conservation,

$$n_c(t) = n - \frac{1}{V}\sum_{\mathbf{k}\neq 0}\langle 0^-|\hat{a}_{\mathbf{k}}^\dagger(t)\hat{a}_{\mathbf{k}}(t)|0^-\rangle, \qquad (6.2)$$

evaluated in the pre-quench state $|0^-\rangle$ at $t = 0^-$. In a homogeneous case, this is equivalent to a solution of the Gross-Petaevskii equation for the condensate order parameter Ψ_0, coupled to the Heisenberg equation of motion for the finite momentum quasi-particles. Focussing on zero temperature, we take the initial state $|0^-\rangle$ to be the vacuum with respect to the quasi-particles $\hat{\alpha}_{\mathbf{k}}$, that diagonalize the initial Hamiltonian, $\hat{H}_i = \sum_{\mathbf{k}} E_{ki}\hat{\alpha}_{\mathbf{k}}^\dagger\hat{\alpha}_{\mathbf{k}}$, characterized by a pre-quench $t = 0^-$ scattering length, a_i.

The corresponding Heisenberg equation of motion

$$i\sigma_z\partial_t\hat{\Phi}_{\mathbf{k}}(t) = \hat{h}_{kf}(t)\cdot\hat{\Phi}_{\mathbf{k}}(t) \qquad (6.3)$$

for $\hat{\Phi}_{\mathbf{k}}(t) = (\hat{a}_{\mathbf{k}}(t), \hat{a}^{\dagger}_{-\mathbf{k}}(t))$ is conveniently encoded in terms of a time-dependent Bogoliubov transformation $U_{kf}(t)$,

$$\hat{\Phi}_{\mathbf{k}}(t) = U_{\mathbf{k}f}(t)\hat{\Psi}_{\mathbf{k}}, \tag{6.4}$$

where

$$U_{kf}(t) \;=\; \begin{pmatrix} u_{kf}(t) & v^{*}_{kf}(t) \\ v_{kf}(t) & u^{*}_{kf}(t) \end{pmatrix} \tag{6.5}$$

and $\hat{\Psi}_{\mathbf{k}} = (\hat{\beta}_{\mathbf{k}}, \hat{\beta}^{\dagger}_{-\mathbf{k}})$ are time-independent bosonic reference operators, that diagonalize the Hamiltonian at the initial time $t = 0^{+}$ after the quench, with $\hat{H}_f(0^{+}) = \sum_{\mathbf{k}} E_{kf}(0^{+})\hat{\beta}^{\dagger}_{\mathbf{k}}\hat{\beta}_{\mathbf{k}}$.

Equivalently, $U^{\dagger}_{kf}(0^{+})h_{kf}(0^{+})U_{kf}(0^{+}) = E_{kf}(0^{+}) = \sqrt{\epsilon_k^2 + 2g_f n_c(0^{+})\epsilon_k}$, fixing the initial condition

$$u_{kf}(0^{+}) \;=\; \sqrt{\frac{1}{2}\left(\frac{\epsilon_k + g_f n_c(0^{+})}{E_f(0^{+})} + 1\right)}, \tag{6.6a}$$

$$v_{kf}(0^{+}) \;=\; -\sqrt{\frac{1}{2}\left(\frac{\epsilon_k + g_f n_c(0^{+})}{E_f(0^{+})} - 1\right)}, \tag{6.6b}$$

for spinor $\psi_{kf}(t) \equiv (u_{kf}(t), v_{kf}(t))$, that evolves according to

$$i\sigma_z \partial_t \psi_{kf}(t) = \hat{h}_{kf}(t) \cdot \psi_{kf}(t). \tag{6.7}$$

As for the Bogoliubov analysis in Sec. II A, because the initial state $|0^{-}\rangle$ is a vacuum of $\hat{\alpha}_k$, it is convenient to further express $\hat{\Phi}_{\mathbf{k}}(t) = (\hat{a}_{\mathbf{k}}(t), \hat{a}^{\dagger}_{-\mathbf{k}}(t))$ in terms of the pre-quench quasi-particle basis $\hat{\Psi}_{\mathbf{k}}(0^{-}) = (\hat{\alpha}_{\mathbf{k}}, \hat{\alpha}^{\dagger}_{\mathbf{k}})$,

$$\hat{\Phi}_{\mathbf{k}}(t) \;=\; U_{kf}(t)U^{-1}_{kf}(0^{+})U_{ki}(0^{-})\hat{\Psi}_{\mathbf{k}}(0^{-}), \tag{6.8a}$$

$$\;\equiv\; U_k(t)\hat{\Psi}_{\mathbf{k}}(0^{-}). \tag{6.8b}$$

The post-quench dynamics is thus fully determined by the self-consistent solutions $\psi_{kf}(t)$ of Eq. (6.7), together with the atom number conservation constraint, (6.2). This can be obtained numerically in essentially exact way, as we will demonstrate in Sec. VI B.

A. Quasi-adiabatic self-consistent approximation

Despite availability of the numerical solution, to gain further physical insight it is of interest to obtain an approximate analytical solution. To this end we note that for a given slowly evolving condensate density satisfying $\dot{n}_c(t)/n \ll E^3_{kf}/(\hbar n g \epsilon_k) = (\epsilon_k)^{1/2}(\epsilon_k + 2gn_c)^{3/2}/(\hbar n g)$ (see Eq. (B8) and [39, 75]), Eq. (6.7) can be well-approximated by an instantaneous, quasi-adiabatic Bogoliubov transformation of $\hat{H}_f(t)$ (see Appendix B),

$$U_{kf}(t) = \begin{pmatrix} u_k(t)e^{-i\int_0^t E_{kf}(t')} & v_k(t)e^{i\int_0^t E_{kf}(t')} \\ v_k(t)e^{-i\int_0^t E_{kf}(t')} & u_k(t)e^{i\int_0^t E_{kf}(t')} \end{pmatrix}. \tag{6.9}$$

In above, $(u_k(t), v_k(t))$ is the instantaneous eigenstate of the single-particle Hamiltonian $\hat{h}_{kf}(t)$, with time dependence entering only through the time dependent condensate density, $n_c(t)$. Such approximation is in the spirit of the WKB quasi-local treatment of a smoothly varying potential [74].

More specifically the solution is given by

$$\begin{aligned} u_k(t) &= \sqrt{\frac{1}{2}\left(\frac{\epsilon_k + g_f n_c(t)}{E_{kf}(t)} + 1\right)}, \\ v_k(t) &= -\sqrt{\frac{1}{2}\left(\frac{\epsilon_k + g_f n_c(t)}{E_{kf}(t)} - 1\right)}, \\ E_{kf}(t) &= \sqrt{\epsilon_k(\epsilon_k + 2g_f n_c(t))}, \end{aligned} \tag{6.10}$$

with initial condition given by (6.6a)(6.6b).

After a tedious but conceptually straightforward calculation that utilizes above relations, we obtain the momentum distribution function

$$\begin{aligned} n_k(t) &= \langle 0^{-}|\hat{a}^{\dagger}_{\mathbf{k}}(t)\hat{a}_{\mathbf{k}}(t)|0^{-}\rangle \\ &= \frac{\epsilon_k^2 + \epsilon_k(g_i n + g_f n + g_f n_c(t)) + 2g_f g_i n_c(t) n + 2g_f n_c(t) n(g_f - g_i)\sin^2(\int_0^t \sqrt{\epsilon_k(\epsilon_k + 2g_f n_c(t'))}dt')}{2\sqrt{\epsilon_k(\epsilon_k + 2g_f n_c(t))}\sqrt{(\epsilon_k + 2g_i n)}\sqrt{(\epsilon_k + 2g_f n)}} - \frac{1}{2}, \end{aligned} \tag{6.11}$$

with the condensate density $n_c(t)$ self-consistently determined according to $n_c(t) = n - \sum_{\boldsymbol{k}\neq 0} n_k(t)$.

By construction, the above expression for $n_k(t = 0)$ reduces to the pre-quench momentum distribution function

$$n_k(t=0) = \frac{1}{2}\left[\frac{\epsilon_k + g_i n_c(0)}{E_{ki}} - 1\right] = n_{ki}, \tag{6.12}$$

as required by continuity. Furthermore for $g_f = g_i$, i.e.,

in the absence of a quench, the time-dependent part of n_k drops out and again reduces to n_{ki}.

Using (6.11) the self-consistency condition reduces to a dimensionless form

$$1 - \hat{n}_c = n_d^0 F_d(\hat{n}_c, \sigma), \tag{6.13}$$

where $n_d^0 = 8/(3\sqrt{\pi})(na_f^3)^{1/2}$ is the depletion corresponding to the ground state of quenched Hamiltonian, $q \equiv \sqrt{k^2/(2mng_f)}$ and $\hat{n}_c(t) \equiv n_c(t)/n$ are dimensionless variables, and

$$F(\hat{n}_c, \sigma, t) = 3\sqrt{2}\int dq q^2 \left[\frac{(q^4 + q^2(\sigma + 1 + \hat{n}_c) + 2\sigma\hat{n}_c + 2\hat{n}_c(1-\sigma)\sin^2(\int_0^t ngt\sqrt{q^2(q^2+2\hat{n}_c)}))}{2\sqrt{q^2(q^2+2\hat{n}_c)}\sqrt{(q^2+2\sigma)}\sqrt{(q^2+2)}} - \frac{1}{2}\right], \tag{6.14}$$

is the quench-induced depletion-enhancement factor.

We solve Eqs.(6.13),(6.14) numerically and plot the depletion fraction $\hat{n}_d(t) = 1 - \hat{n}_c(t)$ as a function of time in Fig. 15.

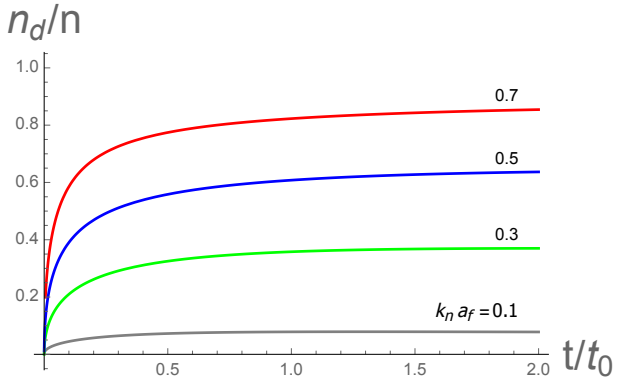

FIG. 15: (Color online) Time evolution of the condensate depletion fraction $n_d(t)/n$ (treated within a quasi-adiabatic self-consistent dynamic field analysis, referring to Eq. (6.13)), following a scattering length quench from $k_n a_i = 0.01$ to various $k_n a_f$ in a resonant Bose gas. Here we normalize the time with the pre-thermalization timescale $t_0 = 1/ng_f = m/(4\pi a_f n)$ associated with $k_n a_f = 1$ (where $k_n \equiv n^{1/3}$).

We observe that the depletion fraction increases smoothly with time on the scale $t_0 = m/(4\pi a_f n)$, reaching a stationary steady-state n_d^{ss}, that is an increasing function of the quench depth $k_n a_f$. Even for a deep quench to a unitary point, the self-consistent treatment ensures that the depletion, always remains below the total atom density. The slow time dependence of $n_d(t)$ justifies the quasi-static approximation for the high momenta ($k \gtrsim 1/\xi$) quasi-particles, but fails for the low-momenta ($k \lesssim 1/\xi$) Goldstone modes. We further note that the asymptotic depletion n_d^{ss} always significantly exceeds the depletion for the ground state corresponding to the quenched scattering length a_f. Thus not surprisingly the thermal equilibrium is never reached in our effectively integrable harmonic model.

Having computed the condensate depletion and the associated condensate density, $n_c(t)$, Eq. (6.11) immediately gives us the momentum distribution function $n_k(t)$, that we illustrate in Fig. 16. Following a quench, the

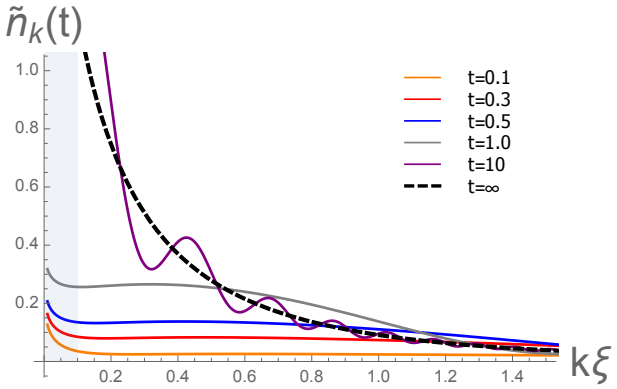

FIG. 16: (Color online) Time evolution of the (column-density) momentum distribution function, $\tilde{n}_{\hat{k}}(\hat{t}) \equiv \int d\hat{k}_z n_{\hat{k}}(\hat{t})$ following a scattering length quench $k_n a_i = 0.01 \to k_n a_f = 0.5$ (where $k_n \equiv n^{1/3}$) in a resonant Bose gas, computed with quasi-adiabatic self-consistent approximation. Here we measure time in units of the pre-thermalization timescale $t_0 = 1/ng_f = m/(4\pi a_f n)$ and momentum in units of inverse coherence length $\xi^{-1} \equiv \sqrt{2mng_f}$. For experimentally relevant atom density, $n = 5.5{*}10^{12} cm^{-3}$, the pre-thermalization timescale $t_0 = 73\mu s$ thus obtained compares favorably with $100\mu s$ observed experimentally [56]. The grey region indicates a range of momenta not resolved in JILA experiments, due to initial inhomogeneous real space density profile and finite trap size.

initially narrow (for $g_i \ll g_f$) momentum distribution function (corresponding to pre-quench BEC state) displays rich dynamics. Within 2-body interaction scale it quickly develops a large momentum tail corresponding to the strong atom-atom interaction g_f. With time, the suddenly turned on interaction promotes an increasing number of atom pairs from the condensate to finite momentum excitations. The momentum distribution tail fills in from high to low momenta as pair-excitation dynamics at momentum k dephases with frequency $2E_{kf}$. Thus, at time t, $n_k(t)$ establishes a pre-thermalized power-

law steady-state for momenta $k > k_{pth}(t)$, latter set by $E_{k_{pth},f}t \approx 1$. Equivalently, it takes time

$$t_{pth} \approx \frac{1}{E_{k_{pth},f}}, \tag{6.15a}$$

$$\sim \begin{cases} 1/k^2, & \text{for } k \gg 1/\xi, \\ 1/k, & \text{for } k \ll 1/\xi, \end{cases} \tag{6.15b}$$

for the pre-thermalization to reach a stationary state down to momentum k, a distinctive feature that is consistent with JILA experiments [56].

As illustrated in Fig. 17, in the long time limit (around 170μ-sec in ^{85}Rb experiments [56]) a quenched Bose gas approaches a pre-thermalized stationary state, as reflected by a time-independent power-law momentum distribution

$$n_k(t) = \frac{\hat{k}^4 + \hat{k}^2(\sigma + 1 + \hat{n}_c^{ss}) + \hat{n}_c^{ss}(1+\sigma)}{2\sqrt{\hat{k}^2(\hat{k}^2 + 2\hat{n}_c^{ss})}\sqrt{(\hat{k}^2 + 2\sigma)}\sqrt{(\hat{k}^2+2)}} - \frac{1}{2},$$
$$\sim C^{ss}/k^4, \qquad \text{for } k\xi \gg 1, \tag{6.16}$$

where $C^{ss} = (4\pi a_f n)^2 \left[n_c^{ss}/n + (1-\sigma)^2\right]$ is the nonequilibrium analog of Tan's contact [39, 76]. Within the above self-consistent Bogoliubov approximation the quasi-particles do not scatter, precluding full thermalization. The resulting final state remains nonequilibrium, completely determined by the depth-quench parameter σ, characterized by a diagonal density matrix ensemble.

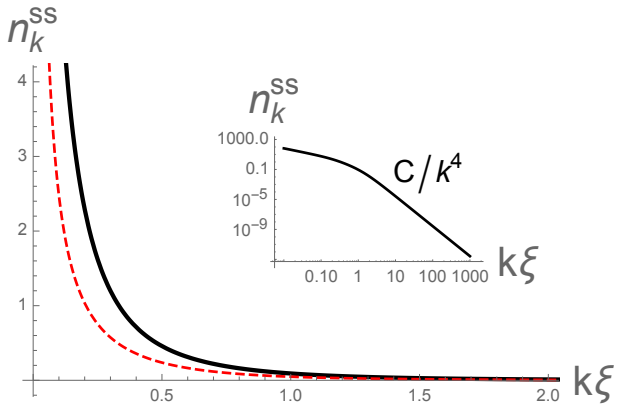

FIG. 17: (Color online) A long-time nonequilibrium steady-state momentum distribution function n_k^{ss} of a resonant Bose gas following a scattering length quench $k_n a_i = 0.01 \to k_n a_f = 0.5$ (solid black curve), as compared to ground state momentum distribution at $k_n a_f$ (red dashed curve). The inset illustrates the emergence of a $1/k^4$ large momentum tail, corresponding to a steady-state "contact".

With the above solution of the self-consistent post-quench dynamics, we can now also calculate other physical observables, such as, for example the structure function measured in Bragg spectroscopy. Using above analysis for $S_{\mathbf{q}}(t)$ in Eq. (4.21) we find

$$S_{\hat{q}}(t) = \coth(\hat{\beta}\hat{q}\sqrt{\hat{q}^2+2\sigma})\frac{\hat{q}}{\sqrt{\hat{q}^2+2\sigma}}$$
$$\times \left(\frac{\sqrt{\hat{q}^2+2}}{\sqrt{\hat{q}^2+2\hat{n}_c(t)}} - \frac{2(1-\sigma)\sin^2(\hat{q}t\sqrt{\hat{q}^2+2\hat{n}_c(t)})}{\sqrt{\hat{q}^2+2}\sqrt{\hat{q}^2+2\hat{n}_c(t)}}\right), \tag{6.17}$$

where $\hat{q} = q/\sqrt{2mng_f}$, $\hat{t} = ng_f t$ and $\hat{\beta} = ng_f\beta$.

The results are then illustrated in Fig. 5 and 18. The role of self-consistency is clear: in Fig. 5, as compared with Fig. 11, self-consistency exchanges the relative position of initial and final asymptotic steady-state curve; while in Fig. 18 it shifts the phase as well as modifies the frequency of the structure function oscillation. We expect these features to be experimentally testable by going to a deep quench regimes, $k_n a_f \gg 1$.

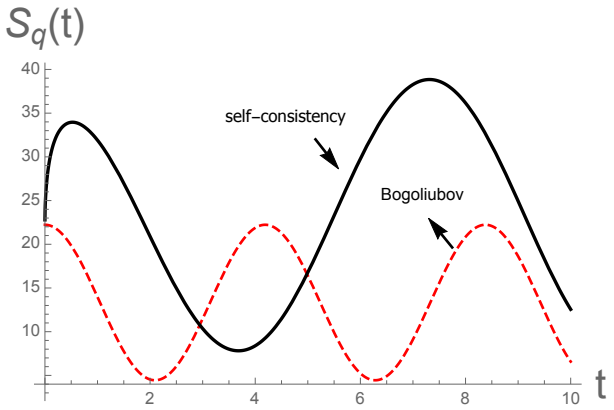

FIG. 18: (Color online) Oscillation of structure function $S_{\mathbf{q}}(t)$ (treated within a quasi-adiabatic self-consistent dynamic field analysis, thick black curve, referring to Eq. (6.17)) as a function of time, following a scattering length quench from $0.1a_f \to a_f$ with $k_n a_f = 0.7$ (where $k_n \equiv n^{1/3}$) at momentum $k\xi = 0.5$, as compared to Bogoliubov approximation (dashed red curve).

We emphasize that above analysis utilizes a quasi-adiabatic approximation, valid for $\dot{n}_c(t)/n \ll E_{kf}^3/(\hbar n g \epsilon_k)$. As mentioned above we expect it to break down for sufficiently small momenta for slow Goldstone modes as well as large $k_n a_f$ value, where $\dot{n}_c(t)/n$ is large.

B. Exact numerical solution to post quench dynamics

In this subsection we test the validity of above quasi-adiabatic approximation by analyzing the post-quench dynamics through an essentially exact numerical solution of the Heisenberg equation of motion (6.7). Consistent

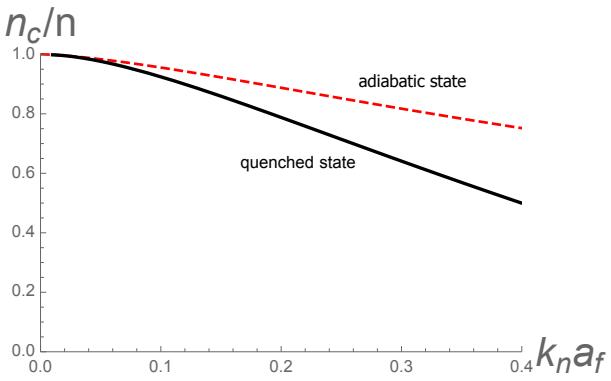

FIG. 19: (Color online) Quenched steady state condensate fraction n_c/n as a function of $k_n a_f$ (solid black curve, treated with quasi-adiabatic self-consistent dynamic field, referring to Eq.(6.13)), as compared with the ground state condensate fraction at $k_n a_f$ (dashed red curve), both calculated with self-consistency on n_c.

with our expectations we find that while the former provides an accurate description for a shallow quench and high momenta, it fails quantitatively (though not qualitatively) for $k_n a_f \gg 1$ and low momenta, $k \ll 1/\xi$.

As derived in previous subsection, the dynamics is governed by Eq. (6.7) for $\psi_{\mathbf{k}}(t) = (u_{kf}(t), v_{kf}(t))$, that relate atomic excitations, $\hat{a}_{\mathbf{k}}$ to Bogoliubov quasi-particles $\hat{\beta}_{\mathbf{k}}$. Here we solve Eq. (6.7) numerically together with the number conservation condition on the condensate fraction. In dimensionless form, the equations of motion are given by

$$\begin{aligned} i\dot{u}_k &= (\hat{k}^2 + \bar{n}(t))u_k + \bar{n}(t)v_k, \\ -i\dot{v}_k &= (\hat{k}^2 + \bar{n}(t))v_k + \bar{n}(t)u_k, \end{aligned} \tag{6.18}$$

with the initial conditions fixed by a requirement that at $t = 0$, $\psi(0^+)$ diagonalizes $\hat{H}_f(0^+)$,

$$\begin{aligned} u_k(t=0) &= \sqrt{\frac{1}{2}[E_{kf}^{-1}(\epsilon_k + n_c(0)g_f) + 1]}, \\ &= \sqrt{\frac{1}{2}\left(\frac{\hat{k}^2+1}{\sqrt{\hat{k}^2(\hat{k}^2+2)}} + 1\right)}, \end{aligned} \tag{6.19a}$$

$$\begin{aligned} v_k(t=0) &= -\sqrt{\frac{1}{2}[E_{kf}^{-1}(\epsilon_k + n_c(0)g_f) - 1]}, \\ &= -\sqrt{\frac{1}{2}\left(\frac{\hat{k}^2+1}{\sqrt{\hat{k}^2(\hat{k}^2+2)}} - 1\right)}, \end{aligned} \tag{6.19b}$$

where $\hat{t} \equiv n g_f t$, $\hat{k}^2 \equiv k^2/(2mng_f)$ and $\bar{n}(t) \equiv n_c(t)/n$.

Decoupling the $u_k(t)$ and $v_k(t)$ components

$$\begin{aligned} \ddot{u} &= [-k^2(k^2 + 2\bar{n}(t)) + i\frac{\dot{\bar{n}}(t)}{\bar{n}(t)}(k^2)]u + \frac{\dot{\bar{n}}(t)}{\bar{n}(t)}\dot{u}, \\ \ddot{v} &= [-k^2(k^2 + 2\bar{n}(t)) - i\frac{\dot{\bar{n}}(t)}{\bar{n}(t)}(k^2)]v + \frac{\dot{\bar{n}}(t)}{\bar{n}(t)}\dot{v}, \end{aligned} \tag{6.20}$$

more clearly reveals the relation of these exact equations to the quasi-adiabatic approximation of previous subsection. Indeed the latter is obtained by neglecting $\dot{\bar{n}}(t)/\bar{n}(t)$ relative to the instantaneous Bogoliubov dispersion $E_{kf}(t)$, clearly only possible for sufficiently large momenta.

To fully account for the self-consistent dynamics of $n_c(t)$, here we solve iteratively the full set of equations (6.20) (or equivalently Eqs.(6.18), (6.19a)(6.19b)) and (6.22). With this solution in hand we can compute an arbitrary physical quantity.

Focussing on experimentally accessible momentum distribution, we compute

$$\begin{aligned} n_k(t) &= \langle 0^- | \hat{a}_{\mathbf{k}}^\dagger(t)\hat{a}_{\mathbf{k}}(t) | 0^- \rangle \\ &= |(u_k(t)\sinh\Delta\theta_k - v_k^*(t)\cosh\Delta\theta_k)|^2, \end{aligned} \tag{6.21}$$

together with the atom number self-consistency condition

$$\begin{aligned} \bar{n}(t) = 1 - \frac{8}{\sqrt{\pi}}(2na_f^3)^{1/2}\int d\hat{k}\hat{k}^2 |(u_k(t)\sinh\Delta\theta_k \\ - v_k^*(t)\cosh\Delta\theta_k)|^2. \end{aligned} \tag{6.22}$$

We illustrate the results in Figs. 1,3, from which we observe that the numerically computed $n_k(t)$ and $n_d(t)$ quite closely qualitatively resemble the approximate quasi-adiabatic counterparts. Yet, they differ quantitatively, particularly in the case of deep quench and for small momenta. The asymptotic time-averaged value of $n_d(t)$ always considerably exceeds the corresponding ground state depletion and thus the pre-thermalized system remains out of equilibrium.

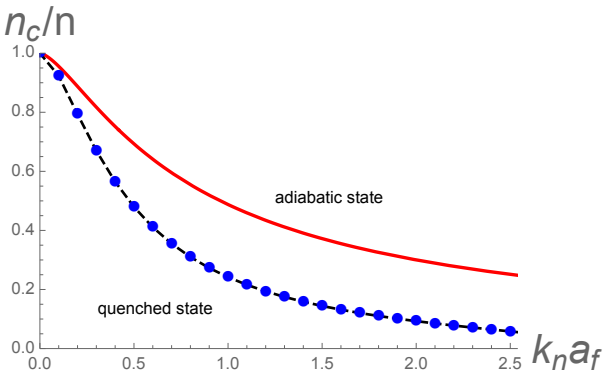

FIG. 20: (Color online) Quenched steady-state condensate fraction (dash-dotted blue curve) as a function of $k_n a_f$, following a quench from $k_n a_i = 0.01 \to k_n a_f$ (where $k_n \equiv n^{1/3}$), as compared to the ground state condensate fraction at $k_n a_f$ (solid red curve, same as in Fig. 2), both calculated within self-consistent dynamic field approximation.

In Fig. 21 we compare the numerical solution with corresponding quantities obtained via various approximate approaches of previous sections. We find that for $k_n a_f \ll 1$, both the quasi-adiabatic self-consistent solution and numerical self-consistent solution, reduce to

that of a straight Bogoliubov approximation, but deviate with increasing depth of the quench, $k_n a_f$. We observe that in contrast to the adiabatic approximation, the full numerical solution predicts that the condensate fraction remains finite for arbitrary large $k_n a_f$, arguing that our earlier conjecture of a nonequilibrium phase transition to a "normal" state is likely incorrect [39].

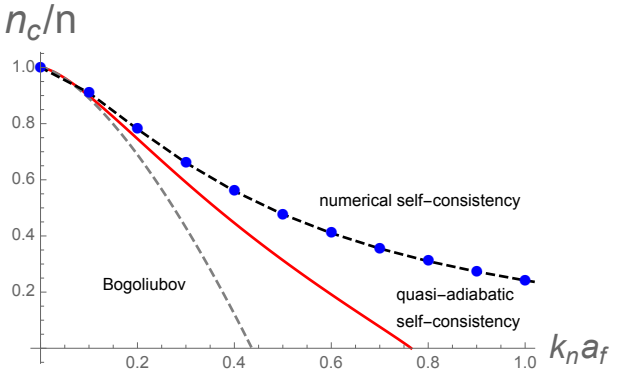

FIG. 21: (Color online) Comparison of results from three different approaches to computation of the post-quench steady state condensate fraction n_c/n: numerical self-consistency (dash-dotted blue), quasi-adiabatic self-consistency (solid red) and Bogoliubov (dashed grey).

C. Generalized Gibbs Ensemble

In the analysis above we found that following a scattering length quench a nonequilibrium state, characterized by a stationary momentum distribution function of atoms emerges in the long time limit. It is thus natural to explore whether this state can be captured by a Generalized Gibbs Ensemble (GGE) [25, 27].

At the simplest level of harmonic Bogoliubov description, the final stationary state is completely determined by the initial post-quench momentum distribution function of the quasi-particles $\hat{\beta}_k$. The latter is in turn specified by the initial, a_i and final a_f scattering lengths, i.e., by the initial ground state $|0^-\rangle$ (vacuum of $\hat{\alpha}_k$) and the post-quench Hamiltonian $\hat{H}(0^+)$, through the relation (4.5) derived in Sec. IV.

Since at this harmonic level the energy eigenvalues E_{kf} for each momentum are separately conserved, the distribution of $\hat{\beta}_{\mathbf{k}}$ occupations can clearly be captured with GGE

$$\hat{\rho}_{GGE} = Z_{GGE}^{-1} e^{-\sum_{\mathbf{k}} \lambda_k E_{kf} \hat{\beta}^\dagger_{\mathbf{k}} \hat{\beta}_{\mathbf{k}}}, \tag{6.23}$$

where $Z_{GGE} = Tr\left[e^{-\sum_{\mathbf{k}} \lambda_{\mathbf{k}} E_{kf} \hat{\beta}^\dagger_{\mathbf{k}} \hat{\beta}_{\mathbf{k}}}\right]$ and λ_k are the Lagrange multipliers (inverse of effective temperatures) for each conserved mode $\mathbf{k}$. These are fixed by requiring

$$n_k^\beta \equiv \langle 0^-|\hat{\beta}^\dagger_{\mathbf{k}} \hat{\beta}_{\mathbf{k}}|0^-\rangle = \langle \hat{\beta}^\dagger_{\mathbf{k}} \hat{\beta}_{\mathbf{k}}\rangle_{GGE} \equiv Tr(\hat{\beta}^\dagger_{\mathbf{k}} \hat{\beta}_{\mathbf{k}} \hat{\rho}_{GGE}). \tag{6.24}$$

The analysis from Sec. IV gives the left hand side

$$n_k^\beta = \frac{1}{4}\left(\frac{E_{kf}}{E_{ki}} + \frac{E_{ki}}{E_{kf}}\right) - \frac{1}{2}, \tag{6.25}$$

determing

$$\lambda_k = \frac{1}{E_{kf}} \ln\left(\frac{n_k^\beta + 1}{n_k^\beta}\right). \tag{6.26}$$

We now want to see if the long-time atomic momentum distribution function $n_k(t \to \infty)$ can be characterized by the GGE.

1. *shallow quench*

For a shallow quench, captured by purely harmonic Bogoliubov approximation we have

$$\begin{aligned} n_k(t) &= \langle 0^-|\hat{a}^\dagger_{\mathbf{k}}(t)\hat{a}_{\mathbf{k}}(t)|0^-\rangle, \\ &= v_k^2 + (u_k^2 + v_k^2)\langle \hat{\beta}^\dagger_{\mathbf{k}}(t)\hat{\beta}_{\mathbf{k}}(t)\rangle \\ &\quad - u_k v_k \langle \hat{\beta}_{\mathbf{k}}(t)\hat{\beta}_{-\mathbf{k}}(t) + \hat{\beta}^\dagger_{\mathbf{k}}(t)\hat{\beta}^\dagger_{-\mathbf{k}}(t)\rangle. \end{aligned} \tag{6.27}$$

In the long time limit, the time-dependence of the off-diagonal last terms dephases away, and only first two terms survive. The steady-state momentum distribution n_k^{ss} then becomes

$$n_k^{ss} = v_k^2 + (u_k^2 + v_k^2)\langle \hat{\beta}^\dagger_{\mathbf{k}} \hat{\beta}_{\mathbf{k}}\rangle \tag{6.28}$$

Since $\langle \hat{\beta}^\dagger_{\mathbf{k}} \hat{\beta}_{\mathbf{k}}\rangle = \langle \hat{\beta}^\dagger_{\mathbf{k}} \hat{\beta}_{\mathbf{k}}\rangle_{GGE}$, it is clear that in this purely harmonic approximation the GGE does describe the steady-state distribution.

2. *deep quench*

As we demonstrated in previous subsections, for a deep quench, a self-consistency of condensate density must be implemented. This results to an effective time dependent Hamiltonian. In the simplest quasi-adiabatic approximation, we find

$$\begin{aligned} n_k(t) &= v_k^2(t) + (u_k^2(t) + v_k^2(t))\langle \hat{\beta}^\dagger_{\mathbf{k}} \hat{\beta}_{\mathbf{k}}\rangle \\ &\quad - u_k(t) v_k(t) \langle \hat{\beta}_{\mathbf{k}}(t)\hat{\beta}_{-\mathbf{k}}(t) + \hat{\beta}^\dagger_{\mathbf{k}}(t)\hat{\beta}^\dagger_{-\mathbf{k}}(t)\rangle. \end{aligned} \tag{6.29}$$

This leads to a steady-state distribution

$$n_k^{ss} = (v_k^{ss})^2 + ((u_k^{ss})^2 + (v_k^{ss})^2)\langle \hat{\beta}^\dagger_{\mathbf{k}} \hat{\beta}_{\mathbf{k}}\rangle, \tag{6.30}$$

where

$$u_k^{ss} = \sqrt{\frac{1}{2}\left(\frac{\epsilon_k + n_c^{ss} g_f}{E_{kf}} + 1\right)}, \tag{6.31a}$$

$$v_k^{ss} = -\sqrt{\frac{1}{2}\left(\frac{\epsilon_k + n_c^{ss} g_f}{E_{kf}} - 1\right)}, \tag{6.31b}$$

$$E_{kf} = \sqrt{{\epsilon_k}^2 + 2 n_c^{ss} g_f \epsilon_k}, \tag{6.31c}$$

and n_c^{ss} the steady-state condensate density determined by the self-consistency condition. The latter spoils the conventional GGE description of the long-time distribution even in this approximation, consistent with Ref. [36] for a O(N) model.

VII. EXCITATION ENERGY

We now turn to a study of the excitation energy E_{exc} following a quench, defined by

$$E_{exc} = \langle 0^-|\hat{H}^f|0^-\rangle - \langle 0_f|\hat{H}^f|0_f\rangle, \tag{7.1}$$

as the difference between the expectation value of the post-quench Hamiltonian in the initial state and the ground state energy of the same Hamiltonian. For a closed system and unitary energy conserving dynamics, this quantity is an important measure of the long time nonequilibrium stationary state, and in particular the resulting temperature for the equilibrated state.

Below, we first study E_{exc} within perturbative Bogoliubov approximation valid for a shallow sudden quench and a dilute gas characterized by $na_s^3 \ll 1$. Within this approximation the ground state energy with repulsive interactions (i.e., here for a resonant problem ignoring the bound molecular state [54, 60]) is given by the LHY result

$$E_{gs} = \langle 0_f|\hat{H}^f|0_f\rangle = \frac{2\pi n a_f}{m}\left[1 + \frac{128}{15\sqrt{\pi}}(na_f^3)^{1/2}\right]. \tag{7.2}$$

Our focus is then on the calculation of $\langle 0^-|\hat{H}^f|0^-\rangle$.

We will then generalize this analysis to arbitrary strength interactions, relating the excitation energy to Tan's contact [76]. We then conclude by studying the excitation energy for a finite-rate ramp.

A. Sudden quench

1. Bogoliubov approximation

Within a sudden quench Bogoliubov approximation a straightforward analytical treatment is possible. To this end, leaving details to Appendix C, we expand the Hamiltonian about the condensed state,

$$\hat{H}_f \approx \frac{g_f}{2V}N^2 + \frac{1}{2}\sum_{\mathbf{k}\neq 0}\left[(\epsilon_k + g_f n)\hat{a}_{\mathbf{k}}^\dagger\hat{a}_{\mathbf{k}} + g_f n\hat{a}_{-\mathbf{k}}\hat{a}_{\mathbf{k}} + h.c.\right], \tag{7.3}$$

that to quadratic order can be diagonalized as analyzed in Sec. II A, giving

$$\hat{H}_f = \frac{1}{2}g_f n^2 V - \sum_{\mathbf{k}\neq 0}\left[\epsilon_k + g_f n_c(0^+) - E_{kf}(0^+)\right] + \sum_{\mathbf{k}\neq 0}E_{kf}(0^+)\hat{\beta}_{\mathbf{k}}^\dagger\hat{\beta}_{\mathbf{k}}. \tag{7.4}$$

The first two constant terms give the LHY ground-state energy (with UV cutoffs in the second term cancelled by the cutoff dependent terms coming from g_f in the first term after it is expressed in terms of scattering length, a_f as detailed in Appendix C.). They clearly cancel in the subtraction in Eq. (7.1), giving excitation energy density $\mathcal{E}_{exc} \equiv E_{exc}/V$

$$\mathcal{E}_{exc} = \frac{1}{V}\sum_{\mathbf{k}\neq 0}E_{kf}(0^+)\left[\langle 0^-|\hat{\beta}_{\mathbf{k}}^\dagger\hat{\beta}_{\mathbf{k}}|0^-\rangle - \langle 0_f|\hat{\beta}_{\mathbf{k}}^\dagger\hat{\beta}_{\mathbf{k}}|0_f\rangle\right]. \tag{7.5}$$

The last term vanishes at $T = 0$, since by definition $|0_f\rangle$ is a vacuum of $\hat{\beta}_{\mathbf{k}}$. Given that $|0^-\rangle$ is a vacuum of the Bogoliubov quasi-particles $\hat{\alpha}_{\mathbf{k}}$ associated with the pre-quench Hamiltonian, $\hat{H}_i$, it is convenient to express $\hat{\beta}_{\mathbf{k}}$ in terms of $\hat{\alpha}_{\mathbf{k}}$, using the relations (4.5), (4.6) worked out in Sec. IV. Evaluating the expectation value

$$\langle 0^-|\hat{\beta}_{\mathbf{k}}^\dagger\hat{\beta}_{\mathbf{k}}|0^-\rangle = \sinh^2\Delta\theta, \tag{7.6}$$

$$= \frac{1}{2}\left[\frac{\epsilon_k + (g_f + g_i)n}{\sqrt{(\epsilon_k + 2g_i n)(\epsilon_k + 2g_f n)}} - 1\right],$$

gives

$$\mathcal{E}_{exc} = \frac{1}{2}\int\frac{d^3k}{(2\pi)^3}\sqrt{\epsilon_k^2 + 2g_f n\epsilon_k} \times\left[\frac{\epsilon_k + (g_f + g_i)n}{\sqrt{(\epsilon_k + 2g_i n)(\epsilon_k + 2g_f n)}} - 1\right]. \tag{7.7}$$

Simple analysis shows that $\mathcal{E}_{exc}$ exhibits a (UV divergent) contribution

$$\mathcal{E}_{exc}^\Lambda = \frac{1}{2}\int^\Lambda\frac{d^3k}{(2\pi)^3}\frac{(g_f - g_i)^2 n^2}{2\epsilon_k}, = \frac{mn^2}{4\pi^2}(g_f - g_i)^2\Lambda. \tag{7.8}$$

set by the microscopic range $r_0 \sim 1/\Lambda$ of the two-body potential. This remains the case even when the couplings $g_{i,f}$ are eliminated in favor of the physical scattering lengths $a_{i,f}$, using

$$g = \frac{\tilde{g}}{1 - \frac{m}{2\pi^2}\tilde{g}\Lambda} = \frac{4\pi}{m}\frac{a_s}{1 - \frac{2}{\pi}a_s\Lambda}, \tag{7.9a}$$

$$\approx \frac{4\pi}{m}a_s(1 + \frac{2}{\pi}a_s\Lambda), \tag{7.9b}$$

and to first order of $a_s\Lambda$ (assuming $a_s\Lambda \ll 1$)

$$\mathcal{E}_{exc}^\Lambda = 4(1-\sigma)^2\frac{n^2 a_f}{m}a_f\Lambda. \tag{7.10}$$

The remaining finite part of $\mathcal{E}_{exc}$ is then given by $\tilde{\mathcal{E}}_{exc} = \mathcal{E}_{exc} - \mathcal{E}_{exc}^\Lambda$,

$$\tilde{\mathcal{E}}_{exc} = -\frac{128\pi^{1/2} a_f n^2}{15m} (n a_f^3)^{1/2} \left[\sigma^{3/2}(3\sigma - 5) + 2\right]. \tag{7.11}$$

It is negative for all $\sigma = g_i/g_f$ and leads to

$$\mathcal{E}_{exc} = 4(1-\sigma)^2 \frac{n^2 a_f}{m} a_f \Lambda - \frac{128\pi^{1/2}}{15} \frac{n^2 a_f}{m} (n a_f^3)^{1/2} \left[\sigma^{3/2}(3\sigma - 5) + 2\right], \tag{7.12}$$

This expression vanishes as $(\sigma-1)^2$ in no quench $\sigma = 1$ limit. Although a negative finite correction $\tilde{\mathcal{E}}_{exc}$ is disconcerting, the total excitation energy density $\mathcal{E}_{exc}$ is indeed positive in the dilute regime $(n a_f^3)^{1/2} \ll 1 \ll a_f \Lambda$, required for the validity of the Bogoliubov approximation.

The potential-range (UV cutoff) dependence of $\mathcal{E}_{exc}$ may at first sight appear surprising (even when expressed in terms of the physical scattering lengths, that renders all equilibrium properties finite). However, as we will see below, this result arises from an unphysical feature of the model protocol, namely an infinitely fast quench. We reexamine this UV dependence below by studying a more physical model with a finite-rate ramp.

2. *beyond Bogoliubov approximation and relation to Tan's contact*

Below we present a more general analysis of the excitation energy, without relying on the expansion about the condensed state, by relating it to other physical quantities like the ground state energy and Tan's contact [76].

We begin with the basic model Hamiltonian of resonant bosons

$$\begin{aligned} \hat{H}_f &= \sum_{\mathbf{k}\neq 0} \epsilon_k \hat{a}^\dagger_{\mathbf{k}} \hat{a}_{\mathbf{k}} + \frac{g_f}{2V} \sum_{\mathbf{k}_1,\mathbf{k}_2,\mathbf{q}} \hat{a}^\dagger_{-\mathbf{k}_1+\mathbf{q}/2} \hat{a}^\dagger_{\mathbf{k}_1+\mathbf{q}/2} \hat{a}_{-\mathbf{k}_2+\mathbf{q}/2} \hat{a}_{\mathbf{k}_2+\mathbf{q}/2}, \\ &= \hat{H}_i + \frac{g_f - g_i}{2V} \sum_{\mathbf{k}_1,\mathbf{k}_2,\mathbf{q}} \hat{a}^\dagger_{-\mathbf{k}_1+\mathbf{q}/2} \hat{a}^\dagger_{\mathbf{k}_1+\mathbf{q}/2} \hat{a}_{-\mathbf{k}_2+\mathbf{q}/2} \hat{a}_{\mathbf{k}_2+\mathbf{q}/2}, \end{aligned} \tag{7.13}$$

where the bare interaction coupling g is expressible in terms of the renormalized coupling $\tilde{g}^{-1} = g^{-1} + m\Lambda/(2\pi^2)$, related to the scattering length $a_s(g)$,

$$\tilde{g} = \frac{4\pi a_s}{m} = \frac{g}{1 + m\Lambda g/(2\pi^2)}. \tag{7.14}$$

With the initial (pre-quench) state $|0^-\rangle \equiv |0_i\rangle$ the vacuum of the pre-quench Hamiltonian, $\hat{H}_i$, the excitation energy density is then given by

$$\begin{aligned} E_{exc} &= \langle 0_i|\hat{H}_i|0_i\rangle - \langle 0_f|\hat{H}_f|0_f\rangle + \frac{g_f - g_i}{2V} \sum_{\mathbf{k}_1,\mathbf{k}_2,\mathbf{q}} \langle 0_i|\hat{a}^\dagger_{-\mathbf{k}_1+\mathbf{q}/2} \hat{a}^\dagger_{\mathbf{k}_1+\mathbf{q}/2} \hat{a}_{-\mathbf{k}_2+\mathbf{q}/2} \hat{a}_{\mathbf{k}_2+\mathbf{q}/2}|0_i\rangle, \\ &= E^i_{gs} - E^f_{gs} + \frac{g_f - g_i}{2V} \sum_{\mathbf{k}_1,\mathbf{k}_2,\mathbf{q}} \langle 0_i|\hat{a}^\dagger_{-\mathbf{k}_1+\mathbf{q}/2} \hat{a}^\dagger_{\mathbf{k}_1+\mathbf{q}/2} \hat{a}_{-\mathbf{k}_2+\mathbf{q}/2} \hat{a}_{\mathbf{k}_2+\mathbf{q}/2}|0_i\rangle. \end{aligned} \tag{7.15}$$

For a dilute weakly interacting gas, $n a_s^3 \ll 1$, we can evaluate the first two (ground state energy) terms within Bogoliubov approximation for the initial and final Hamiltonians, using the LHY result, Eq. (2.14) for g_i, g_f. The last term can be related to Tan's contact.

To this end, we first note that the expectation value of the quartic interaction is related to Tan's contact [76, 78],

$$C = (mg)^2 \langle \hat{\psi}^\dagger \hat{\psi} \hat{\psi}^\dagger \hat{\psi} \rangle, \tag{7.16}$$

that in Bogoliubov approximation is given by

$$C \approx (4\pi n a_s)^2 \left(1 + \frac{64}{3}(n a_s^3/\pi)^{1/2}\right), \tag{7.17}$$

and is UV cutoff $\Lambda = 1/r_0$ independent. The ground state energy density is also expressible in terms of the contact

$$\mathcal{E}_{gs} = \frac{1}{V}\sum_{\mathbf{k}} \epsilon_k \left(n_k - \frac{C}{k^4}\right) + \frac{C}{8\pi m a_s}, \quad (7.18a)$$

$$\approx \frac{2\pi n^2 a_s}{m}\left(1 + \frac{128}{15}(n a_s^3/\pi)^{1/2}\right), \quad (7.18b)$$

with the last equality computed within the Bogoliubov limit.

Using Eq. (7.15) and (7.16), the excitation energy density is thus given by:

$$\mathcal{E}_{exc} = \mathcal{E}^i_{gs} - \mathcal{E}^f_{gs} + \frac{1}{2}(g_f - g_i)\langle 0_i|\hat{\psi}^\dagger\hat{\psi}\hat{\psi}^\dagger\hat{\psi}|0_i\rangle,$$
$$= \mathcal{E}^i_{gs} - \mathcal{E}^f_{gs} + \frac{(g_f - g_i)}{2m^2 g_i^2} C_i. \quad (7.19)$$

Recalling from scattering analysis, that the microscopic UV cutoff-dependent interaction g is given by

$$g = \frac{4\pi a}{m}\left(1 - \frac{2}{\pi} a_s/r_0\right)^{-1}, \quad (7.20)$$

allows us to express $\mathcal{E}_{exc}$ in terms of the more physical scattering lengths

$$\mathcal{E}_{exc} = \mathcal{E}^i_{gs} - \mathcal{E}^f_{gs} + \frac{C_i}{8\pi m a_i^2}(a_f - a_i)\frac{1 - \frac{2}{\pi}a_i/r_0}{1 - \frac{2}{\pi}a_f/r_0}. \quad (7.21)$$

As is clear from $a_s(g)$ in (7.14) plotted in Fig. 6, the scattering length falls into two distinct ranges $0 < |a_s| < \frac{1}{2}\pi r_0$ and $|a_s| > \frac{1}{2}\pi r_0$, where from (7.14) the latter is only accessible for attractive interactions, $g < 0$. Analyzing above expression in the first range and within the Bogoliubov approximation (using (7.17),(7.18b)), to lowest order we recover the UV cutoff dependent result (7.10) of the previous subsection,

$$\mathcal{E}_{exc} \approx \frac{2\pi n^2}{m}(a_i - a_f)\left[1 - \frac{1 - \frac{2}{\pi}a_i/r_0}{1 - \frac{2}{\pi}a_f/r_0}\right], \quad (7.22)$$

$$\approx \frac{4n^2}{m}(a_i - a_f)^2/r_0 \quad (7.23)$$

In the complementary more physically interesting regime $|a_s| > \frac{1}{2}\pi r_0$, we instead have

$$\mathcal{E}_{exc} = \mathcal{E}^i_{gs} - \mathcal{E}^f_{gs} + \frac{C_i}{8\pi m}(a_i^{-1} - a_f^{-1}), \quad (7.24)$$

that in the Bogoliubov limit $n a_s^3 \ll 1$ (i.e., $r_0 \ll |a_s| \ll n^{-1/3}$) reduces to

$$\mathcal{E}_{exc} \approx \frac{4\pi n^2 a_i}{m}\left[1 - \frac{1}{2}\left(\frac{a_f}{a_i} + \frac{a_i}{a_f}\right)\right]. \quad (7.25)$$

For weak (no bound state) attractive interactions $a_i < 0$ this expression is positive and as required vanishes for the case of no-quench, $\sigma = a_f/a_i = 1$.

For a strong resonant interactions, beyond Bogoliubov regime, excitation energy reduces to

$$\mathcal{E}_{exc} = \frac{1}{V}\sum_{\mathbf{k}} \epsilon_k \left(\delta n^i_k - \delta n^f_k\right) + \frac{1}{4\pi m}\left[\frac{C_i}{a_i} - \frac{1}{2}\frac{C_i + C_f}{a_f}\right], \quad (7.26)$$

where $\delta n_k \equiv n_k - C/k^4$ is the momentum distribution with large momentum tail subtracted off.

We observe, that for $a_s > 0$ the excitation energy appears to be negative. However, in this regime, $a_s > \frac{1}{2}\pi r_0$, for $a_s > 0$ the interaction g is necessarily attractive (see (7.14) showing that for $g > 0$, a_s is limited below $\frac{1}{2}\pi r_0$) and exhibits a molecular bound state that lies below atomic BEC continuum. Thus the initial purely atomic condensate state with $a_s > 0$ is therefore not a ground state (the molecular bound state is) and thus there is no a priori reason to expect for the change in energy to be positive under a quench. We thus conjecture that the negative excitation energy $\varepsilon_{exc} < 0$ is a reflection of such resonant interaction.

Finally, as we will show next, the UV cutoff dependent excitation energy, (7.23) is a reflection of the unphysical infinitely fast quench, a divergence that in a more physical situation of a finite-rate ramp is cut off by the ramp rate.

B. Finite-rate ramp

In this subsection we analyze the excitation energy following a finite-rate ramp of the coupling strength, for simplicity focussing on a linear ramp, defined by Eq. (5.1), (5.5) in Sec. V, characterized by a dimensionless rate γ and related ramp time $\tau \equiv (1 - \sigma)/(n g_f \gamma)$. Below we will show that above short-scale divergence for a sudden quench is regularized by a finite ramp rate γ.

1. *scaling analysis*

To this end we first conjecture that for a finite-rate ramp (nonzero ramp time) the dominant singular part of excitation energy is generalized to

$$\mathcal{E}^\Lambda_{exc}(\gamma) = \frac{4(\sigma - 1)^2 n^2 a_f}{m} a_f \Lambda f(E_\Lambda \tau), \quad (7.27)$$
$$= \frac{4(\sigma - 1)^2 n^2 a_f}{m} a_f \Lambda f\left(E_\Lambda (1 - \sigma)/(n g_f \gamma)\right),$$

where $E_\Lambda = \Lambda^2/2m \approx 1/(2m r_0^2)$ is the UV cutoff energy scale (corresponding to range of the potential $r_0 \sim \Lambda^{-1}$), that sets the ramp rate scale.

We can deduce the asymptotic form of the scaling function $f(x)$ from the knowledge of the behavior of $\mathcal{E}^\Lambda_{exc}(\gamma)$ in sudden quench and adiabatic limits. In the former case of $\gamma \to \infty$, cleary $f(x) = 1$ so that (7.10) is recovered. In the latter case of $\gamma \to 0$, we expect the system to track

the ground state and thus $\mathcal{E}^{\Lambda}_{exc}(\tau\to\infty)\to 0$, and require for the UV cutoff Λ to drop out.

The latter condition thus requires that $f(x\to\infty) = \kappa/\sqrt{x}$ (κ is a dimensionless constant), so that

$$\mathcal{E}^{\Lambda}_{exc}(\gamma) \underset{\gamma\to 0}{=} \kappa\frac{8\sqrt{2\pi}n^2a_f}{m}(na_f^3)^{1/2}(1-\sigma)^{3/2}\sqrt{\gamma}, \quad (7.28a)$$

$$\equiv \frac{1}{4}\kappa\mathcal{E}_0(1-\sigma)^{3/2}\sqrt{\gamma}, \quad (7.28b)$$

scaling as the square-root of the ramp rate, with $\mathcal{E}_0 \equiv 32\sqrt{2\pi}\frac{n^2a_f}{m}(na_f^3)^{1/2}$. This is consistent with the general predictions [77], with the specific exponent of 1/2 appearing here.

Before turning to a more microscopic analysis, we note that an estimate of experimental ramp rate is $\gamma\approx 10^{-10}$ eV and of UV energy cutoff $E_\Lambda\approx 10^{-7}$ eV [56]. Thus, in JILA experiments $E_\Lambda/\gamma\gg 1$, with the finite ramp rate expecting to cutoff the dependence on the microscopic cutoff Λ, and the excitation energy scaling proportional to $\mathcal{E}_{exc}\sim\sqrt{\gamma}$.

2. *microscopic and numerical analysis*

As a complementary approach, we can use a microscopic model of a finite-rate ramp protocol, Sec. V, together with a numerical analysis to compute the resulting excitation energy.

Leaving the detailed calculations to Appendix C we find that the energy right after the finite-rate ramp is given by

$$\mathcal{E}_{total} = 2\pi\frac{n^2a_f}{m} + 32\sqrt{2\pi}\frac{n^2a_f}{m}(na_f^3)^{1/2}\int dkk^2\left[(k^2+1)|v_k(\tau)|^2 - \frac{1}{2}(u_k(\tau)v_k^*(\tau)+v_k(\tau)u_k^*(\tau)) + \frac{1}{4k^2}\right], \quad (7.29)$$

where $u_k(t), v_k(t)$ are solutions of Eqs.(5.4a)(5.4b) (see Eq. (C9)). Subtracting the LHY ground state energy density $\mathcal{E}_{gs}$ (7.2), the excitation energy density is then given by

$$\mathcal{E}_{exc} = \mathcal{E}_{total} - \mathcal{E}_{gs} = \mathcal{E}_0 f(\sigma,\Lambda,\gamma), \quad (7.30)$$

where

$$f(\sigma,\Lambda,\gamma) = \int dkk^2\Big[(k^2+1)|v_k(\tau)|^2 - \frac{1}{2}\left(u_k(\tau)v_k^*(\tau)+v_k(\tau)u_k^*(\tau)\right) + \frac{1}{4k^2}\Big] - \frac{4\sqrt{2}}{15} \quad (7.31)$$

is a dimensionless function that can be evaluated using numerical solutions for $u_k(\tau)$ and $v_k(\tau)$.

Displaying the results in Fig. 22, we observe that for a small ramp rate γ, the cutoff dependence drops out of the excitation energy, as curves with different cutoffs Λ collapse. In the opposite limit of $\gamma\to\infty$, the excitation energy recovers the linear cutoff-depedence displayed for the sudden quench case, in Eq. (7.10).

We also verify the square-root $\sqrt{\gamma}$ prediction of the scaling theory for slow ramp rate, (7.28b), in Fig. 4, a "zoom-in" of Fig. 22 around small γ. Fitting our numerical solution to a power-law scaling form predicted by Eq. (7.28b), we find the exponent to be 0.53, in good agreement with 1/2 emerging from our general scaling analysis. We suspect that this small discrepancy is a combination of slight numerical errors and weak crossover from slow to fast ramp; the exact exponent of 1/2 should emerge only in the strictly asymptotic limit of slow ramp.The σ (quench depth) dependence in Eq. (7.28b) is also confirmed by inspecting Fig. 23.

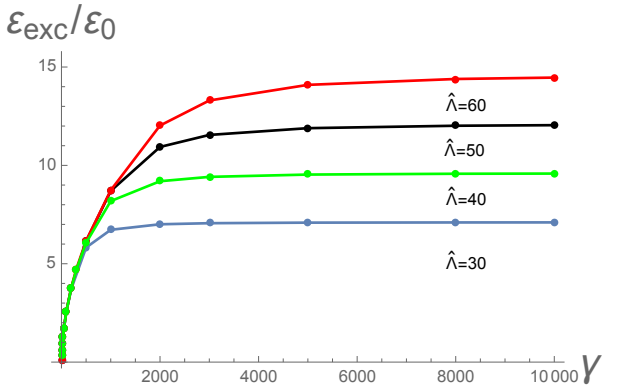

FIG. 22: (Color online) Excitation energy (scaled by LHY correction to the ground state energy) following a scattering length ramp $0.5a_f\to a_f$ as a function of ramp rate γ for different scaled momentum cutoff $\hat{\Lambda}=\Lambda\xi$ (here $\xi\equiv 1/\sqrt{2mng_f}$ is the coherence length). For large ramp rate γ (fast ramp), the excitation energy $\mathcal{E}_{exc}$ (defined in the text) grows linearly with the UV cutoff Λ, while for small rate (slow ramp) the cutoff dependence drops out and is replaced by a square-root of the ramp rate γ.

With this we conclude our analysis of the excitation energy and turn to the study of the dynamic analog of Tan's contact [76].

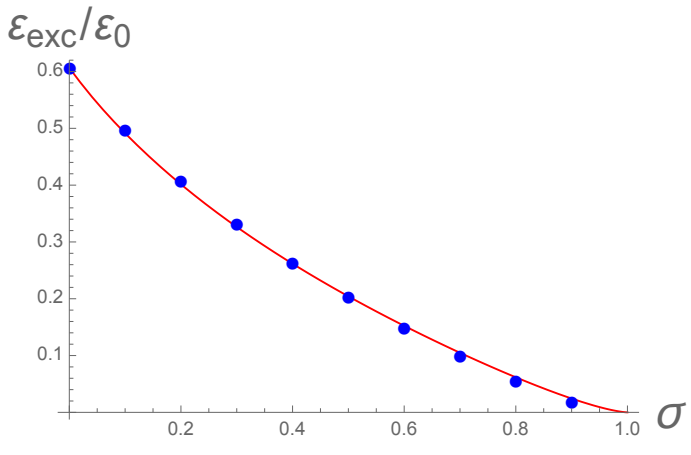

FIG. 23: (Color online) Excitation energy (scaled by LHY correction to the ground state energy) following a scattering length ramp from $a_i \to a_f$ as a function of quench depth $\sigma = a_i/a_f$. The blue data points are obtained for each chosen σ at dimensionless ramp $\hat{\gamma} \equiv (1-\sigma)/(\tau n g_f) = 10$ and scaled momentum cutoff $\hat{\Lambda} = \Lambda\xi = 60$; the red curve represents fitting function $y = 0.58(1-x)^{3/2}$.

VIII. CONTACT

A. Ground state contact

Contact, C is a remarkable physical parameter introduced by Tan [76], that enters in a large variety of physical observables. Most notably, it appears as a coefficient of the universal large momentum tail of the ground-state momentum distribution function

$$C = \lim_{k\to\infty} k^4 n_k \tag{8.1}$$

and as a response of the ground-state energy density $\mathcal{E}_{gs} \equiv E_{gs}/V$ to the tuning of the scattering length, the so-called adiabatic theorem,

$$\begin{aligned} C &= -8\pi m \frac{d\mathcal{E}_{gs}}{da_s^{-1}}, && \text{(8.2a)} \\ &= (mg)^2 \langle \hat{\psi}^\dagger \hat{\psi}^\dagger \hat{\psi}\hat{\psi}\rangle, && \text{(8.2b)} \end{aligned}$$

with the second relation to the interaction energy (already noted in the previous section) obtained via the Hellmann-Feynman theorem [74]. As we show in Appendix D 1, above can be straightforwardly evaluated in the ground state within the dilute Bogoliubov approximation [79]. Though contact is quite different for fermions and bosons, in equilibrium, these relations are expected to hold independent of statistics.

The contact was first successfully measured in the ground state of stable fermionic gases, with relations experimentally verified [63]. More recently, the contact was studied in a resonant bosonic gas via Bragg spectroscopy, utilizing the adiabatic theorem, (8.2a)) [64] and more directly from the large frequency $1/\omega^{3/2}$ tail (frequency analog of $1/k^4$ momentum tail, (8.1); see (4.35)) of the RF spectroscopy signal [64]. However, because a resonant Bose gas is fundamentally unstable and evaporates through the three-body decay, these measurements are intrinsically nonequilibrium, requiring a dynamical analysis of the contact.

B. Dynamical contact

We thus examine the contact and its associated relations for a resonant Bose gas dynamics following a quench. Immediately after the quench the states remain unchanged $|0^-\rangle = |0^+\rangle$ and only the coupling changes, $g_i \to g_f$. Thus, the relation between two forms of C defined in (8.2a) and (8.2b) remains valid,

$$\begin{aligned} C_{dE}(0^+) &= -8\pi m \frac{d\mathcal{E}_f}{da_f^{-1}} \\ &= (mg_f)^2 \langle 0^+|\hat{\psi}^\dagger\hat{\psi}^\dagger\hat{\psi}\hat{\psi}|0^+\rangle \\ &= \left(\frac{g_f}{g_i}\right)^2 C_E(0^-), \end{aligned} \tag{8.3}$$

despite the fact that $|0^+\rangle$ is not an eigenstate of $\hat{H}(0^+) \equiv \hat{H}_f$ and thus Hellmann-Feynman theorem no longer applies.

However, the contact C_{dE} is then clearly not continuous across the quench, and using (7.14),(7.20) acquires a UV cutoff dependence $\Lambda = 1/r_0$, that drops out only in the $a_{i,f} \gg r_0$ limit

$$\begin{aligned} C_{dE}(0^+) &= \left(\frac{g_f}{g_i}\right)^2 C_E(0^-), && \text{(8.4a)} \\ &= C_E(0^-), \quad a_{i,f} \gg r_0, && \text{(8.4b)} \\ &= \left(\frac{a_f}{a_i}\right)^2 \left(1 + \frac{4}{\pi r_0}(a_f - a_i)\right) C_E(0^-), \quad a_{i,f} \ll r_0 && \text{(8.4c)} \end{aligned}$$

.

This is consistent with cutoff dependence found in the excitation energy, (7.23). On the other hand the momentum distribution function only depends on the state and is thus continuous across the quench. Thus, the contact C_n, defined by the large momentum tail of the distribution function, (8.1) is continuous across the quench and is therefore distinct from C_E.

Utilizing the analysis of Sec. IV, we next compute these contact quantities at time t after the quench. We first study the contact $C_E(t)$ defined by the quartic interaction, (8.2b). Relegating the calculation details to Appendix D 2, within the Bogoliubov approximation we find

$$C_E(t) = (4\pi n a_f)^2 + F_C(\sigma, t) C^f_{LHY}, \tag{8.5}$$

where the C^f_{LHY} is the LHY correction to the ground state contact for quenched Hamiltonian with a_f

$$C^f_{LHY} = (4\pi n a_f)^2 \frac{64}{3\sqrt{\pi}} (n a_f^3)^{1/2} \tag{8.6}$$

and the time-dependent enhancement factor due to the quench is given by

$$F_C(\sigma,t)=\frac{\sigma^{3/2}+3\sqrt{\sigma}+3\sqrt{1-\sigma}\arccos\sqrt{\sigma}}{4} + \frac{3\sqrt{2}}{8}\int dy y^2 \frac{y(1-\sigma)}{(y^2+2)\sqrt{y^2+2\sigma}} \times\cos[2\hat{t}\sqrt{y^2(y^2+2)}] \tag{8.7}$$

and illustrated in Fig. 24.

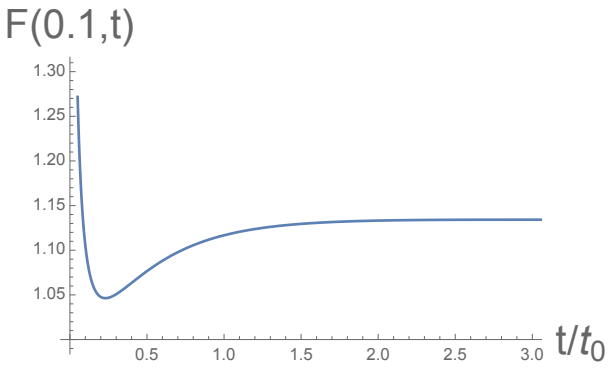

FIG. 24: (Color online) Contact enhancement factor $F_C(\sigma,t)$ above the corresponding ground state value as a function of time following a scattering length quench $0.1a_f\to a_f$, in units of pre-thermalization time scale $t_0=\hbar/ng_f=m/(4\pi a_f n\hbar)$. For a typical ^{85}Rb experiment with $n=5\times10^{12}cm^{-3}$, $a_s=1100a_0$, $t_0\approx360\mu s$.

Immediately after the quench, at $t=0^+$, the quantity $F_C(\sigma,t)$ can be evaluated analytically, giving the contact

$$C_E(0^+)=(4\pi n a_f)^2\left[1+\frac{64}{3\sqrt{\pi}}(na_i^3)^{1/2}\right] + 64\pi a_f^2 n^2\Lambda(a_f-a_i), \tag{8.8}$$

which is the Bogoliubov limit of the general result in Eq. (8.4c). This UV cutoff-dependence is reflected in the large value of the numerically evaluated contact near $t=0^+$, in Fig. 24. As time evolves after a quench, the contact decreases dramatically within a short window of time, with the cutoff-dependence quickly vanishing. After reaching a minimum it then slowly grows to a finite steady-state value, C_{ss}.

At long times, the sinusoid in (8.7) averages out and contact reaches a steady-state value

$$h(\sigma)\equiv F_C(\sigma,t\to\infty)=\frac{\sigma^{3/2}+3\sqrt{\sigma}+3\sqrt{1-\sigma}\arccos\sqrt{\sigma}}{4} \tag{8.9}$$

plotted in Fig. 25. This steady-state contact is greater than the contact in the ground state for the same scattering length a_f.

Finally, we examine the contact associated with the tail of the momentum distribution function after the quench,

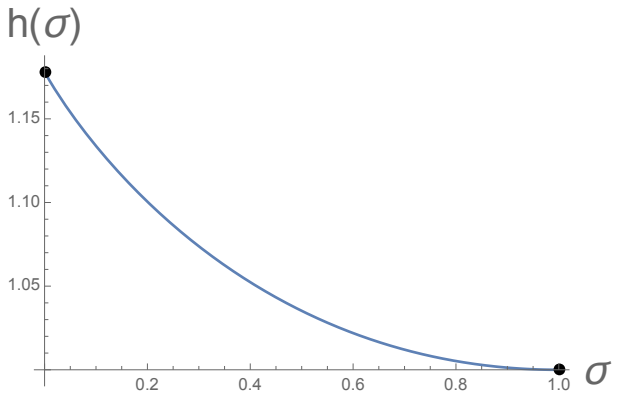

FIG. 25: (Color online) Asymptotic contact enhancement factor $h(\sigma)\equiv F_C(\sigma,t\to\infty)$ following a scattering length quench $a_i\to a_f$ as a function of quench depth $\sigma=a_i/a_f$. Two dots correspond to maximum enhancement $h(0)=3\pi/8$ (noninteracting initial state or unitarity final state) and minimum enhancement $h(1)=1$ (no quench), respectively.

which is given by Eq. (6.11) following a deep quench and Eq. (4.14) for a shallow quench, respectively [80]. From these we straightforwardly obtain

$$C_n=\lim_{k\to\infty}k^4n_k=(4\pi a_f n)^2\left[\frac{n_c^{ss}}{n}+(1-\sigma)^2\right] \tag{8.10}$$

and the shallow quench result is obtained by setting $n^{ss}=n$ using Bogoliubov approximation. Clearly, this is also independent of time. Thus, out of equilibrium, the three forms of the contact, C_n, C_E, C_{dE} no longer coincide, like they do in the ground state.

Above analysis of various forms of contact in the nonequilibrium state thus shows that no direct relation of the coefficient of the $1/\omega^{3/2}$ tail in RF spectroscopy [64] to the equilibrium contact and its other ground state relations can be made.

IX. SUMMARY AND OPEN DIRECTIONS

In this manuscript we studied the dynamics of a resonant Bose gas following shallow and deep scattering length quenches and ramps, confining to a metastable regime of a positive scattering length. Utilizing a dynamic field theory extension of the Bogoliubov theory, which self-consistently accounts for a large depletion and a time-dependent condensate density, we approximately solved for the full post-quench evolution of the system. From this we then computed a variety of physical observables, such as the evolution of the momentum distribution function, the associated condensate depletion, the time-dependent structure function, the RF spectroscopy signal, the excitation energy and various forms of a "nonequilibrium contact". We found, that following initial transient dynamics, the Bose gas exhibits a prethermalization to a stationary state (characterized e.g.,

by a stationary momentum distribution function) that differs qualitatively from the corresponding ground state. Because of integrability of the approximate model, that does not include quasi-particles scattering, the system never exhibits full thermalization to a ground state. Despite the simplicity of our model and approximate analysis, our results are in reasonable qualitative agreement with recent JILA experiments [56].

Although we made significant progress in understanding the post-quench dynamics of a resonant Bose system, our work leaves a number questions for a future investigation. Our present study utilized a single-channel model and focussed on the upper-branch physics with a tunable positive scattering length, thereby neglecting the closed molecular channel. The latter may in fact be quite significant, enriching the dynamics by allowing coherent condensate oscillations not only into pairs of atomic quasi-particles in the upper branch, but also into molecular condensate and molecular quasi-particles. This extension can be quite naturally treated within a two-channel model, where the closed molecular channel is explicitly included. It would allow one to address the dynamics not only within the superfluid phase but across quantum and classical phase transitions, most notably across the quantum Ising transition between atomic and molecular superfluids and throughout the atomic-molecular phase diagram [51–53].

Another crucial ingredient missing in our model is the quasi-particle scattering. This is responsible for a time-independent quasi-particle momentum distribution function, that is completely fixed by the initial state, characterized by a_i and the final scattering length a_f. This feature is responsible for the absence of thermalization of the system. It is thus desirable to extend the present model to include quasi-particle scattering, that can be handled through the Boltzmann equation for the quasi-particle distribution function. In such a generalized model, the dynamics of the atomic observables (e.g., atomic momentum distribution and structure functions) will consist of two contributions, Heisenberg evolution of atoms due to quasi-particle unitary dynamics, coupled to the evolution of the quasi-particle momentum distribution function governed by the Boltzmann equation with collision integrals. We expect that such dynamics will exhibit a second, longer time scale, set by the quasi-particle scattering that will lead to true long-time thermalization.

Finally, to treat the effects of interactions more systematically, it is desirable to have a full nonequilibrium Schwinger-Keldysh field theoretic formulation. We leave these and a number of other open question for future research [59].

Acknowledgments

We thank P. Makotyn, D. Jin, and E. Cornell for sharing their data with us before publication, and acknowledge them, A. Andreev, D. Huse, V. Gurarie, and A. Kamenev for stimulating discussions. This research was supported by the NSF through DMR-1001240, and by the Simons Investigator award from the Simons Foundation.

Appendix A: Energy conservation

In this appendix we study the time evolution of the total energy following a deep quench. Although energy is conserved under exact unitary evolution of a closed system, it is less clear whether it remains so for the time-dependent self-consistent Bogoliubov approximation employed in deep quenches. We demonstrate below that within this approximation, that neglects anomalous averages of finite momentum excitations, the total energy is indeed conserved.

To this end we study the time derivative of the full time-dependent Hamiltonian, including the constant mean-field parts derived in Sec. II, (2.24). It is given by

$$\hat{H}_{total} = \sum_{\mathbf{k}\neq 0}\left[(\epsilon_k + g n_c(t))\hat{a}^\dagger_{\mathbf{k}}\hat{a}_{\mathbf{k}} + \frac{g}{2}n_c(t)(\hat{a}_{\mathbf{k}}\hat{a}_{-\mathbf{k}} + \hat{a}^\dagger_{\mathbf{k}}\hat{a}^\dagger_{-\mathbf{k}})\right] + g[n_c(t)n_d(t) + \frac{1}{2}n_c^2(t) + n_d^2(t)], \tag{A1}$$

where g is the final interaction g_f to which the system is quenched, and the energy is evaluated as

$$E_{total}(t) = \langle 0^-|\hat{H}_{total}(t)|0^-\rangle = E_1(t) + E_2(t) + E_3(t). \tag{A2}$$

The time derivative of last mean-field term, E_3 is given by

$$\begin{aligned}\frac{dE_3}{dt} &= g[\dot{n}_c n_d + n_c\dot{n}_d + n_c\dot{n}_c + 2n_d\dot{n}_d],\\ &= g n_d\dot{n}_d,\end{aligned} \tag{A3}$$

where we used the atom conservation constraint $n = n_c(t) + n_d(t)$, giving $\dot{n}_c(t) + \dot{n}_d(t) = 0$.

A time derivative of the first term $E_1(t)$ is

$$\begin{aligned}\frac{dE_1}{dt} &\equiv \frac{d}{dt}\sum_{\mathbf{k}\neq 0}(\epsilon_k + g n_c(t))\,\langle 0^-|\hat{a}^\dagger_{\mathbf{k}}(t)\hat{a}_{\mathbf{k}}(t)|0^-\rangle,\\ &= \sum_{\mathbf{k}\neq 0} g\dot{n}_c\langle\hat{a}^\dagger_{\mathbf{k}}\hat{a}_{\mathbf{k}}\rangle + (\epsilon_k + g n_c(t))\langle\dot{\hat{a}}^\dagger_{\mathbf{k}}\hat{a}_{\mathbf{k}} + \hat{a}^\dagger_{\mathbf{k}}\dot{\hat{a}}_{\mathbf{k}}\rangle,\end{aligned} \tag{A4}$$

and of the second term $E_2(t)$

$$\begin{aligned}\frac{dE_2}{dt} &\equiv \frac{g}{2}\frac{d}{dt}\sum_{\mathbf{k}\neq 0} n_c(t)\langle 0^-|\hat{a}_{\mathbf{k}}(t)\hat{a}_{-\mathbf{k}}(t) + \hat{a}^\dagger_{\mathbf{k}}(t)\hat{a}^\dagger_{-\mathbf{k}}(t)|0^-\rangle,\\ &= \sum_{\mathbf{k}\neq 0}\frac{g}{2}\dot{n}_c\langle\hat{a}_{\mathbf{k}}\hat{a}_{-\mathbf{k}} + \hat{a}^\dagger_{\mathbf{k}}\hat{a}^\dagger_{-\mathbf{k}}\rangle + \frac{g}{2}n_c\langle\dot{\hat{a}}_{\mathbf{k}}\hat{a}_{-\mathbf{k}} + \hat{a}_{\mathbf{k}}\dot{\hat{a}}_{-\mathbf{k}}\\ &\quad + \dot{\hat{a}}^\dagger_{\mathbf{k}}\hat{a}^\dagger_{-\mathbf{k}} + \hat{a}^\dagger_{\mathbf{k}}\dot{\hat{a}}^\dagger_{-\mathbf{k}}\rangle.\end{aligned} \tag{A5}$$

Using the Heisenberg equation of motion to eliminate time derivatives of atom operators we find

$$\begin{aligned}\dot{\hat{a}}_{\mathbf{k}} &= \frac{1}{i}[(\epsilon_k + gn_c)\hat{a}_{\mathbf{k}} + gn_c\hat{a}^\dagger_{-\mathbf{k}}],\\ \dot{\hat{a}}_{-\mathbf{k}} &= \frac{1}{i}[(\epsilon_k + gn_c)\hat{a}_{-\mathbf{k}} + gn_c\hat{a}^\dagger_{\mathbf{k}}].\end{aligned} \tag{A6}$$

With this (A4) and (A5) reduce to

$$\frac{dE_1}{dt} = g\dot{n}_c n_d + \frac{1}{i}\sum_{\mathbf{k}\neq 0} gn_c(\epsilon_k + gn_c)\langle \hat{a}^\dagger_{\mathbf{k}}\hat{a}^\dagger_{-\mathbf{k}} - \hat{a}_{\mathbf{k}}\hat{a}_{-\mathbf{k}}\rangle \tag{A7}$$

and

$$\begin{aligned}\frac{dE_2}{dt} &= \sum_{\mathbf{k}\neq 0}\frac{g}{2}\dot{n}_c\langle \hat{a}_{\mathbf{k}}\hat{a}_{-\mathbf{k}} + \hat{a}^\dagger_{\mathbf{k}}\hat{a}^\dagger_{-\mathbf{k}}\rangle\\ &+ \frac{gn_c}{i}((\epsilon_k + gn_c)\langle \hat{a}_{\mathbf{k}}\hat{a}_{-\mathbf{k}} - \hat{a}^\dagger_{\mathbf{k}}\hat{a}^\dagger_{-\mathbf{k}}\rangle.\end{aligned} \tag{A8}$$

For the total energy we then obtain,

$$\frac{dE_{total}}{dt} = \sum_{\mathbf{k}\neq 0}\frac{g}{2}\dot{n}_c[\langle \hat{a}_{\mathbf{k}}\hat{a}_{-\mathbf{k}}\rangle + \langle \hat{a}^\dagger_{\mathbf{k}}\hat{a}^\dagger_{-\mathbf{k}}\rangle] \approx 0, \tag{A9}$$

where in the last approximation we neglected anomalous correlator of excited atoms. More precisely, following Sotiriadis and Cardy [35], we observe that while the conventional definition of the energy is not conserved, the shifted one $E_{shifted} \equiv E_{total} - \frac{g}{2}\int dt\dot{n}_c[\langle \hat{a}_{\mathbf{k}}\hat{a}_{-\mathbf{k}}\rangle + \langle \hat{a}^\dagger_{\mathbf{k}}\hat{a}^\dagger_{-\mathbf{k}}\rangle]$ approximately is.

Appendix B: $U(t)$ for quasi-adiabatic approximation

In this section, we fill in the technical details leading to $U(t)$ for quasi-adiabatic approximation in Eq. (6.9). The operator part of time-dependent Hamiltonian is

$$\begin{aligned}\hat{H}(t) &= \frac{1}{2}\sum_{\mathbf{k}\neq 0}((\epsilon_k + n_c(t)g_f)(\hat{a}^\dagger_k\hat{a}_{\mathbf{k}} + \hat{a}^\dagger_{-\mathbf{k}}\hat{a}_{-\mathbf{k}})\\ &+ n_c(t)g_f(\hat{a}^\dagger_{\mathbf{k}}\hat{a}^\dagger_{-\mathbf{k}} + \hat{a}_{\mathbf{k}}\hat{a}_{-\mathbf{k}})).\end{aligned} \tag{B1}$$

It can be instantaneously diagonalized by

$$\begin{pmatrix}\hat{a}_{\mathbf{k}}(t)\\ \hat{a}^\dagger_{-\mathbf{k}}(t)\end{pmatrix} = \begin{pmatrix}u_k(t) & v_k(t)\\ v_k(t) & u_k(t)\end{pmatrix}\begin{pmatrix}\hat{\gamma}_{\mathbf{k}}(t)\\ \hat{\gamma}^\dagger_{-\mathbf{k}}(t)\end{pmatrix}, \tag{B2}$$

and rewritten as

$$\begin{aligned}\hat{H}(t) &= -\frac{1}{2}\sum_{\mathbf{k}\neq 0}(\epsilon_k + n_c(t)g - E_{kf}(t))\\ &+\frac{1}{2}\sum_{\mathbf{k}\neq 0}E_{kf}(t)(\hat{\gamma}^\dagger_{\mathbf{k}}\hat{\gamma}_{\mathbf{k}} + \hat{\gamma}^\dagger_{-\mathbf{k}}\hat{\gamma}_{-\mathbf{k}}),\end{aligned} \tag{B3}$$

where

$$\begin{aligned}u_k(t) &= \sqrt{\frac{1}{2}(\frac{\epsilon_k + g_f n_c(t)}{E_k(t)} + 1)},\\ v_k(t) &= -\sqrt{\frac{1}{2}(\frac{\epsilon_k + g_f n_c(t)}{E_k(t)} - 1)},\\ E_{kf}(t) &= \sqrt{\epsilon_k(\epsilon_k + 2g_f n_c(t))}.\end{aligned} \tag{B4}$$

The time-dependence of $\hat{\gamma}^\dagger_{\mathbf{k}}(t)$ and $\hat{\gamma}_{\mathbf{k}}(t)$ is obtained from the Heisenberg equation of motion,

$$\frac{d\hat{\gamma}_{\mathbf{k}}}{dt} = i[\hat{\gamma}_{\mathbf{k}}, \hat{H}] + \frac{\partial\hat{\gamma}_{\mathbf{k}}}{\partial t}, \tag{B5}$$

where the last term accounts for the explicit time-dependence in Hamiltonian. To compute it we first express $\hat{\gamma}^\dagger_{\mathbf{k}}(t)$ and $\hat{\gamma}_{\mathbf{k}}(t)$ in terms of $\hat{a}^\dagger_{\mathbf{k}}(t)$ and $\hat{a}_{\mathbf{k}}(t)$.

$$\begin{pmatrix}\hat{\gamma}_{\mathbf{k}}(t)\\ \hat{\gamma}^\dagger_{-\mathbf{k}}(t)\end{pmatrix} = \begin{pmatrix}u_k(t) & -v_k(t)\\ -v_k(t) & u_k(t)\end{pmatrix}\begin{pmatrix}\hat{a}_{\mathbf{k}}(t)\\ \hat{a}^\dagger_{-\mathbf{k}}(t)\end{pmatrix}, \tag{B6}$$

Then

$$\begin{aligned}\frac{\partial}{\partial t}\begin{pmatrix}\hat{\gamma}_{\mathbf{k}}(t)\\ \hat{\gamma}^\dagger_{-\mathbf{k}}(t)\end{pmatrix} &= \begin{pmatrix}\dot{u}_k(t) & -\dot{v}_k(t)\\ -\dot{v}_k(t) & \dot{u}_k(t)\end{pmatrix}\begin{pmatrix}\hat{a}_{\mathbf{k}}(t)\\ \hat{a}^\dagger_{-\mathbf{k}}(t)\end{pmatrix},\\ &= \begin{pmatrix}\dot{u}_k(t) & -\dot{v}_k(t)\\ -\dot{v}_k(t) & \dot{u}_k(t)\end{pmatrix}\begin{pmatrix}u_k(t) & v_k(t)\\ v_k(t) & u_k(t)\end{pmatrix}\begin{pmatrix}\hat{\gamma}_{\mathbf{k}}(t)\\ \hat{\gamma}^\dagger_{-\mathbf{k}}(t)\end{pmatrix},\\ &= \begin{pmatrix}0 & \frac{g\dot{n}_c(t)\epsilon_k}{2E^2_{kf}}\\ \frac{g\dot{n}_c(t)\epsilon_k}{2E^2_{kf}} & 0\end{pmatrix}\begin{pmatrix}\hat{\gamma}_{\mathbf{k}}(t)\\ \hat{\gamma}^\dagger_{-\mathbf{k}}(t)\end{pmatrix}.\end{aligned} \tag{B7}$$

Now the equation of motions become

$$\frac{d}{dt}\begin{pmatrix}\hat{\gamma}_{\mathbf{k}}(t)\\ \hat{\gamma}^{\dagger}_{-\mathbf{k}}(t)\end{pmatrix}=\begin{pmatrix}-iE_{kf}(t) & \frac{g\dot{n}_c(t)\epsilon_k}{2E^2_{kf}}\\ \frac{g\dot{n}_c(t)\epsilon_k}{2E^2_{kf}} & iE_{kf}(t)\end{pmatrix}\begin{pmatrix}\hat{\gamma}_{\mathbf{k}}(t)\\ \hat{\gamma}^{\dagger}_{-\mathbf{k}}(t)\end{pmatrix}. \tag{B8}$$

Assuming $\dot{n}_c(t)$ changes slowly compared to other timescales (or more explicitly $\dot{n}_c(t)/n \ll E^3_{kf}/(\hbar n g\epsilon_k)$), we can ignore the off-diagonal terms in (B8) and have

$$\frac{d}{dt}\begin{pmatrix}\hat{\gamma}_{\mathbf{k}}(t)\\ \hat{\gamma}^{\dagger}_{-\mathbf{k}}(t)\end{pmatrix}\approx\begin{pmatrix}-iE_{kf}(t) & 0\\ 0 & iE_{kf}(t)\end{pmatrix}\begin{pmatrix}\hat{\gamma}_{\mathbf{k}}(t)\\ \hat{\gamma}^{\dagger}_{-\mathbf{k}}(t)\end{pmatrix}, \tag{B9}$$

from which we can solve $\hat{\gamma}^{\dagger}_{\mathbf{k}}(t)$ and $\hat{\gamma}_{\mathbf{k}}(t)$ as

$$\hat{\gamma}_{\mathbf{k}}(t)=\hat{\gamma}_{\mathbf{k}}e^{-i\int_0^t dt' E_{kf}(t')},\qquad \hat{\gamma}^{\dagger}_{-\mathbf{k}}(t)=\hat{\gamma}^{\dagger}_{-\mathbf{k}}e^{i\int_0^t dt' E_{kf}(t')}, \tag{B10}$$

thus

$$\begin{aligned}\begin{pmatrix}\hat{a}_{\mathbf{k}}(t)\\ \hat{a}^{\dagger}_{-\mathbf{k}}(t)\end{pmatrix}&=\begin{pmatrix}u_k(t) & v_k(t)\\ v_k(t) & u_k(t)\end{pmatrix}\begin{pmatrix}e^{-i\int_0^t dtE_{kf}(t')} & 0\\ 0 & e^{i\int_0^t dtE_{kf}(t')}\end{pmatrix}\begin{pmatrix}\hat{\gamma}_{\mathbf{k}}\\ \hat{\gamma}^{\dagger}_{-\mathbf{k}}\end{pmatrix},\\ &=\begin{pmatrix}u_k(t)e^{-i\int_0^t dtE_{kf}(t')} & v_k(t)e^{i\int_0^t dtE_{kf}(t')}\\ v_k(t)e^{-i\int_0^t dtE_{kf}(t')} & u_k(t)e^{i\int_0^t dtE_{kf}(t')}\end{pmatrix}\begin{pmatrix}\hat{\gamma}_{\mathbf{k}}\\ \hat{\gamma}^{\dagger}_{-\mathbf{k}}\end{pmatrix}.\end{aligned} \tag{B11}$$

Comparing this with Eq. (6.4) , we find

$$U(t)=\begin{pmatrix}u_k(t)e^{-i\int_0^t dtE_{kf}(t')} & v_k(t)e^{i\int_0^t dtE_{kf}(t')}\\ v_k(t)e^{-i\int_0^t dtE_{kf}(t')} & u_k(t)e^{i\int_0^t dtE_{kf}(t')}\end{pmatrix}. \tag{B12}$$

Appendix C: Energy after quench

In this section we evaluate the total energy of the system after the sudden quench. Separating the energy into kinetic part and interaction part

$$\langle 0^-|\hat{H}^f|0^-\rangle=\langle 0^-|\hat{H}^f_{KE}|0^-\rangle+\langle 0^-|\hat{H}^f_{int}|0^-\rangle, \tag{C1}$$

with

$$\hat{H}^f_{KE}=\frac{1}{2}\sum_{\mathbf{k}\neq 0}\epsilon^0_k(\hat{a}^{\dagger}_{\mathbf{k}}\hat{a}_{\mathbf{k}}+\hat{a}^{\dagger}_{-\mathbf{k}}\hat{a}_{-\mathbf{k}}), \tag{C2}$$

$$\hat{H}^f_{int}=\frac{1}{2}Vg_fn^2+\frac{1}{2}\sum_{\mathbf{k}\neq 0}[ng_f(\hat{a}^{\dagger}_{\mathbf{k}}\hat{a}_{\mathbf{k}}+\hat{a}^{\dagger}_{-\mathbf{k}}\hat{a}_{-\mathbf{k}})+ng_f(\hat{a}^{\dagger}_{\mathbf{k}}\hat{a}^{\dagger}_{-\mathbf{k}}+\hat{a}_{\mathbf{k}}\hat{a}_{-\mathbf{k}})], \tag{C3}$$

we then use Bogoliubov transformation to evaluate them respectively by expressing $\hat{a}_{\mathbf{k}}$ in terms of pre-quench basis $\hat{\alpha}_{\mathbf{k}}$, obtaining

$$\hat{H}_{KE}=\sum_{\mathbf{k}\neq 0}\epsilon_k\hat{a}^{\dagger}_{\mathbf{k}}\hat{a}_{\mathbf{k}}=\sum_{\mathbf{k}\neq 0}\epsilon_k\left(|u_k|^2\hat{\alpha}^{\dagger}_{\mathbf{k}}\hat{\alpha}_{\mathbf{k}}-u^*_kv_k\hat{\alpha}^{\dagger}_{\mathbf{k}}\hat{\alpha}^{\dagger}_{-\mathbf{k}}-u_kv^*_k\hat{\alpha}_{-\mathbf{k}}\hat{\alpha}_{\mathbf{k}}+|v_k|^2\hat{\alpha}_{-\mathbf{k}}\hat{\alpha}^{\dagger}_{-\mathbf{k}}\right), \tag{C4}$$

and

$$\begin{aligned}\hat{H}_{int}=&\frac{1}{2}Vg_fn^2+ng_f\sum_{\mathbf{k}\neq 0}[|v_k|^2-\frac{1}{2}(u^*_kv_k+u_kv^*_k)]\\ &+\frac{1}{2}ng_f\sum_{\mathbf{k}\neq 0}\Big[\left(|u^2_k|+|v^2_k|-(u^*_kv_k+u_kv^*_k)\right)(\hat{\alpha}^{\dagger}_{\mathbf{k}}\hat{\alpha}_{\mathbf{k}}+\hat{\alpha}^{\dagger}_{-\mathbf{k}}\hat{\alpha}_{-\mathbf{k}})+(u^2_k+v^2_k-2u_kv_k)(\hat{\alpha}^{\dagger}_{\mathbf{k}}\hat{\alpha}^{\dagger}_{-\mathbf{k}}+\hat{\alpha}_{\mathbf{k}}\hat{\alpha}_{-\mathbf{k}})\Big].\end{aligned} \tag{C5}$$

Since $\hat{\alpha}_{\mathbf{k}}|0^-\rangle = 0$, we have

$$\langle 0^-|\hat{H}_{KE}|0^-\rangle = \sum_{\mathbf{k}\neq 0} \epsilon_k |v_k|^2, \tag{C6}$$

and

$$\langle 0^-|\hat{H}^f_{int}|0^-\rangle = \frac{1}{2}V\tilde{g}_f n^2 + n\tilde{g}_f \sum_{\mathbf{k}\neq 0}\left[|v_k|^2 - \frac{1}{2}(u_k^* v_k + u_k v_k^*) + \frac{n\tilde{g}_f}{4\epsilon_k}\right], \tag{C7}$$

during which coupling g has been expanded to second order

$$g = \frac{4\pi a}{m} + \frac{(4\pi a)^2}{m^2 V}\sum_{\mathbf{k}\neq 0}\frac{1}{2\epsilon_k} \equiv \tilde{g} + \frac{\tilde{g}^2}{V}\sum_{\mathbf{k}\neq 0}\frac{1}{2\epsilon_k}. \tag{C8}$$

Therefore, the total energy is

$$\begin{aligned} E_{tot}(t=0^+) &= \langle 0^-|\hat{H}_{KE} + \hat{H}_{int}|0^-\rangle, \\ &= \frac{1}{2}V\tilde{g}_f n^2 + n\tilde{g}_f \sum_{\mathbf{k}\neq 0}\left[\left(\frac{\epsilon_k}{n\tilde{g}} + 1\right)|v_k|^2 - \frac{1}{2}(u_k^* v_k + u_k v_k^*) + \frac{n\tilde{g}_f}{4\epsilon_k}\right], \\ &= \frac{2\pi n a_f}{m} + \frac{32\sqrt{2\pi}na_f}{m}(na_f^3)^{1/2}\int dk k^2\left[(k^2+1)|v_k|^2 - \frac{1}{2}(u_k v_k^* + v_k u_k^*) + \frac{1}{4k^2}\right]. \end{aligned} \tag{C9}$$

For a sudden quench, the expressions for u_k and v_k are simple

$$\begin{aligned} u_k &= \sqrt{\frac{1}{2}\left(\frac{\epsilon_k + n\tilde{g}_i}{\sqrt{\epsilon_k(\epsilon_k + 2n\tilde{g}_i)}} + 1\right)}, \\ v_k &= -\sqrt{\frac{1}{2}\left(\frac{\epsilon_k + n\tilde{g}_i}{\sqrt{\epsilon_k(\epsilon_k + 2n\tilde{g}_i)}} - 1\right)}. \end{aligned} \tag{C10}$$

Plugging Eq. (C10) into (C6) and (C7), we obtain the kinetic energy as

$$\begin{aligned} \langle 0^-|\hat{H}_{KE}|0^-\rangle &= \sum_{\mathbf{k}\neq 0}\frac{1}{2}\epsilon_k\left(\frac{\epsilon_k + n\tilde{g}_i}{\sqrt{\epsilon_k(\epsilon_k + 2n\tilde{g}_i)}} - 1\right), \\ &= \frac{1}{2}n\tilde{g}_i(2m\tilde{g}_i n)^{3/2}\frac{4\pi V}{(2\pi)^3}\int dy y^2\left[\frac{y^2+1}{\sqrt{y^2(y^2+2)}} - 1\right], \\ &= N\frac{4a_i n}{m}\Lambda a_i - \frac{128\sqrt{\pi}a_i n}{5m}N(na_i^3)^{1/2}, \end{aligned} \tag{C11}$$

the interaction energy as

$$\begin{aligned} \langle 0^-|\hat{H}^f_{int}|0^-\rangle &= \frac{1}{2}V\tilde{g}_f n^2 + \frac{1}{2}n\tilde{g}_f\sum_{\mathbf{k}\neq 0}(\epsilon_k/\sqrt{\epsilon_k(\epsilon_k + n\tilde{g}_f)} - 1 + n\tilde{g}_f/2\epsilon_k), \\ &= \frac{1}{2}Vn^2\tilde{g}_f + \frac{1}{2}n\tilde{g}_f(2m\tilde{g}_f n)^{\frac{3}{2}}\frac{4\pi V}{(2\pi)^3}\int dy y^2\left(\frac{y}{\sqrt{y^2+2\sigma}} - 1 + \frac{1}{2y^2}\right), \\ &= \frac{2\pi a_f n}{m}N\left[1 + \frac{64}{3}\left(\frac{na_i^3}{\pi}\right)^{\frac{1}{2}}\right] + (1-2\sigma)N\frac{4a_f n}{m}\Lambda a_f, \end{aligned} \tag{C12}$$

and the total energy as

$$E_{tot} = \langle 0^-|\hat{H}_{KE} + \hat{H}_{int}|0^-\rangle = \frac{4(1-\sigma)^2 n a_f}{m}Na_f\Lambda - \frac{128\sqrt{\pi}na_i}{5m}N(na_i^3)^{1/2} + \frac{2\pi n a_f}{m}N\left[1 + \frac{64}{3\sqrt{\pi}}(na_i^3)^{1/2}\right], \tag{C13}$$

which is Eq. (7.12) in the text. The ground state energy can be easily obtained by setting $\sigma = 1$, and one obtains

$$E_{tot} = \frac{2\pi a_s n}{m}N[1 + \frac{128}{15}(\frac{na_s^3}{\pi})^{\frac{1}{2}}]. \tag{C14}$$

as the cutoff dependences of kinetic energy and interaction energy cancel each other, recovering the LHY result as expected.

Appendix D: Contact

1. Ground state contact

In this paper, we follow E. Braaten et.al [78] and take the working definition of contact to be

$$C = (mg)^2\langle \int dr\hat{\psi}^\dagger(r,t)\hat{\psi}^\dagger(r,t)\hat{\psi}(r,t)\hat{\psi}(r,t))\rangle = 2m^2 g\langle \hat{H}_{int}\rangle/V. \tag{D1}$$

At $T=0$ for $na_s^3 \ll 1$, the interaction energy of Bose gas is given in Appendix C. For ground state, $\langle O|\hat{H}_{int}|O\rangle$ can be evaluated by applying $\sigma = 1$ to Eq. (C12), which gives

$$\begin{aligned}\langle O|\hat{H}_{int}|O\rangle &= \frac{2\pi a_s Nn}{m}\left[1+\frac{64}{3\sqrt{\pi}}(na_s^3)^{1/2}\right] - \frac{4\Lambda a_s^2 Nn}{m}, \\ &= 2Nn/m\left[a_s\pi\left(1+\frac{64}{3\sqrt{\pi}}(na_s^3)^{1/2}\right) - 2a_s^2\Lambda\right].\end{aligned} \tag{D2}$$

The last term contains the same divergence as the bare interaction g, and we show below they exactly cancel each other to give a finite contact.

$$\begin{aligned}C &= 2m^2 g\langle O|\hat{H}_{int}|O\rangle/V, \\ &= 2m^2\left(\frac{4\pi a_s}{m}+\frac{8\Lambda a_s^2}{m}\right)\langle O|\hat{H}_{int}|O\rangle/V, \\ &= 8m(\pi a_s + 2\Lambda a_s^2)\langle O|\hat{H}_{int}|O\rangle/V, \\ &= (4\pi a_s)^2 n^2\left[1+\frac{64}{3\sqrt{\pi}}(na_s^3)^{1/2}+\frac{128}{3\pi^{3/2}}a_s\Lambda(na_s^3)^{1/2}+O(\Lambda^2 a_s^2)\right].\end{aligned} \tag{D3}$$

Thus to the order of $(na_s^3)^{1/2}$, the contact value for ground state at $T=0$ is

$$C = (4\pi a_s)^2 nN\left[1+\frac{64}{3\sqrt{\pi}}(na_s^3)^{1/2}\right]. \tag{D4}$$

For bosons in thermal equilibrium, one central Tan's relation is the adiabatic theorem, which relates the energy change with respect to scattering length to the contact. The theorem states the following thing

$$C = 8\pi m a_s^2 \frac{d\mathcal{E}_{gs}}{da_s}. \tag{D5}$$

Since the ground state energy is given by Eq. (7.2), it is straightforward to show that

$$8\pi m a_s^2 \frac{d\mathcal{E}_{gs}}{da_s} = (4\pi a_s n)^2\left[1+\frac{64}{3\sqrt{\pi}}(na_s^3)^{\frac{1}{2}}\right]. \tag{D6}$$

Thus we have verified the adiabatic theorem in ground state.

Another important Tan's relation is the momentum theorem, which relates contact to the high momentum tail of the momentum distribution function

$$C = \lim_{k\to\infty} k^4 n_k. \tag{D7}$$

For ground state at $T=0$, momentum distribution n_k is given by Eq. (2.13), giving

$$\lim_{k\to\infty} k^4 n_k = C_0 + O(1/k^2), \tag{D8}$$

with $C_0 = (4\pi a_s n)^2$. Thus we recover the lowest order of contact obtained in Eq. (D4).

We can also generalize the contact to large na_s^3 case. From Eq. (2.24), the ground state energy is modified as

$$\begin{aligned}\mathcal{E}_{gs} &= \langle O|\hat{H}_{total}|O\rangle \\ &= \frac{2\pi a_s V n^2}{m}\left[1+\left(\frac{n_d}{n}\right)^2+\frac{128(na_s^3)^{1/2}}{15\sqrt{\pi}}\left(\frac{n_c}{n}\right)^{5/2}\right].\end{aligned} \tag{D9}$$

Then the adiabatic theorem gives

$$\begin{aligned} C &= 8\pi m a_s^2 \frac{d\mathcal{E}_{gs}}{da_s} \\ &= (4\pi a_s n)^2 \left[1 + \left(\frac{n_d}{n}\right)^2 + \frac{64(na_s^3)^{1/2}}{3\sqrt{\pi}} \left(\frac{n_c}{n}\right)^{5/2}\right]. \end{aligned} \tag{D10}$$

It is straightforward to verify that this also agrees with contact obtained via Eq. (D1). Here, condensate density n_c and depletion density n_d are determined self-consistently by Eq. (3.2).

2. Dynamical contact

An important quantity to determine dynamical contact is the interaction energy $\langle 0^-|\hat{H}^f_{int}|0^-\rangle$. In this section, still assuming a sudden quench, we further study the dynamics of interaction energy and focus on its asymptotic long time limit, and use it to construct the dynamical contact as in Eq. (D1). Using Eq. (4.2a) to decompose $\hat{a}_k$ into post-quench basis $\hat{\beta}_k(t)$, as $\hat{\beta}_k(t)$ evolve simply according to Eq. (4.8), combined with Eq. (C3), we obtain

$$\begin{aligned} &\langle 0^-|\hat{H}^f_{int}|0^-\rangle \\ &= \frac{1}{2}Vg_f n^2 - \frac{1}{2}\sum_{\mathbf{k}\neq 0} ng \frac{\epsilon_k + 2ng_f - \sqrt{\epsilon_k(\epsilon_k+2ng_f)}}{\epsilon_k + 2ng_f} + \frac{1}{2}\sum_{\mathbf{k}\neq 0} \frac{\epsilon_k gn}{\sqrt{\epsilon_k(\epsilon_k+2ng_f)}}[\langle \beta^\dagger_{\mathbf{k}}\beta_{\mathbf{k}}\rangle + \langle \beta^\dagger_{-\mathbf{k}}\beta_{-\mathbf{k}}\rangle \\ &\quad + \langle \beta^\dagger_{\mathbf{k}}\beta^\dagger_{-\mathbf{k}}\rangle e^{2iE_k t} + \langle \beta_{\mathbf{k}}\beta_{-\mathbf{k}}\rangle e^{-2iE_k t},] \\ &= \frac{1}{2}Vg_f n^2 + \frac{(n\tilde{g}_f)^2}{4\epsilon_k} - \frac{1}{2}\sum_{\mathbf{k}\neq 0} ng_f \frac{\epsilon_k + 2ng_f - \sqrt{\epsilon_k(\epsilon_k+2ng_f)}}{\epsilon_k + 2ng_f} + \sum_{\mathbf{k}\neq 0}\frac{1}{2}\epsilon_k ng_f[\frac{\epsilon_k + ng_f + ng_i - \sqrt{(\epsilon_k+2ng_i)(\epsilon_k+2ng_f)}}{(\epsilon_k+2ng_f)\sqrt{\epsilon_k(\epsilon_k+2ng_i)}}, \\ &\quad + \frac{n(g_f-g_i)}{(\epsilon_k+2ng_f)\sqrt{\epsilon_k(\epsilon_k+2ng_i)}}\cos[2t\sqrt{\epsilon_k(\epsilon_k+2ng_f)}]. \end{aligned} \tag{D11}$$

Rescaling time and momentum and taking the integral, we obtain

$$\begin{aligned} \langle 0^-|\hat{H}^f_{int}|0^-\rangle &= \frac{1}{2}Ng_f n + \frac{1}{2}ng_f(2mg_f n)^{\frac{3}{2}}\frac{4\pi V}{(2\pi)^3}\int dy y^2 \\ &\quad \times [y\frac{y^2+1+\sigma-\sqrt{(y^2+2\sigma)(y^2+2)}}{(y^2+2)\sqrt{y^2+2\sigma}} + \frac{y}{\sqrt{y^2+2\sigma}} - 1 + \frac{1}{2y^2} + \frac{y(1-\sigma)}{(y^2+2)\sqrt{y^2+2\sigma}}\cos(2\hat{t}\sqrt{y^2(y^2+2)}] \\ &= \frac{2Nna_f\pi}{m}[1 + F_C(\sigma,t)\frac{64}{3\sqrt{\pi}}(na_f^3)^{1/2})] - \frac{4Nna_f^2\Lambda}{m}, \end{aligned} \tag{D12}$$

where $F_C(\sigma,t) = h(\sigma) + T(t,\sigma,\Lambda)$ and

$$h(\sigma) = \frac{\sigma^{3/2} + 3\sqrt{\sigma} + 3\sqrt{1-\sigma}\arccos\sqrt{\sigma}}{4}, \tag{D13}$$

$$T(t,\sigma,\Lambda) = \frac{3\sqrt{2}}{8}\int dy y^2 \frac{y(1-\sigma)}{(y^2+2)\sqrt{y^2+2\sigma}} \times \cos[2\hat{t}\sqrt{y^2(y^2+2)}]. \tag{D14}$$

Following Eq. (D3), to the order of $(na^3)^{1/2}$ we obtain the dynamical contact after a quench,

$$C_E(t) = (4\pi n a_f)^2 + F_C(\sigma,t)C^f_{LHY}, \tag{D15}$$

given in Eq. (8.5) of the main text. In the asymptotically long time limit, $T(t\to\infty,\sigma,\Lambda)\to 0$.

3. RF spectroscopy

In this appendix, we dervie Eq. (4.34) of Sec. IV C. With $\hat{J}_I(t) = e^{i\int_0^t dt'\hat{H}_0}\hat{J}e^{-i\int_0^t dt'\hat{H}_0}$,

$$\begin{aligned}
\langle\hat{J}(t)\rangle &= \langle\psi|\hat{J}(t)|\psi\rangle, \\
&= \langle\psi|e^{i\int_0^t dt'(\hat{H}_0+\hat{H}_1(t'))}Je^{-i\int_0^t dt'(\hat{H}_0+\hat{H}_1(t'))}|\psi\rangle, \\
&= \langle\psi_I(t)|\hat{J}_I(t)|\psi_I(t)\rangle, \\
&= \langle\psi|e^{i\int_0^t dt'(\hat{H}_0+\hat{H}_{RF}(t'))}e^{-i\int_0^t dt'\hat{H}_0}\hat{J}_I(t)e^{i\int_0^t dt'\hat{H}_0}e^{-i\int_0^t dt'(\hat{H}_0+\hat{H}_{RF}(t'))}|\psi\rangle, \\
&= \langle\psi|T^*\left[e^{i\int_0^t dt'\hat{H}^I_{RF}(t')}\right]\hat{J}_I(t)T\left[e^{-i\int_0^t dt'\hat{H}^I_{RF}(t')}\right]|\psi\rangle, \\
&= -i\int_0^t dt'\langle\psi|\left[\hat{J}_I(t),\hat{H}^I_{RF}(t')\right]|\psi\rangle.
\end{aligned} \tag{D16}$$

The state $|\psi\rangle = |\alpha_0, 0_b\rangle$ a product state of a vacuum of b atoms, $|0_b\rangle$ and a SF condensate of a atoms, $|\alpha_0\rangle$, corresponding to the $t = 0^-$ state (ground state for $T = 0$: $\hat{a}_{\mathbf{k}}|\alpha_0\rangle = 0$) *before* the ramp (quench) to a new scattering length, which we will take to be a vacuum of Bogoliubov quasi-particles for $t = 0^-$ interactions at $T = 0$.

Plugging the expressions for $\hat{J}_I(t)$ and $\hat{H}_1(t)$ into above equation, we obtain the current as

$$\begin{aligned}
\langle\hat{J}(t)\rangle = &\int_0^t dt'\sum_{\mathbf{k},\mathbf{k}'}\langle\psi|\Big[I(t)\hat{b}^\dagger_{\mathbf{k}}(t)\hat{a}_{\mathbf{k}}(t) - I^*(t)\hat{a}^\dagger_{\mathbf{k}}(t)\hat{b}_{\mathbf{k}}(t) \\
&+ ign_0\sum_{\mathbf{k}}(\hat{a}_{-\mathbf{k}}(t)\hat{a}_{\mathbf{k}}(t) - \hat{a}^\dagger_{\mathbf{k}}(t)\hat{a}^\dagger_{-\mathbf{k}}(t)), \quad I(t')\hat{b}^\dagger_{\mathbf{k}'}(t')\hat{a}_{\mathbf{k}'}(t') + I^*(t')\hat{a}^\dagger_{\mathbf{k}'}(t')\hat{b}_{\mathbf{k}'}(t')\Big]|\psi\rangle, \\
= &\int_0^t dt'\sum_{\mathbf{k},\mathbf{k}'}I(t)I^*(t')\langle\psi|(\hat{a}_{\mathbf{k}}(t)\hat{a}^\dagger_{\mathbf{k}'}(t')\hat{b}^\dagger_{\mathbf{k}}\hat{b}_{\mathbf{k}'} - \hat{a}^\dagger_{\mathbf{k}'}(t')\hat{a}_{\mathbf{k}}(t)\hat{b}_{\mathbf{k}'}\hat{b}^\dagger_{\mathbf{k}})|\psi\rangle e^{i\epsilon_k t - i\epsilon_{k'}t' + i\omega_0(t-t')} + c.c., \\
= &-\int_0^t dt'\sum_{\mathbf{k}}I^*(t')I(t)\langle\alpha_0|\hat{a}^\dagger_{\mathbf{k}}(t')\hat{a}_{\mathbf{k}}(t)|\alpha_0\rangle e^{i(\epsilon_k+\omega_0)(t-t')} + c.c.,
\end{aligned} \tag{D17}$$

Now the RF spectroscopy signal can be evaluated as

$$\begin{aligned}
N_b(\omega_{RF}) &= -\int_0^\infty dt\langle\hat{J}(t)\rangle \\
&= \int_0^\infty dt\int_0^t dt'\sum_{\mathbf{k}}I^*(t')I(t)\langle\alpha_0|\hat{a}^\dagger_{\mathbf{k}}(t')\hat{a}_{\mathbf{k}}(t)|\alpha_0\rangle e^{i(\epsilon_k+\omega_0)(t-t')} + c.c., \\
&= \frac{1}{2}\int_0^\infty dt\int_0^\infty dt'\sum_{\mathbf{k}}I^*(t')I(t)\langle\alpha_0|\hat{a}^\dagger_{\mathbf{k}}(t')\hat{a}_{\mathbf{k}}(t)|\alpha_0\rangle e^{i(\epsilon_k+\omega_0)(t-t')} + c.c..
\end{aligned} \tag{D18}$$

where we utilized the $t \to t'$ symmetry to simplify the integral.

Plugging the correlator in Eq. (4.12) into Eq. (D18), we obtain

$$
\begin{aligned}
N_b(\omega_{RF}) &= \frac{1}{2}\int_0^\infty dt \int_0^\infty dt' \sum_{\mathbf{k}} I^*(t')I(t)\langle\alpha_0|\hat{a}^\dagger_{\mathbf{k}}(t')\hat{a}_{\mathbf{k}}(t)|\alpha_0\rangle \times e^{i(\epsilon_k+\omega_0)(t-t')} + c.c.,\\
&= \frac{1}{2}\int_0^\infty dt \int_0^\infty dt' \sum_{\mathbf{k}} I_0^2 e^{-(t'-t_0)^2/\tau^2} e^{-(t-t_0)^2/\tau^2} \times [e^{i(\epsilon_k+\omega_0-\omega_{RF}-E_k)(t-t')} u_k^2(\sinh\Delta\theta_k)^2 + e^{i(\epsilon_k+\omega_0-\omega_{RF}+E_k)(t-t')}\\
&\quad \times v_k^2(\cosh\Delta\theta_k)^2 + \frac{1}{2}u_k v_k \sinh 2\Delta\theta_k (e^{i(\epsilon_k+\omega_0-\omega_{RF}+E_k)t} e^{-i(\epsilon_k+\omega_0-\omega_{RF}-E_k)t'} + e^{i(\epsilon_k+\omega_0-\omega_{RF}-E_k)t} e^{-i(\epsilon_k+\omega_0-\omega_{RF}+E_k)t'})]\\
&= \pi\tau^2 I_0^2 \sum_{\mathbf{k}} [e^{-\frac{1}{2}(\epsilon_k+\omega_0-\omega_{RF}-E_k)^2\tau^2} u_k^2(\sinh\Delta\theta_k)^2 + e^{-\frac{1}{2}(\epsilon_k+\omega_0-\omega_{RF}+E_k)^2\tau^2} v_k^2(\cosh\Delta\theta_k)^2 + \frac{1}{2}u_k v_k \sinh 2\Delta\theta_k\\
&\quad \times (e^{-\frac{1}{4}(\epsilon_k+\omega_0-\omega_{RF}-E_k)^2\tau^2 - \frac{1}{4}(\epsilon_k+\omega_0-\omega_{RF}+E_k)^2\tau^2}) \cos(2Et_0)],\\
&= \pi\tau^2 I_0^2 \sum_{\mathbf{k}} [e^{-\frac{1}{2}(\epsilon_k+\omega_0-\omega_{RF}-E_k)^2\tau^2} u_k^2(\sinh\Delta\theta_k)^2 + e^{-\frac{1}{2}(\epsilon_k+\omega_0-\omega_{RF}+E_k)^2\tau^2} v_k^2(\cosh\Delta\theta_k)^2\\
&\quad + \frac{1}{2}u_k v_k \sinh 2\Delta\theta_k \times (e^{-\frac{1}{2}((\epsilon_k+\omega_0-\omega_{RF})^2+E_k^2)\tau^2} \cos(2Et_0))],
\end{aligned}
\tag{D19}
$$

which gives Eq. (4.34) of the main text. In above derivation we have used $\hat{b}_{\mathbf{k}}(t) = \hat{b}_{\mathbf{k}} e^{i\epsilon_k t}$ for atoms in the non-interacting hyperfine state, dropped the number non-conserving $\hat{b}^\dagger\hat{b}^\dagger$,$\hat{b}\hat{b}$ terms, neglecting a weak condensation that is always in principle induced by the linear coupling to the a-Bose condensate during the time that the RF coupling pulse is on.

[1] C. Chin, *et al.*, Rev. Mod. Phys. **82**, 1225 (2010).
[2] I. Bloch, J. Dalibard, and W. Zwerger, Rev. Mod. Phys. **80**, 885 (2008).
[3] M. W. Zwierlein, *et al.*, Nature (London) **435**, 1047 (2005).
[4] V. Gurarie and L. Radzihovsky, Ann. Phys. (NY) **322**, 2 (2007)
[5] M. Bartenstein, *et al.*, Phys. Rev. Lett. **92**, 120401 (2004).
[6] C. A. Regal, M. Greiner, D. S. Jin, Phys. Rev. Lett. **92**, 040403 (2004).
[7] T. L. Ho, Phys. Rev. Lett. **92**, 090402 (2004).
[8] M. Y. Veillette, D. E. Sheehy, and L. Radzihovsky, Phys. Rev. A **75**, 043614 (2007).
[9] P. Nikolic and S. Sachdev, Phys. Rev. A **75**, 033608 (2007).
[10] G. Partridge, *et al.*, Science **311**, 503505 (2006).
[11] L. Radzihovsky and D. Sheehy, Rep. Prog. Phys. **73**, 076501 (2010); Phys. Rev. Lett. **96**, 060401 (2006).
[12] Greiner, Markus, *et al.*, Nature (London) **415**, 39 (2002).
[13] S. Doniach, Phys. Rev. B **24**, 5063 (1981).
[14] D. Jaksch, *et al.*, Phys. Rev. Lett. **81**, 3108 (1998).
[15] K. M. O'Hara, *et al.*, Science **298**, 2179 (2002).
[16] Z. Shen, L. Radzihovsky, and V. Gurarie, Phys. Rev. Lett. **109**, 245302 (2012).
[17] C. H. Cheng, and S-K. Yip, Phys. Rev. Lett. **95**, 070404 (2005).
[18] V. Gurarie, L. Radzihovsky, and A. V. Andreev, Phys. Rev. Lett. **94**, 230403 (2005).
[19] C. A. Regal, *et al.*, Phys. Rev. Lett. **90**, 053201 (2003).
[20] G. B. Jo, *et al.*, Science **325**, 1521 (2009).
[21] A. Polkovnikov, *et al.*, Rev. Mod. Phys. **83**, 863 (2011).
[22] M. A. Cazalilla, *et al.*, Rev. Mod. Phys. **83**, 1405 (2011).
[23] T. Langen, R. Geiger, and J. Schmiedmayer, Annu. Rev. Condens. Matter Phys. **6**, 201(2015).
[24] M. Srednicki, Phys. Rev. A **50**, 888 (1994).
[25] M. Rigol, D. Vanja, and M. Olshanii, Nature (London) **452**, 854 (2008).
[26] T. Kinoshita, W. Trevor, and D. S. Weiss, Nature (London) **440**, 900 (2006).
[27] M. Rigol, *et al.*, Phys. Rev. Lett. **98**, 050405 (2007).
[28] E. Altman and A. Vishwanath, Phys. Rev. Lett. **95**, 110404 (2005).
[29] R. A. Barankov, L. S. Levitov, and B. Z. Spivak, Phys. Rev. Lett. **93**, 160401 (2004).
[30] A. V. Andreev, V. Gurarie, and L. Radzihovsky, Phys. Rev. Lett. **93**, 130402 (2004).
[31] E. A. Yuzbashyan, O. Tsyplyatyev, and B. L. Altshuler. Phys. Rev. Lett. **96**, 097005 (2006).
[32] A. Mitra and T. Giamarchi, Phys. Rev. Lett. **107**, 150602 (2011).
[33] V. Gurarie, J. Stat. Mech. **2013**, 02014 (2013).
[34] P. Calabrese and J. Cardy, Phys. Rev. Lett. **96**, 136801 (2006).
[35] S. Sotiriadis and J. Cardy, Phys. Rev. B **81**, 134305 (2010).
[36] A. Chandran, *et al.*, Phys. Rev. B **88**, 024306 (2013).
[37] S. S. Natu and E. J. Mueller, Phys. Rev. A **87**, 053607 (2013).
[38] C. L. Hung, V. Gurarie, and C. Chin, Science **341**, 1213 (2013).
[39] X. Yin and L. Radzihovsky, Phys. Rev. A **88**, 063611

(2013).
[40] A. Bacsi and D. Balazs, Phys. Rev. B **88**, 155115 (2013).
[41] A. Mitra, Phys. Rev. B **87**, 205109 (2013).
[42] M. Fagotti, *et al.*, Phys. Rev. B **89**, 125101 (2014).
[43] N. Nessi, A. Iucci, and M. A. Cazalilla, Phys. Rev. Lett. **113**, 210402 (2014).
[44] R. A. Barankov, L. S. Levitov, and B. Z. Spivak, Phys. Rev. Lett. **93**, 160401 (2004).
[45] M. S. Foster, *et al.*, Phys. Rev. B **88**, 104511 (2013).
[46] M. S. Foster, *et al.*, Phys. Rev. Lett. **113**, 076403 (2014).
[47] E. A. Donley, *et al.*, Nature (London) **417**, 529 (2002).
[48] N. R. Claussen, *et al.*, Phys. Rev. Lett. **89**, 010401 (2002).
[49] S. J. J. M. F. Kokkelmans and M. J. Holland, Phys. Rev. Lett. **89**, 180401 (2002).
[50] A. Rancon, *et al.*, Phys. Rev. A **88**, 031601 (2013).
[51] L. Radzihovsky, J. I. Park, and P. B. Weichman. Phys. Rev. Lett. **92**, 160402 (2004).
[52] M. W. J. Romans, *et al.*, Phys. Rev. Lett. **93**, 020405 (2004).
[53] L. Radzihovsky, P. B. Weichman, and J. I. Park, Ann. Phys. (NY) **323**, 2376 (2008).
[54] D. Borzov, *et al.*, Phys. Rev. A **85**, 023620 (2012).
[55] L. Bonnes and S. Wessel, Phys. Rev. B **84**, 054510 (2011).
[56] P. Makotyn, *et al.*, Nature Physics **10**, 116 (2014)
[57] D. S. Petrov and G. V. Shlyapnikov, Phys. Rev. A **64**, 012706 (2001).
[58] J. L. Song and F. Zhou, Phys. Rev. Lett. **103**, 025302 (2009).
[59] X. Yin and L. Radzihovsky, unpublished
[60] T. L. Ho, Phys. Rev. Lett. **108**, 195301 (2012).
[61] Although we refer to the initial state as the ground, for a bosonic system on the BEC side, it is not, as lower-lying molecular (and higher number cluster) states exist. However, on short time scales relevant to experiments, we confine our analysis to the upper-branch [54, 60], valid for the initial preparation far detuned from the Feshbach resonance [56].
[62] A. G. Sykes, *et al.*, Phys. Rev. A **89**, 021601 (2014)
[63] J. T. Stewart, *et al.*, Phys. Rev. Lett. **104**, 235301 (2010).
[64] R. J. Wild, *et al.*, Phys. Rev. Lett. **108**, 145305 (2012).
[65] N. N. Bogoliubov, J. Phys. U.S.S.R. **11**, 23 (1947)
[66] A. L. Fetter and J. D. Walecka, *Quantum theory of many-particle systems* (Courier Corporation, 2003).
[67] J. Zinn-Justin, *Quantum field theory and critical phenomena* (Clarendon, Oxford, 1989).
[68] T. D. Lee, K. Huang, and C. N. Yang, Phys. Rev. **106**, 1135 (1957).
[69] P. M. Chaikin and T. C. Lubensky, *Principles of condensed matter physics* (Cambridge University Press, Cambridge, 2000).
[70] V. N. Popov, *Functional Integrals and Collective Modes* (Cambridge University Press, New York, 1987, Chap. 6)
[71] M. H. Anderson, *et al.*, Science **269**, 198 (1995).
[72] K. B. Davis, *et al.*, Phys. Rev. Lett. **75**, 3969 (1995).
[73] S. B. Papp, *et al.*, Phys. Rev. Lett. **101**, 135301 (2008).
[74] R. Shankar, *Principles of quantum mechanics* (Springer Science Business Media, 2012).
[75] B. Kain and H. Ling, Phys. Rev. A **90**, 063626 (2014)
[76] S. Tan, Ann. Phys. (NY) **323**, 2952 (2008).
[77] A. Polkovnikov and V. Gritsev, Nature Physics **4**, 477 (2008).
[78] E. Braaten and L. Platter, Phys. Rev. Lett. **100**, 205301 (2008).
[79] A. Schakel, arXiv:1007.3452
[80] J. P. Corson and J. L. Bohn, Phys. Rev. A **91**, 013616 (2015)